

# Search for associations containing young stars (SACY)

## VII. New stellar and substellar candidate members in the young associations<sup>★,★★</sup>

P. Elliott<sup>1,2</sup>, A. Bayo<sup>3</sup>, C. H. F. Melo<sup>1</sup>, C. A. O. Torres<sup>4</sup>, M. F. Sterzik<sup>5</sup>, G. R. Quast<sup>4</sup>, D. Montes<sup>6</sup>, and R. Brahm<sup>7,8</sup>

<sup>1</sup> European Southern Observatory, Alonso de Cordova 3107, Vitacura Casilla 19001, Santiago 19, Chile  
e-mail: pe210@exeter.ac.uk

<sup>2</sup> School of Physics, University of Exeter, Stocker Road, Exeter, EX4 4QL

<sup>3</sup> Departamento de Física y Astronomía, Facultad de Ciencias, Universidad de Valparaíso, Av. Gran Bretaña 1111, 5030 Casilla, Valparaíso, Chile

<sup>4</sup> Laboratório Nacional de Astrofísica/MCT, Rua Estados Unidos 154, 37504-364 Itajubá (MG), Brazil

<sup>5</sup> European Southern Observatory, Karl-Schwarzschild-Str. 2, D-85748 Garching, Germany

<sup>6</sup> Departamento de Astrofísica y Ciencias de la Atmósfera, Facultad de Ciencias Físicas, Universidad Complutense de Madrid, 28040 Madrid, Spain

<sup>7</sup> Instituto de Astrofísica, Facultad de Física, Pontificia Universidad Católica de Chile, Av. Vicuña Mackenna 4860, 7820436 Macul, Santiago, Chile

<sup>8</sup> Millennium Institute of Astrophysics, Av. Vicuña Mackenna 4860, 7820436 Macul, Santiago, Chile

Received 4 February 2016; accepted 7 March 2016

### ABSTRACT

**Context.** The young associations offer us one of the best opportunities to study the properties of young stellar and substellar objects and to directly image planets thanks to their proximity (<200 pc) and age ( $\approx 5$ -150 Myr). However, many previous works have been limited to identifying the brighter, more active members ( $\approx 1 M_{\odot}$ ) owing to photometric survey sensitivities limiting the detections of lower mass objects.

**Aims.** We search the field of view of 542 previously identified members of the young associations to identify wide or extremely wide (1000-100,000 au in physical separation) companions.

**Methods.** We combined 2MASS near-infrared photometry ( $J$ ,  $H$ ,  $K$ ) with proper motion values (from UCAC4, PPMXL, NOMAD) to identify companions in the field of view of known members. We collated further photometry and spectroscopy from the literature and conducted our own high-resolution spectroscopic observations for a subsample of candidate members. This complementary information allowed us to assess the efficiency of our method.

**Results.** We identified 84 targets (45:  $0.2$ - $1.3 M_{\odot}$ , 17:  $0.08$ - $0.2 M_{\odot}$ , 22:  $<0.08 M_{\odot}$ ) in our analysis, ten of which have been identified from spectroscopic analysis in previous young association works. For 33 of these 84, we were able to further assess their membership using a variety of properties (X-ray emission, UV excess,  $H_{\alpha}$ , lithium and KI equivalent widths, radial velocities, and CaH indices). We derive a success rate of 76–88% for this technique based on the consistency of these properties.

**Conclusions.** Once confirmed, the targets identified in this work would significantly improve our knowledge of the lower mass end of the young associations. Additionally, these targets would make an ideal new sample for the identification and study of planets around nearby young stars. Given the predicted substellar mass of the majority of these new candidate members and their proximity, high-contrast imaging techniques would facilitate the search for new low-mass planets.

**Key words.** data analysis open clusters and associations: general proper motions stars: kinematics and dynamics stars: low-mass

## 1. Introduction

The very first members of the TW Hydrae association, one of the youngest ( $\approx 10$  Myr) and closest ( $\approx 50$  pc) young associations, were identified more than two and a half decades ago (de la Reza et al. 1989). The authors noted that a handful of isolated T Tauri

stars with high Galactic latitudes shared similar Galactic kinematics.

These young stars have been identified using a variety of properties (X-ray emission, lithium absorption,  $H_{\alpha}$  emission, common Galactic kinematics, visible, and near-infrared photometry) to identify co-moving groups and distinguish them from older field stars. However, a common property of much of these works was the identification of stars with spectral types earlier than  $\approx K0$ . This was the result of the sensitivities of surveys, such as HIPPARCOS (Perryman et al. 1997) and the ROSAT all-sky survey (RASS; Voges et al. 1999), which were used to build the samples. Recently there have been many works focussed on identifying the lower mass members of the young associations e.g. Shkolnik et al. (2012); Schlieder et al. (2012b); Rodriguez et al. (2013); Malo et al. (2014); Kraus et al. (2014); Gagné et al. (2015); Binks & Jeffries (2016). Again, these surveys use a vari-

\* Based on FEROS observations obtained during CNTAC programme CN2015B-9 and observations made with the HERMES spectrograph mounted on the 1.2 m Mercator Telescope at the Spanish Observatorio del Roque de los Muchachos of the Instituto de Astrofísica de Canarias.

\*\* Appendices A, B, C, and D are available in electronic form at <http://www.aanda.org>. Table E is only available at the CDS via anonymous ftp to <http://cdsarc.u-strasbg.fr> (<ftp://123.45.678.9>) or via <http://cdsarc.u-strasbg.fr/viz-bin/qcat?J/A+A/XXX/XXX>

ety of techniques, however, the initial samples of low-mass candidate members are usually built upon multiple-catalogue photometry combined with proper motions. The candidates are then followed up using mid or high resolution to produce radial velocities (RVs) and signatures of youth, such as  $H_\alpha$  emission and lithium absorption. As a result of the optical magnitudes of these targets (typically  $V > 14$  mag.) the observations are very time expensive, therefore refinement of the initial sample is crucial where possible.

The identification of further low-mass members in the young associations is extremely important for a number of reasons. These targets offer us one of the best opportunities to image exoplanets using high-contrast imaging. The dimmer host star in addition to a hotter planet (because of its youth) significantly reduces contrast constraints (Chauvin et al. 2015; Bowler et al. 2013). Additionally, the young associations currently appear to be very incomplete for low-mass stars. This incompleteness means the initial mass function is very poorly constrained below  $\approx 1 M_\odot$ . Therefore, no meaningful comparison can be made between the IMFs of young associations, formed in low-density regions, and those of higher density clusters.

The work presented here forms part of larger project to study multiplicity in the young associations (Elliott et al. 2014, 2015). These works have used the search for associations containing young stars (SACY) dataset. Stars are defined as members of distinct associations in this dataset by the convergence method (Torres et al. 2006). In this work we extend the membership list including high-probability targets identified in other works; see Section 2 for details. The targets identified in this work are candidate wide companions to these previously identified high-probability members. In that respect this work differs from the majority of previous works aimed at identifying new members and is more similar to works related to wide binaries (Caballero 2009, 2010; Alonso-Floriano et al. 2015). The formation mechanism and implications of such wide (1000-100,000 au) companions will be discussed in further work. Additionally detection limits derived from the analysis presented here will form part of another study combining radial velocities, adaptive optics (AO)-imaging and 2MASS photometry to derive multiplicity statistics across 8 orders of magnitude in physical separation in the young associations. In this work we present the technique we employed to identify the wide companion candidates, an evaluation of our method (using available literature and our own high-resolution spectroscopy observations) and the list of candidate members with their current membership status.

The manuscript is arranged as follows. Section 2 explains how the sample for this work was formed. Section 3 details our technique for identifying new members. Section 4 outlines the sources where we gathered additional information. Section 5 describes the high-resolution spectra we analysed for a subsample of identified targets. Section 6 discusses the properties of the candidates we identified. Section 7 concludes this work evaluating the success of the technique.

## 2. The sample

We collated high-probability members from a collection of prominent moving group works to date (Torres et al. 2008; Zuckerman et al. 2011; Malo et al. 2014; Kraus et al. 2014; Elliott et al. 2014; Murphy & Lawson 2015), which cover a wide range of spectral types (B2-M5) and ages ( $\sim 5$ -150 Myr), totalling 542 targets in nine associations. A summary of the associations can be found in Table 1. We did not put any constraints on the mass of the known members as we want to maximise our

**Table 1.** Summary of the associations studied in this work.

Ass.	Ass. ID	Age	Age ref.	No. of objects
AB Dor	ABD	100-150	2,7	105
Argus	ARG	40-44	1,7	77
$\beta$ -Pic	BPC	21-26	1,3,4,7	69
Carina	CAR	35-45	1,3,7	48
Columba	COL	35-42	1,3,7	78
$\epsilon$ -Cha	ECH	5-10	1,5,7	24
Octans	OCT	30-40	1,6,7	62
Tuc-Hor	THA	33-45	1,3,7	56
TW Hydrae	TWA	10-12	1,3,7	23

**References.** 1: Torres et al. (2006), 2: da Silva et al. (2009), 3: Bell et al. (2015), 4: Binks & Jeffries (2014), 5: Murphy et al. (2013), 6: Murphy & Lawson (2015), 7: Torres et al. in prep.

sample size. However, we are limited in sensitivity to wide companions depending on the position of the source on the sky, its proper motion, and density of objects in the field of view (FoV), as discussed in Section 3. The targets that make up the sample and their basic properties are listed in Table D.1.

## 3. Searching for new members as very wide companions

To identify very wide companions we used the point source catalogue of 2MASS (Cutri et al. 2003) for near-infrared photometry ( $J, H, K$ ). We combined this with proper motions from the naval observatory merged astrometric dataset (NOMAD), the proper motion extended catalogue (PPMXL), and the United States naval observatory (USNO) CCD astrograph catalogue (UCAC4) (Zacharias et al. 2005; Roeser et al. 2010; Zacharias et al. 2012, respectively).

One aim of this search was to produce robust detection limits of our entire sample out to 100,000 au in physical separation from the known member. These limits will be used in further work as explained in Section 1. We first calculated the angular query needed to achieve a physical search radius out to 100,000 au using the distance to the source (either from parallax ESA 1997; van Leeuwen 2007 or derived kinematically using the convergence method Torres et al. 2006). We then converted the apparent magnitude of any sources in the FoV into absolute magnitude, assuming the distance of the known member. Using the available photometry ( $J, H, K$ ) we constructed colour-magnitude diagrams ( $H-K, K$  and  $J-K, K$ ) for each FoV. We used the evolutionary tracks of Baraffe et al. (2015), with the age of the association that the member belongs to. We then used the photometry with derived statistical uncertainties and kinematic criteria (detailed below) to classify potential companions.

### 3.1. Computing statistical photometric uncertainties

The three photometric bands of 2MASS ( $J, H, K$ ) do not offer a very wide range of colours to distinguish young objects from contamination. Additionally proper motion values are only projected motions and therefore the distance to the object can be a severe limiting factor. For those reasons we took the time to produce photometric criteria that would limit the number of false-positives whilst attempting to minimise the possibility of true companion rejection.

First of all, for the entire sample we computed the standard deviation of the difference between the colour of the

isochrone and 2MASS photometry for each object. The values were  $\sigma_{H-K}=0.06$  mag and  $\sigma_{J-K}=0.16$  mag for the colours  $H-K$  and  $J-K$ , respectively. This provided an estimate of the difference between the models and observations. We used the generous criteria of  $2\sigma$  for both colours, however, the source must agree in both of these colours to be classified as a potential companion.

The colour and magnitude are related quantities and therefore an offset in magnitude can dramatically affect the agreement in colour. An unresolved (equal-mass) companion can affect the magnitude of a source by up to  $\approx 0.8$  mag. We therefore adopted this value as our upper uncertainty on the absolute magnitude. The effect of unresolved companions is asymmetric with respect to the magnitude, i.e. it only ever increases this value. For the lower limit, we computed the average difference (0.15 mag.) between the isochrone and the known member; in the cases that the known member was fainter than its isochrone, we used  $2\sigma$  as our criterion again.

We performed the analysis on a subset of the primary sources in our sample to test the effectiveness of our derived criteria. Of 198 primaries, 188 were initially identified correctly. Of the ten sources that were not identified, seven were known sources with two or more components in their photometry (such as HD 217379, identified as a triple-lined spectroscopic binary in Elliott et al. 2014). These are rare cases, however we do not want to exclude any sources (companions also have a small probability of being in an SB3 configuration) and therefore we increased the upper limit on the magnitude (1.2 mag.). With this new criterion we identified 195 / 198 of our primaries. Of the three sources (T Cha, CP-681894, TWA 22) that were still not identified, two have near-infrared photometric excesses (T Cha is a well-known disc system (Weintraub 1990) and CP-681894 shows strong  $H_\alpha$  emission and K-band excess, indicative of accretion (Schütz et al. 2005)). The other target, TWA 22 is a very tight, near equal-mass binary system (Bonney et al. 2009). Using the resolved photometry this system would have been classified correctly. However, with the unresolved 2MASS photometry the system appears too red for its magnitude. Owing to its proximity ( $\approx 18$  pc) and its age (10-20 Myr) the effect of the unresolved companion is exaggerated, however such young, nearby, low-mass (system mass:  $220 \pm 21 M_{Jup.}$ ) systems are very rare in our sample. Therefore, we proceeded with the criteria described above.

This may induce a small bias in the way that we search for our companions, i.e. we could potentially exclude sources with strong infrared excess. However, only 3 / 198 were not classified because of their excess (1.5%). Additionally the frequency of primordial discs for the ages of the young associations is very low. For example, at 5 Myr the frequency is  $\approx 10\%$  and for populations older than 10 Myr  $< 5\%$ , (see Figure 1 of Mamajek 2009). Furthermore this effect is less and less prominent as the mass of the companion decreases. Andrews et al. (2013) showed that, for a sample of stars with spectral types earlier than M8.5 in Taurus, the disc mass decreases with the stellar mass. If we consider this in terms of infrared photometry the excess scales with the luminosity of the object, i.e. a significant excess, considering the same detection threshold, is less likely for a lower mass star. Furthermore, if we assume a flat-mass ratio, as observed in many regions (including close,  $\approx 10$ -1000 au, visual binaries in young associations; Elliott et al. 2015) this bias becomes even less significant.

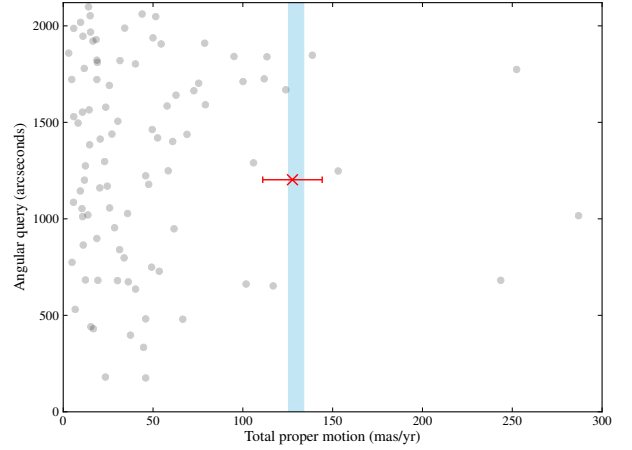


**Fig. 1.** Graphical demonstration of our contamination / detection method for target Kap Psc (distance: 50 pc). The red markers indicate proper motion compatible sources (with  $3\sigma$  uncertainties) and the grey markers indicate incompatible sources. The blue shaded space is the  $3\sigma$  boundary of the proper motion of the primary target. The extent of the angular query is  $2000''$ , equivalent to 100,000 au at 50 pc.

### 3.2. Using near-infrared photometry and proper motions to find wide companions

Any source that met the criteria described above was classified as a potential companion within the FoV. We then cross-matched all of these sources with the catalogues of UCAC4, PPMXL, and NOMAD, in that order of preference based on uncertainties, completeness, and catalogue-catalogue agreement, to collect the proper motion values.

Finding physical extremely wide companions is limited by the projected motion of the target on the sky. In most cases we do not have access to parallax or radial velocity values; we only have access to proper motion, which is intrinsically linked to its distance. Additionally the Galactic position of the target is a limiting factor, i.e. targets close to the Galactic plane (and close to the Sun) are likely to have a high number of sources in their FoV; this increases the false-positive probability even with the imposed photometric constraints. Our targets are of different ages, at different distances and spatial positions and therefore there are many competing factors in estimating the contribution of contamination. We treated the contamination of each source individually to find potential companions and also to derive the maximum angular separation space that we could probe. This method provides us with detection limits in angular separation, which is crucial for our broader statistical analysis to be presented in future work (Elliott et al. in prep.).

For sources with low or intermediate proper motion ( $< 20$  mas) the chance of contamination increases significantly. In many works authors decide to use a hard cut-off (i.e. only considering sources with proper motions above a certain, somewhat arbitrary, threshold). However, information on the population can be lost as a source with intermediate proper motion is not analysed at all. Below is a description of the method we employed to maximise the physical separation space we can query without significant contamination.

Figure 1 graphically demonstrates our method for a primary target in our sample. The total proper motion, the x-axis, is defined as  $\sqrt{\mu_{\alpha,*}^2 + \mu_{\delta}^2}$ . Therefore, two sources may share the

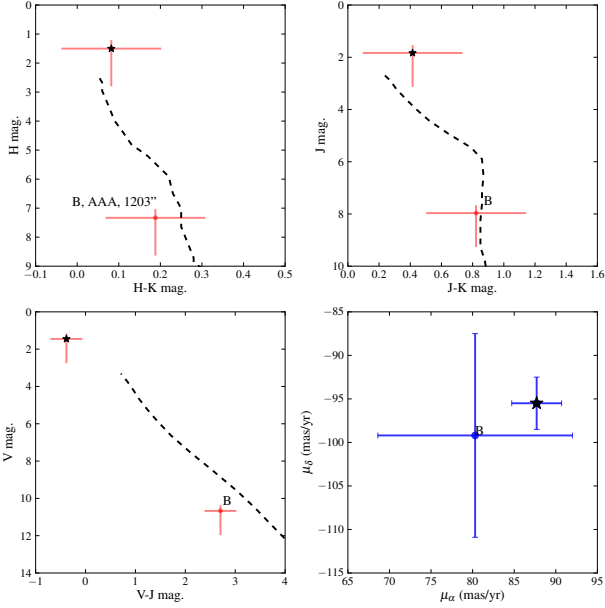


**Fig. 2.** *Top left, top right, and bottom left panels:* colour-magnitude diagrams for Kap Psc+2MASS J23270114+0055200 in  $(H-K, K)$ ,  $(J-K, K)$ , and  $(V-J, V)$ , respectively. The text next to the marker indicates the component designation, the quality flags of the 2MASS photometry and angular separation from the primary. The dotted lines are the evolutionary tracks of Baraffe et al. (2015) using the age of the moving group. *Bottom right panel:* Proper motion values of the primary and companion.

same total proper motion, however, not the same angle of projected motion. It is this angle that distinguishes proper motion-compatible sources (red markers) from incompatible sources (grey markers).

All markers in Figure 1 are sources with compatible 2MASS photometry. The grey circles show sources with an incompatible proper motion vector ( $\geq 3\sigma$  discrepancy), the red marker (at  $\approx 1200''$ , 57,000 au) represents sources with a compatible proper motion vector, and the blue shaded area is  $3\sigma$  proper motion space of the primary target. The total queried FoV is equivalent to 100,000 au. We use the point at which the total proper motion of the primary crosses any region in the parameter space with 2 or more incompatible sources as our maximum angular separation. This is a very conservative estimate but proved very powerful. If the total proper motion of the primary never crosses any such regions we set our sensitivity to a radial physical distance of 100,000 au, as in Figure 1.

Figure 2 shows a summary of the photometry ( $V, J, H, K$ ) and proper motion of the potential companion from Figure 1. The agreement in the colour  $V-K$  is generally very poor and is discussed more thoroughly in Section 6.8. For the inner angular query we use the limit given by the PSF of 2MASS ( $\approx 3''$ ) that relates to a physical inner limit of 18–570 au for our nearest and furthest sources, respectively.

#### 4. Further information from catalogues and literature

Table 2 summarises the catalogues and works with which we cross-matched our sample to gain further photometry, spectroscopy, kinematics, and information of multiplicity. Where the

cross-match was successful we collated any available notes of the source from the works.

We also compared our results to other works that have focussed on very wide companions to stars in the moving groups (Kastner et al. 2011, 2012; Scholz et al. 2005; Looper et al. 2010; Feigelson et al. 2006; Alonso-Floriano et al. 2015). A detailed comparison of these targets can be found in Appendix B. Additionally we queried Simbad (Wenger et al. 2000) for each object to collate any noteworthy features, analysis, and further parameters available.

#### 4.1. Photometry from the Catalina survey

We used the Catalina survey (Drake et al. 2009), aimed at identifying optical transients, covering  $33,000 \text{ deg}^2$  of the sky, to analyse optical photometric variability. We cross-matched our sample with the second data release via the online multi-object search service<sup>1</sup>. From this cross-match there were 235 matches. This was significantly reduced to 55 matches, considering objects fainter than 13 mag. to avoid saturation. We checked the light curves of all 55 of these objects for any signs of variability using a Lomb-Scargle periodogram via the astroML python package (Vanderplas et al. 2012) and derived  $V$  magnitudes, based on the median value of those data, for objects with 3 or more epochs of data (see Figure 3 for an example). However, the median values we derived were, in most cases, much higher (0.5–1.0 mag.) than those catalogued in NOMAD and URAT1. This discrepancy is most likely down to the transformation from unfiltered photometry to  $V$  magnitudes. In this analysis we do not use the median magnitudes derived from Catalina photometry because of this large discrepancy. However, any variability or periodicity seen in an objects light curve is included as a flag in Table E and is discussed further in Section 6.8.

#### 4.2. Previous searches for members of young associations

Some of the works listed in Table 2 and additionally other works are specifically concerned with identifying new members of the young associations. Below we note any overlap between our identified objects and other works. We are interested in not only confirming the youth of the objects, but also in analysing their radial velocity agreement with their associated known member.

- Malo et al. (2013): There were two objects identified here that are in common (2MASS J01034210+4051158, 2MASS J21100535-1919573). Both objects have compatible radial velocity values with their associated primary stars.
- Gagné et al. (2015): We found one object in common (2MASS J11020983-3430355), which was also identified in Teixeira et al. (2008) and is discussed in more detail in Appendix B. This object has compatible radial velocity with its associated primary.
- Shkolnik et al. (2012): There were three objects in common (2MASS J01034210+4051158, 2MASS J04373746-0229282, and 2MASS J12573935+3513194). The radial velocity values were consistent with their primary stars for the first two sources. The third source is a spectroscopic binary and therefore its radial velocity is not consistent with its associated primary star, see Appendix A. Owing to a lack of data its system velocity cannot be derived at this time.

<sup>1</sup> [http://nessi.cacr.caltech.edu/cgi-bin/getmulticonedb\\_release2.cgi](http://nessi.cacr.caltech.edu/cgi-bin/getmulticonedb_release2.cgi)

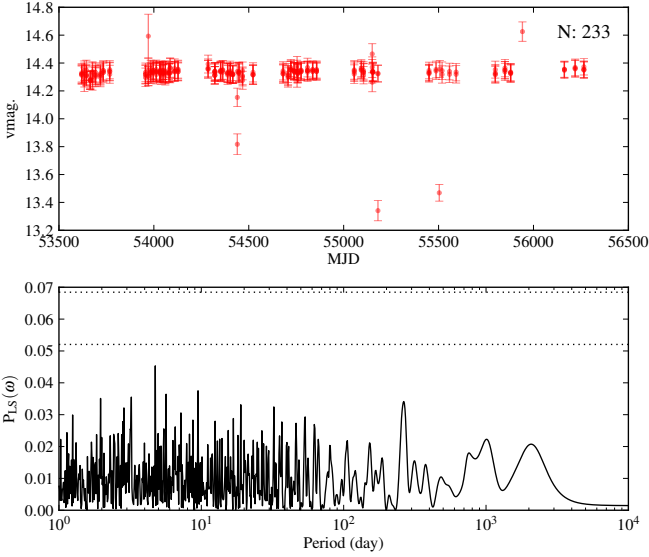


**Fig. 3.** *Top panel:* light curve of optical magnitudes for a candidate member in our sample (2MASS J02103888-4557248);  $N$  is the total number of data points. *Bottom panel:* Lomb-Scargle periodogram for the data presented in the top panel. The dashed lines represent the levels of significance:  $1\sigma$  and  $5\sigma$ .

- [Schlieder et al. \(2012b\)](#): We found one object in common (2MASS J05015665+0108429), which has compatible radial velocity with its associated primary.
- [Rodriguez et al. \(2013\)](#): We found one object in common (2MASS J02105345-4603513), which is most likely a spectroscopic binary. The target has an incompatible radial velocity and is discussed in more detail in Appendix A.
- [Kraus et al. \(2014\)](#): Although we included the bonafide member list from this work, we did not include identified candidate members. There was one successful match with these candidate members (2MASS J00302572-6236015). This source has compatible radial velocity with its associated primary.
- [Alonso-Floriano et al. \(2015\)](#): The authors identified 36 potential wide binaries, and 16 of these systems only had one stellar component previously classified as a member of the  $\beta$ -Pic moving group. We recovered 15/16 of these new identifications.

The one detection we did not recover we conclude is not a physical wide companion (V4046 Sgr – GSC 07396-00759); see Appendix B for details.

## 5. Spectroscopic parameters and observations

High-resolution optical spectra allow us to compute radial velocity values and look for signatures of youth. In the following analysis, we computed EWs for the gravity-sensitive atomic alkali lines of K I (7699 Å) and Na I (8194.8 Å), see [Martin \(1997\)](#). Additionally, EWs of  $H_{\alpha}$ , associated with activity, and lithium which is used as an age indicator; see [Barrado y Navascués et al. \(1999\)](#); [Binks & Jeffries \(2014\)](#).

To produce the spectroscopic quantities described above we used the line-fitting method described in [Bayo et al. \(2011\)](#). This automatic line measurement procedure has been improved and includes a local pseudo-continuum iterative identification pro-

**Table 2.** Surveys and catalogues cross-matched with the sample presented.

Code	Reference	Parameters
NO04	<a href="#">Nordström et al. (2004)</a>	RV
BA12	<a href="#">Bailey et al. (2012)</a>	RV
EL14	<a href="#">Elliott et al. (2014)</a>	RV
MA14	<a href="#">Malo et al. (2014)</a>	RV, $H_{\alpha}$ , Li, $L_x$
RAVE	<a href="#">Kordopatis et al. (2013)</a>	RV
DE15	<a href="#">Desidera et al. (2015)</a>	RV, Li
RO13	<a href="#">Rodriguez et al. (2013)</a>	RV, $H_{\alpha}$ , Li, NaI
RI06	<a href="#">Riaz et al. (2006)</a>	RV, $H_{\alpha}$ , $L_x/L_{bol}$ , CaH1,2,3
BE15	<a href="#">Bell et al. (2015)</a>	V mag.
IPHAS	<a href="#">Barentsen &amp; et al. (2014)</a>	$H_{\alpha}$
GALEX	<a href="#">Bianchi et al. (2011)</a>	NUV, FUV mag.
URAT1	<a href="#">Zacharias et al. (2015)</a>	R, B, V mag.
CATA	<a href="#">Drake et al. (2009)</a>	V mag. (+ variability)
ASAS	<a href="#">Pojmanski (2002)</a>	V mag. (+ variability)
RO13	<a href="#">Rodriguez et al. (2013)</a>	RV
SH12	<a href="#">Shkolnik et al. (2012)</a>	RV
SC12	<a href="#">Schlieder et al. (2012b)</a>	RV, SpT
SPM4	<a href="#">Girard et al. (2011)</a>	B, V mag.
RE09	<a href="#">Reiners &amp; Basri (2009)</a>	RV, Li presence
RI15	<a href="#">Riviere-Marichalar et al. (2015)</a>	RV, $H_{\alpha}$
M013	<a href="#">Moór et al. (2013)</a>	RV, Li, $H_{\alpha}$ , $L_x/L_{bol}$
GO06	<a href="#">Gontcharov (2006)</a>	RV, V mag.
DE12	<a href="#">de Bruijne &amp; Eilers (2012)</a>	RV
FR13	<a href="#">Frith et al. (2013)</a>	RV
MO08	<a href="#">Morin et al. (2008)</a>	RV
LO10	<a href="#">Looper et al. (2010)</a>	RV
KH07	<a href="#">Kharchenko et al. (2007)</a>	RV
HO91	<a href="#">Hoffleit &amp; Jaschek (1991)</a>	RV
LE13	<a href="#">Lépine et al. (2013)</a>	$H_{\alpha}$ , CaH2,3
MO01a	<a href="#">Montes et al. (2001)</a>	RV
LO06	<a href="#">López-Santiago et al. (2006)</a>	RV, Li
MA10	<a href="#">Maldonado et al. (2010)</a>	RV
WISE	<a href="#">Wright et al. (2010)</a>	W1, W2, W3, W4
RI14	<a href="#">Riedel et al. (2014)</a>	V mag.
VI56	<a href="#">Vyssotsky (1956)</a>	V mag.
ME06	<a href="#">Mermilliod (2006)</a>	V mag.
LA01	<a href="#">Lawson et al. (2001)</a>	V mag.
KH09	<a href="#">Kharchenko et al. (2009)</a>	V mag.
NOMAD	<a href="#">Zacharias et al. (2005)</a>	B, V, R mag.
WDS	<a href="#">Mason et al. (2001)</a>	Multiplicity
MA13	<a href="#">Malo et al. (2013)</a>	RV, $H_{\alpha}$ , Li
GSC	<a href="#">Lasker et al. (2008)</a>	B, U, V mag.
TYC	<a href="#">Høg et al. (2000)</a>	B, V mag.
3XMM	<a href="#">Xmm-Newton Survey Science Centre (2013)</a>	X-ray: flux
CHAN	<a href="#">Evans et al. (2010)</a>	X-ray: flux
BSC	<a href="#">Voges et al. (1999)</a>	X-ray: counts, HR
FSC	<a href="#">Voges et al. (2000)</a>	X-ray: counts, HR

cess and Monte Carlo solutions on this identification process to take the normalisation contribution to the uncertainties of the line measurements into account.

### 5.1. Existing observations

We searched the public archives of four high-resolution spectrographs (UVES/VLT, FEROS/2.2m, HARPS/3.6m, and HIRES/KECK). We found one HARPS spectrum for target 2MASS J23485048-2807157 (Prog. ID: 92.C-0224) and one HIRES spectrum for target 2MASS J02455260+0529240 (Prog. ID: U033Hr). The radial velocities were computed using a binary mask (SpT: K0) to produce a cross-correlation function (CCF) as described in [Queloz \(1995\)](#); [Elliott et al. \(2014\)](#). The spectroscopic quantities are shown in Table 3. We could not compute EWs for Na I or K I for the HARPS observation

because of the wavelength coverage of the spectrum (3780–6910 Å).

## 5.2. New observations

To further classify identified candidates we obtained new high-resolution spectra using HERMES/Mercator and FEROS/2.2 m. The details of the observations are presented below.

**HERMES:** Spectroscopic observations were obtained at the 1.2 m Mercator Telescope at the *Observatorio del Roque de los Muchachos* (La Palma, Spain) on 14–18 December 2015 with HERMES, High Efficiency and Resolution Mercator Echelle Spectrograph (Raskin et al. 2011). Using the high-resolution mode (HRF), the spectral resolution is 85000 and the wavelength range is from  $\lambda$ 3800 Å to  $\lambda$ 8750 Å approximately. All the obtained *echelle* spectra were reduced with the automatic pipeline (Raskin et al. 2011) for HERMES. We were limited to brighter targets to keep the integration times below 2000 seconds for a signal-to-noise ratio (S/N)  $\geq 30$  at 6500 Å. When the observations were taken we were not aware that 3/4 of these targets had existing radial velocity values. However, with the newly obtained spectra we were able to compare our values to those of the literature, increase our sensitivity to single-lined spectroscopic binaries, and additionally calculate EWs of spectral lines.

**FEROS:** We observed five newly identified candidate members using FEROS on 25-12-2015. These observations were taken with the standard FEROS setup (2'' fibre aperture, R~48,000, 3600–9200 Å) in OBJCAL mode, using the ThAr+Ne lamp for simultaneous wavelength calibration. The targets were faint ( $V \approx 13$ –14.8 mag.) and therefore the S/N was low ( $\leq 20$ ). To calculate accurate radial velocities for these spectra, we used a dedicated pipeline built from a modular code (CERES, Brahm et al. in prep.) that is capable of processing data in a homogeneous and optimal way coming from different echelle spectrographs. A description of a similar pipeline developed for the Coralie spectrograph can be found in Jordán et al. (2014). This FEROS pipeline is able to achieve a long-term RV precision of 5 m/s in the high S/N limit. In the case of low S/N data ( $\sim 20$ ), the optimal extraction routine of the pipeline coupled with the careful treatment of systematics, allows it to obtain RV precisions of  $\sim 20$ –30 m/s. In order to increase the accuracy of the wavelength solution, the bluest ( $\lambda < 3900$  Å) and reddest ( $\lambda > 6700$  Å) orders are not used. Some features such as the NaI and KI doublets are in the reddest orders and therefore are unavailable in these 1D reduced spectra. For the calculation of all EWs and indices from molecular bands, we used the standard reduced products from the MIDAS pipeline. Unfortunately the low S/N of our observations prevented us from continuum identification and extraction in several wavelengths regions. One of these regions was Li I (6708 Å), which is affected by a strong Ar emission line originated from the contiguous comparison fibre. We therefore do not analyse the Li I region from these FEROS spectra.

A summary of the observations and derived spectroscopic properties are shown in Table 3 for the HERMES and FEROS observations.

## 6. Properties of candidates from our search

Discussions of individual objects with discrepant/dubious spectroscopic parameters (denoted by a "N" or "?" in *Member?* column of Table 4) can be found in Appendix A. The detailed spectroscopic, kinematic and photometric properties of all identified targets and their respective references can be found in Table E.

For a brief summary of the 84 targets identified in this work and their membership status see Table 4. Below we compare individual kinematic, spectroscopic, and photometric properties of identified targets with our original sample and other young sources to assess the success of our method.

Spectral types were calculated by converting effective temperatures using the relationship for pre-main-sequence stars from Pecaut & Mamajek (2013). The effective temperatures were derived from fitting the SEDs (produced using the VOSA tool; Bayo et al. 2008) with the evolutionary models of Baraffe et al. (2015).

### 6.1. Identification of existing members as wide companions to other known members

Using our method we identified known members of the moving groups as potential wide companions to other known members in our sample.

This effectively reduced our sample size of primaries from 581 to 567. We used these sources to check whether our method based on 2MASS photometry and proper motion is consistent for sources with derived photometric distances and Galactic velocities. Table 5 summarises the results and notes any companions to the sources that could affect their photometry ( $< 3''$ ) and therefore their distance estimation. The uncertainties on the Galactic velocities are  $\sim 1$  kms $^{-1}$ . To quantify the agreement between components in these 14 cases, we first calculated the standard deviation of (U, V, W) Galactic velocities for the known members in each association. We compared this to the magnitude of the differences between the Galactic velocities grouped as in Table 5. We found that 13/14 targets had dispersions below the standard deviation of their respective association, the left panel of Figure 4 shows this result graphically. Additionally, the right panel shows the photometric distances derived between the primary and its associated companion for all 14 systems. These two results are a very good indication that these targets do in fact form physically wide multiple systems rather than being the result of a projection effect due to the spatial density of stars. The formation, abundance, and dynamical evolution of wide binaries in the young associations will be discussed in further work (Elliott et al. in prep.). We do not refer to these targets as *identified in this work*, they form part of the *original sample* in any discussion presented here.

### 6.2. Radial velocities

In Figure 5 we show a comparison of radial velocities between targets identified in this work (companions) and their associated known member for the 23 targets with both measurements. If these companions formed very wide binary systems with their associated known member, we would expect a 1:1 relation between the two quantities within uncertainties. As can be seen, we do indeed see this relation for the majority of targets (18/23). As these targets share the same proper motion and radial velocity, by assuming the same distance, they share the same Galactic velocity. Some of the known members are part of spectroscopic binary systems, these are indicated by crosses in Figure 5. The plotted radial velocities of the known members are the gamma (system) velocities and therefore the effect of the spectroscopic component has been accounted for. The quality of this correction depends on how much of the orbital phase has been covered by previous radial velocity observations. However, as shown by the agreement between the values, this does not have a sig-

**Table 3.** Summary of targets and their derived properties for high-resolution spectra analysed in this work.

2MASS ID	RV (km s <sup>-1</sup> )	Na I (8194.8) (Å)	K I (7699) (Å)	H <sub>γ</sub> (Å)	Li I (mÅ)	T <sub>eff</sub> (K)	SpT	SpT ref.	Obs.
01334282-0701311	-14.934±0.003	0.26±0.01	0.17±0.01	2.00±0.11	64±3	5830	G1	1	HERMES
01373545-0645375	11.689±0.002	0.329±0.026	0.210±0.003	1.202±0.101	101±10	5200	G6	2	HERMES
03281095+0409075	10.952±0.667	0.146±0.048	0.196±0.044	2.727±0.329	124±16	5900	F6	2	HERMES
04373746-0229282	22.047±0.031	1.052±1.162	0.769±0.034	-2.142±0.127	61±23	3750	M1.1	3	HERMES
01354915-0753470	6.487±0.029	0.69±0.09	0.69±0.05	-0.06±0.02	...	3500	M4	4	FEROS
03074909-2750467	16.512±0.171	1.21±0.08	1.21±0.13	-12.80±1.11	...	3500	M4	4	FEROS
04515223-4640497	51.188±0.019	0.35±0.03	0.49±0.05	-0.03±0.01	...	4800	K6	4	FEROS
07013945-4231370	24.339±0.025	-0.001±0.002	0.45±0.07	0.33±0.22	...	4300	K4	4	FEROS
08371456-5517343	81.314±0.019	-0.15±0.07	0.001±0.001	0.70±0.10	...	4850	K9	4	FEROS
23485048-2807157	7.430±0.032	...	...	1.63±0.17	140±10	5200	G8	2	HARPS
02455260+0529240	88.502±0.053	...	0.912±0.039	-2.462±0.216	...	3100	M1	2	HIRES

**References.** 1: Gray et al. (2006), 2: T<sub>eff</sub> conversion from VOSA spectral energy distribution (Bayo et al. 2008), 3: Shkolnik et al. (2012), 4: estimation from FEROS data reduction.

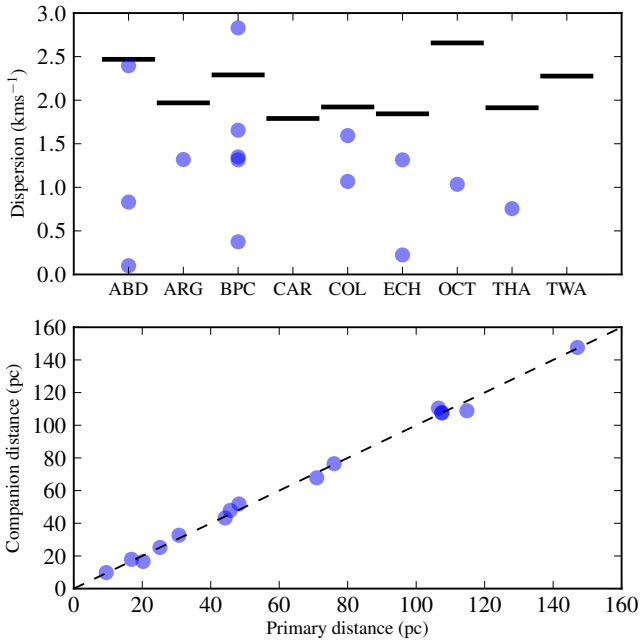


**Fig. 4.** *Top panel:* black markers represent the magnitude of the standard deviation in Galactic velocities (U, V, W) for each association. The blue markers are the absolute difference between companions and their associated primary star, as shown in Table 5. *Bottom panel:* photometric distances derived from the convergence method for companions and their associated known member.

nificant effect. The suspected single-lined spectroscopic binary 2MASS J02105345-4603513 is highlighted by an open black circle and discussed, along with the other four discrepant targets in Appendix A.

### 6.3. Identification of young objects combining GALEX, 2MASS, and WISE photometry

Some previous works have focussed on identifying new late-type members (M0-M5) detecting their predicted enhanced UV emission (Shkolnik et al. 2012; Rodriguez et al. 2013). The con-

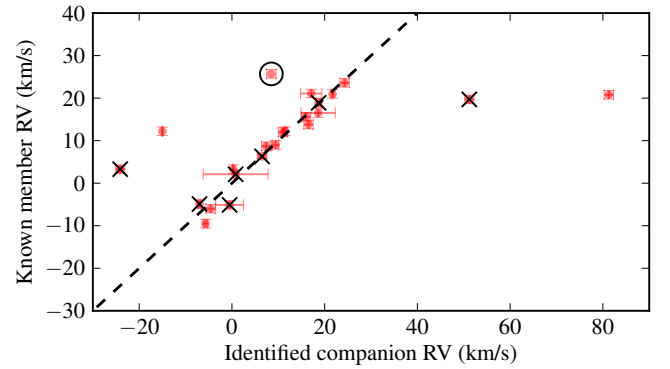


**Fig. 5.** Radial velocity of identified targets in this work versus radial velocity of their associated known member. The dotted line represents a 1:1 relation in the quantities. Crosses indicate the known member is a spectroscopic binary (plotted radial velocity is the system(γ) velocity). The open circle represents the suspected single-lined spectroscopic binary 2MASS J02105345-4603513.

vective envelopes of these low-mass stars combined with their differential rotation produces strong magnetic dynamos. These dynamos lead to enhanced chromospheric and coronal activity, which increases UV emission and X-ray emission (see Section 6.4), respectively.

**Table 4.** Basic properties and membership status of targets identified in this work.

2MASS identifier	Dist. <sup>(a)</sup> (pc)	SpT	V (mag.)	K (mag.)	Mass (M <sub>⊙</sub> )	μ <sub>α,*</sub> (mas/yr)	μ <sub>δ</sub> (mas/yr)	Ass.	Quantity <sup>(b)</sup>	Ref.	Mem? <sup>(c)</sup>
00341993+2528147	49.9	M4	...	10.7	0.23	90.7 ± 4.1	-105.3 ± 4.1	ABD			...
01034210+4051158	29.6	K7	12.9	8.5	0.41	132.0 ± 8.0	-164.0 ± 8.0	ABD	H <sub>α</sub> , X, CaH, UV	1, 5	Y
02103888-4557248	73.7	K5	14.6	11.4	0.25	48.2 ± 1.6	-1.5 ± 1.6	ABD	FI	5	...
02105345-4603513	73.7	M4	15.2	10.3	0.44	53.2 ± 1.8	-10.2 ± 1.8	ABD	RV, X, UV	2	Y?
02123342+2356379	36.6	M4	17.0	11.0	0.12	131.0 ± 8.0	-158.0 ± 8.0	ABD			...
02484213+2716185	50.7	M5	18.8	13.8	0.04	62.4 ± 5.2	-127.3 ± 5.2	ABD			...
03331403+4615194	34.3	F5	11.8	7.6	0.63	64.7 ± 4.0	-172.4 ± 3.6	ABD	RV, H <sub>α</sub> , CaH	14	Y
04080429+0143548	55.3	K9	14.5	10.9	0.23	29.9 ± 4.6	-88.7 ± 5.2	ABD			...
04575034-0652070	45.0	M2	15.6	11.3	0.14	41.3 ± 4.3	-103.1 ± 5.2	ABD			...
05060187-1543564	78.9	M1	...	14.1	0.05	18.7 ± 4.0	-50.2 ± 4.1	ABD			...
05105505-0410563	76.9	M4	15.9	10.8	0.38	19.0 ± 3.4	-54.4 ± 3.7	ABD			...
05274075-0930438	21.9	M3	...	9.7	0.14	61.6 ± 5.1	-172.7 ± 5.1	ABD			...
05454276-1450198	75.8	M4	...	13.6	0.06	10.7 ± 4.1	-51.6 ± 4.1	ABD			...
07285117-3015527	15.7	M4	13.4	8.1	0.25	-45.7 ± 3.4	17.2 ± 3.5	ABD	RV	9	Y
07435039-7940252	80.6	K9	16.2	12.4	0.15	-6.7 ± 3.8	49.3 ± 3.9	ABD			...
07453522-7940136	80.6	F5	12.1	8.9	0.82	-16.5 ± 2.5	42.2 ± 2.5	ABD			...
09281506-7815223	116.5	F5	8.6	7.7	0.22	-25.8 ± 1.1	21.9 ± 1.1	ABD			...
12573935+3513194	19.3	M4	13.0	8.0	0.33	-281.8 ± 3.6	-147.0 ± 6.7	ABD	RV, CaH, H <sub>α</sub>	4, 14	Y?
17360095-1320580	46.3	M0	15.3	11.7	0.11	-4.1 ± 6.0	-108.7 ± 6.3	ABD			...
23270114+0055200	47.2	K5	14.0	10.6	0.23	80.3 ± 3.9	-99.2 ± 3.9	ABD			...
23485048-2807157	42.2	G8	9.1	7.1	0.87	99.2 ± 0.9	-100.9 ± 1.7	ABD	RV, Li, H <sub>α</sub> , X	5	Y
23514340+3127045	42.8	M4	14.1	9.5	0.38	96.5 ± 3.3	-86.6 ± 3.6	ABD	UV	5	Y
03262220+2313122	16.9	M4	16.4	10.7	0.04	247.0 ± 8.0	-96.0 ± 8.0	ARG	FI	5	...
06494841-2858025	120.8	M4	15.6	11.5	0.30	-15.7 ± 4.3	20.0 ± 4.3	ARG			...
07013945-4231370	101.0	K4	13.9	10.9	0.38	-9.9 ± 1.1	34.6 ± 1.1	ARG	KI, RV, H <sub>α</sub>	5	Y
07283006-4908589	82.8	F8	8.8	7.6	1.18	-25.4 ± 0.8	48.8 ± 1.3	ARG	RV, Li	5, 6	Y
08374680-5252307	152.3	K2	14.5	12.3	0.28	1.7 ± 1.9	6.2 ± 1.8	ARG			...
09394669-2133023	93.3	M5	18.0	14.4	0.04	-41.4 ± 4.0	15.8 ± 4.0	ARG			...
01334282-0701311	24.0	G1	5.8	4.3	0.97	175.2 ± 1.0	-82.3 ± 1.0	BPC	RV, Li	5, 16	N
01354915-0753470	37.9	M4	13.8	9.8	0.13	88.6 ± 5.1	-42.2 ± 5.1	BPC	H <sub>α</sub> , KI, RV	5	Y?
01373545-0645375	24.0	G6	7.7	5.8	0.89	171.3 ± 1.0	-98.5 ± 1.0	BPC	X, RV, Li, H <sub>α</sub>	5, 15, 16	Y
02160734+2856530	39.5	M2	15.7	11.6	0.04	92.9 ± 3.1	-64.0 ± 3.2	BPC			...
04373746-0229282	29.4	M1	10.6	6.4	0.78	45.9 ± 1.3	-63.6 ± 1.2	BPC	Li, RV, CaH, H <sub>α</sub> , KI, X	1, 4	Y
05015665+0108429	24.2	M4	12.9	7.7	0.28	33.2 ± 2.2	-89.1 ± 3.1	BPC	X, RV, CaH, H <sub>α</sub>	5, 7, 14	Y
05195327+0617258	71.0	M5	18.3	12.4	0.05	13.7 ± 4.0	-38.1 ± 4.0	BPC	X	5	Y
14141700-1521125	30.2	M3	15.6	8.8	0.18	-117.4 ± 8.0	-196.6 ± 8.0	BPC	UV	5	Y
17483374-5306118	71.0	M2	13.7	9.3	0.47	-2.5 ± 2.0	-51.7 ± 2.0	BPC			...
18011138-5125594	48.1	M0	14.8	11.3	0.07	-9.8 ± 5.2	-84.5 ± 5.1	BPC			...
18420483-5554126	51.9	M4	15.1	9.9	0.20	13.4 ± 3.5	-73.9 ± 3.7	BPC	H <sub>α</sub> , X, CaH, UV	1, 5	Y
18480637-6213470	52.4	F6	7.3	6.1	1.26	16.1 ± 2.0	-80.3 ± 2.0	BPC	Li, RV	8	Y
18580464-2953320	82.6	M3	12.8	8.8	0.75	15.4 ± 2.4	-45.6 ± 2.4	BPC	RV	8	Y
19223409-5429181	48.3	M0	14.0	10.7	0.10	32.0 ± 2.4	-87.8 ± 2.5	BPC			...
20085122-2740536	48.0	M3	16.3	11.8	0.05	40.4 ± 4.0	-61.7 ± 4.0	BPC			...
20321797-2600432	48.3	M5	18.6	13.0	0.01	50.0 ± 4.9	-70.1 ± 4.9	BPC			...
21100461-1920302	32.6	M4	13.1	7.6	0.47	87.0 ± 1.4	-94.4 ± 3.1	BPC	RV, UV	5, 9	Y
21212446-6654573	30.2	G9	9.0	6.4	0.84	90.5 ± 1.0	-90.9 ± 1.6	BPC	X, RV	5, 17	Y?
02590322-4232450	103.3	M3	15.0	10.3	0.52	41.1 ± 2.3	0.0 ± 1.5	CAR	UV	5	Y
03074909-2750467	54.6	M4	12.5	10.2	0.24	59.6 ± 5.3	-16.4 ± 17.6	CAR	RV	5	Y
08371456-5517343	180.8	K9	13.9	10.3	0.79	-7.9 ± 1.8	9.7 ± 1.9	CAR	H <sub>α</sub> , RV	5	N
09594633-7227360	83.6	M2	15.8	12.0	0.13	-37.4 ± 3.4	23.0 ± 3.4	CAR			...
01525509-5222266	83.4	M1	17.0	12.4	0.09	52.6 ± 7.0	-7.5 ± 7.0	COL			...
02005969-1608428	80.9	M4	18.0	13.9	0.04	51.1 ± 4.9	-25.0 ± 4.9	COL			...
02015050-1614575	80.9	M2	16.7	13.7	0.04	50.0 ± 3.8	-30.6 ± 3.8	COL			...
03212872-1048588	128.1	M3	...	13.7	0.08	24.7 ± 4.0	-28.2 ± 4.0	COL			...
03255277-3601161	107.5	M4	15.4	10.6	0.47	33.9 ± 2.8	-4.1 ± 2.8	COL			...
03281095+0409075	81.5	F6	8.8	7.2	1.26	46.7 ± 0.7	-37.0 ± 0.8	COL	RV, Li	5	Y
03400260+5441003	35.4	M5	17.7	12.0	0.04	102.0 ± 4.0	-109.2 ± 4.0	COL			...
03471077+5138276	57.5	M2	15.6	11.8	0.09	60.1 ± 3.7	-67.5 ± 3.8	COL			...
04423261+0905471	105.6	M3	15.8	11.0	0.37	31.7 ± 3.9	-41.3 ± 3.9	COL			...
04515223-4640497	68.1	K6	14.3	11.7	0.13	27.7 ± 2.5	17.1 ± 2.6	COL	H <sub>α</sub> , RV	5	N
05005830-4100023	76.3	M4	14.7	9.6	0.54	32.6 ± 1.5	9.6 ± 2.8	COL			...
05301939-1916161	115.1	K2	...	9.1	0.86	17.8 ± 3.1	-0.6 ± 2.3	COL			...
05374880+0233088	70.8	M3	14.2	9.5	0.52	16.8 ± 3.7	-44.6 ± 4.0	COL			...
09151348-7605020	117.5	K2	9.4	6.9	1.17	-31.2 ± 1.0	23.3 ± 1.0	ECH			...
12201867-7417202	114.8	M0	15.0	11.6	0.07	-39.5 ± 3.1	7.7 ± 3.0	ECH			...



2MASS identifier	Dist. <sup>(a)</sup> (pc)	SpT	V (mag.)	K (mag.)	Mass (M <sub>⊙</sub> )	μ <sub>α,*</sub> (mas/yr)	μ <sub>δ</sub> (mas/yr)	Ass.	Quantity <sup>(b)</sup>	Ref.	Mem? <sup>(c)</sup>
02174439+3330409	34.5	M3	16.3	11.8	0.05	44.8 ± 4.1	-52.5 ± 4.1	OCT			...
06251922-6630435	126.1	M2	16.4	12.1	0.22	-13.0 ± 3.8	25.4 ± 3.3	OCT			...
17420077-8608464	132.0	K5	12.9	9.6	0.80	9.2 ± 1.2	-25.5 ± 1.2	OCT			...
23315208+1956142	6.1	M4	10.3	5.3	0.26	543.2 ± 1.6	-44.6 ± 1.6	OCT	H <sub>α</sub> , RV, CaH, X	5, 10, 14	Y
00230961-6139143	44.6	M3	16.7	12.2	0.04	79.8 ± 2.7	-49.3 ± 2.6	THA			...
00302572-6236015	42.5	M4	12.2	7.5	0.71	95.2 ± 0.9	-48.0 ± 0.9	THA	Li, H <sub>α</sub> , RV	11	Y
02455260+0529240	54.3	M1	13.4	9.2	0.41	71.9 ± 2.9	-41.5 ± 3.0	THA	RV, UV	5	N
03153814-0339004	49.2	M3	16.8	12.1	0.05	65.4 ± 4.2	-47.4 ± 4.2	THA			...
03365153-4957314	43.3	K5	12.4	9.8	0.20	124.5 ± 2.2	-75.7 ± 2.1	THA			...
03484041-3738198	50.7	M2	13.3	8.7	0.51	79.0 ± 1.1	-4.5 ± 1.1	THA	X, RV	5, 12	Y
04354718-1210374	62.3	M3	...	12.0	0.08	58.0 ± 4.8	-26.4 ± 4.2	THA			...
04485254-5043145	54.8	M3	16.9	12.2	0.06	43.6 ± 5.3	19.0 ± 5.0	THA			...
05154763-0931041	77.5	M5	17.8	14.0	0.03	39.5 ± 5.6	-8.0 ± 5.6	THA			...
06350229-6951519	68.4	K2	11.9	8.6	0.72	21.8 ± 1.5	41.6 ± 1.4	THA	RV	9	Y
11020983-3430355	51.0	M8	21.2	11.9	0.02	-77.0 ± 9.5	-19.5 ± 9.5	TWA	H <sub>α</sub> , CaH	13	Y
11130416-4516056	96.2	M0	15.7	11.7	0.08	-41.0 ± 3.2	4.0 ± 3.0	TWA	Fl	5	...
12073145-3310222	53.8	K9	14.5	11.0	0.06	-62.7 ± 1.8	-32.3 ± 1.4	TWA	Fl	5	...
12090628-3247453	53.8	M1	16.1	12.0	0.02	-68.1 ± 2.0	-40.2 ± 2.7	TWA			...
12354893-3950245	73.0	M5	12.1	8.9	0.42	-48.6 ± 1.7	-21.3 ± 1.6	TWA	X	5	Y

**Notes.** <sup>(a)</sup> Distance taken from the bonafide member that the target is associated with. <sup>(b)</sup> Optical flaring from Catalina photometry (Fl) is not used to assess the membership of targets. <sup>(c)</sup> Based on quantities listed in column *Quantity*: consistent radial velocity (RV), H<sub>α</sub> EW (H<sub>α</sub>), Li absorption (Li), X-ray emission (X), UV/IR photometric criteria discussed in Section 6.3: UV, CaH indices (CaH). Those systems with either a flag of "Y" or "N" are discussed in Appendix A.

**References.** 1: Riaz et al. (2006), 2: Rodriguez et al. (2013), 3: Kharchenko et al. (2007), 4: Shkolnik et al. (2012), 5: This work, 6: Desidera et al. (2015), 7: Schlieder et al. (2012b), 8: Moór et al. (2013), 9: Kordopatis et al. (2013), 10: Morin et al. (2008), 11: Kraus et al. (2014), 12: Hoffleit & Jaschek (1991), 13: Kordopatis et al. (2013), 13: Scholz et al. (2005), 14: Lépine et al. (2013), 15: Delorme et al. (2012), 16: Gontcharov (2006), 17: Torres et al. (2006)

Rodríguez et al. (2011) combined near-IR photometry with UV emission to identify young, late-type (M0-M5) stars in Upper Scorpius and TW Hydrae. The dotted-line box in Figure 6 shows the criteria imposed Rodríguez et al. (2013) to identify new members using NUV and infrared photometry. We plotted identified candidates and known members that have all the necessary photometry (NUV,  $J$ ,  $W1$ , and  $W2$ ). The few identified targets that have photometry in all four bands are either compatible, i.e. candidate young M dwarfs within the boxed area, or consistent with previous members of earlier spectral type. Additionally, three of the targets matching this criteria have X-ray detections. These sources have the largest  $L_x/L_{bol}$  values shown in Figure 7 (smaller than -3) for targets identified in this work. Objects matching the criteria are listed in Table 4. The success rate of this technique, as derived in Rodríguez et al. (2013), was  $\approx 75\%$ .

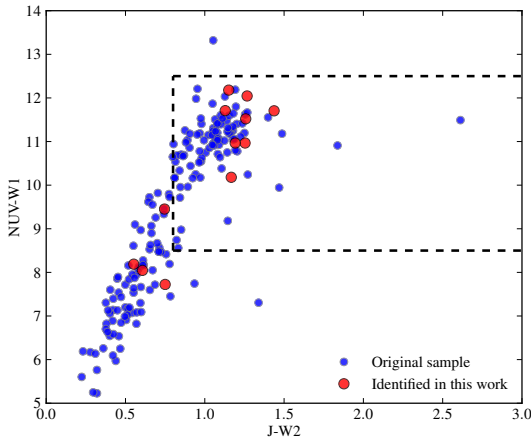


**Fig. 6.** Colour-colour diagram for  $J$ - $W2$ ,  $NUV$ - $W2$  for new (red) and known (blue) members of the moving groups. The boxed area represents the criteria described in Rodríguez et al. (2013) used to classify potential young M dwarfs.

#### 6.4. X-ray sources

The original SACY sample was constructed from optical counterparts to X-ray bright sources from the ROSAT all-sky survey (BSC; Voges et al. 1999). We additionally queried the faint X-ray catalogue of ROSAT (FSC; Voges et al. 2000), the serendipitous source catalogue of XMM (3XMM; Xmm-Newton Survey Science Centre 2013) and the Chandra source catalogue (CSC; Evans et al. 2010).

##### 6.4.1. X-ray emission

3XMM is the most recent serendipitous source catalogue from pointed observed using XMM-Newton. Using Figure 8 of Watson et al. (2009) (2XMM catalogue) the lower limit of X-ray flux (0.2-2.0 keV) ranges between  $10^{-15}$  –  $10^{-14}$   $\text{erg cm}^{-2} \text{s}^{-1}$ , depending on the sky coverage. On average the XMM catalogue provides fluxes one order of magnitude fainter than ROSAT (Voges et al. 1999). We cross-matched our detections with 3XMM for sources within  $6''$ , and an upper search radius encompassed  $>99\%$  of positional uncertainties; see Figure 11 of Watson et al. (2009). We additionally searched the Chandra source catalogue (Evans et al. 2010) for sources within  $5''$  using

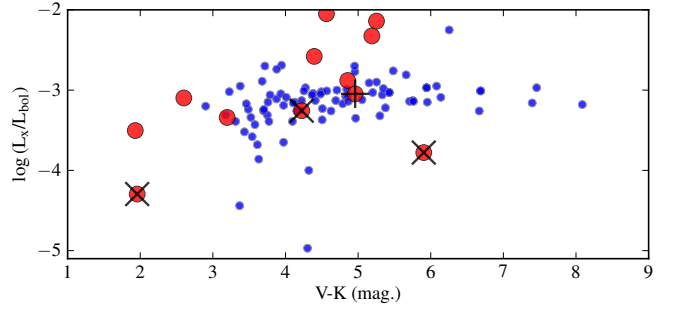


**Fig. 7.** V-K colour versus  $\log(L_x/L_{bol})$  for the original sample (blue) and for targets identified in this work (red). The crosses represent targets identified as close ( $<0.3''$ ) binaries; the luminosities are not corrected for unresolved components. The plus symbols represent sources with a variability flag in the 3XMM catalogue.

the CSCview<sup>2</sup> programme to access data in the 0.2-2.0 keV energy regime. Our search yielded five sources with X-ray data (3: XMM, 1: FSC, 3: BSC, 1: CSC).

In the case of ROSAT data we converted the count rate and hardness-ratio (HR1) to X-ray flux using the formulation of Fleming et al. (1995); these values are for energies in the range 0.1-2.4 keV. For CSC and XMM data the fluxes are available directly in the catalogues, and we used the energies in the range 0.2-2.0 keV to calculate total fluxes for an approximately equal comparison to fluxes derived from ROSAT data. We converted the fluxes to luminosities assuming the distance to the target was that of its associated known member.

We calculated bolometric luminosities of our targets using the VOSA tool (Bayo et al. 2008), which collates multi-band photometry from many reliable catalogues and fits both evolutionary models and black-body curves. The values were calculated based on best-fit atmospheric models (Allard et al. 2012) using available photometry and are listed in Table E. For the nine members identified in this work with available X-ray data, we calculated the X-ray to bolometric luminosity ratio ( $L_x/L_{bol}$ ). Three additional sources had a previously calculated values from Riaz et al. (2006) and Rodríguez et al. (2013), which we also used. The results are presented in Figure 7.

Typical values for young ( $<100$  Myr) sources are  $10^{-5}$  –  $10^{-3}$  with saturation at  $\approx 10^{-3}$  (Riaz et al. 2006; Zuckerman et al. 2004). One source (GJ 3305 AB) was identified previously as an X-ray bright, wide component ( $66''$ ) to HD 29391 by Feigelson et al. (2006). The ratio we calculate in this work is in agreement with that derived previously.

Ten of the 12 sources are clearly consistent as they have ratios of -3.5 or lower. The target at (5.9, -4.3) is a proposed member of AB Doradus (2MASS J23485048-2807157); given its colour and age (estimates range from 100-145 Myr for the moving group) this target is still not ruled out as a young source from analysis of its X-ray emission (see Figure 4 of Zuckerman et al. (2004)). Additionally it has strong lithium absorption and consistent radial velocity with its associated primary. The remaining source (2MASS J05195327+0617258, at 2.0, -3.8) has a very low estimated mass ( $0.05 M_{\odot}$ ) and is a proposed member of the  $\beta$ -Pic moving group. We did not find any additional

<sup>2</sup> <http://cda.cfa.harvard.edu/cscview/>

information on this object, however its calculated ratio is still consistent with being a young member.

#### 6.4.2. X-ray non-detections

Using the all sky ROSAT surveys (RASS; Voges et al. 1999, 2000) we also investigated non-detections based on expected  $L_x/L_{\text{bol}}$  values for young sources. As shown in Figure 4 of Zuckerman et al. (2004), young sources with a  $B-V$  colour  $>0.7$  mag have  $L_x/L_{\text{bol}}$  values that are larger than  $-3.5$ . From our analysis (see Figure 7), we see the majority of sources also have values  $-3.5$  or larger. We used the bolometric luminosities calculated using VOSA (Bayo et al. 2008) for the 50 sources in the colour range  $B-V > 0.7$  mag, to calculate expected X-ray fluxes ( $f_x = L_{\text{bol}} \times 10^{-3.5/4\pi D^2}$ ) based on this ratio. The detection limit of RASS is  $\approx 2 \times 10^{-13}$  erg s $^{-1}$  (Schmitt et al. 1995), 44/50 targets had predicted fluxes below this limit. For the six sources with apparent non-detections we re-queried the RASS catalogues, extending the search radius beyond the positional error. Two of the six had nearby detections that were extremely extended, causing the positional offset of the source to lie within the radius of the detection, which could account for an apparent non-detection in this region. We do not use the further four non-detections as a further youth constraint of the objects as one cannot be certain if these are reliable non-detections from the catalogue data. For reference, the BSC catalogue has sky coverage of 92% at a brightness limit of 0.1 cts s $^{-1}$  (Voges et al. 1999).

#### 6.5. Gravity-sensitive features

We were able to calculate Na I and KI EWs for 11 objects from our spectroscopic observations. Figure 8 shows the results for the EWs of KI for objects identified here and objects studied in Shkolnik et al. (2011), which focussed on identifying nearby ( $<25$  pc) young M dwarfs. We only show objects classified as M0 or later, the region where KI EWs distinguish between younger and older populations. All four objects have EWs consistent with youth, including the radial velocity-discrepant target 2MASS J02455260+0529240.

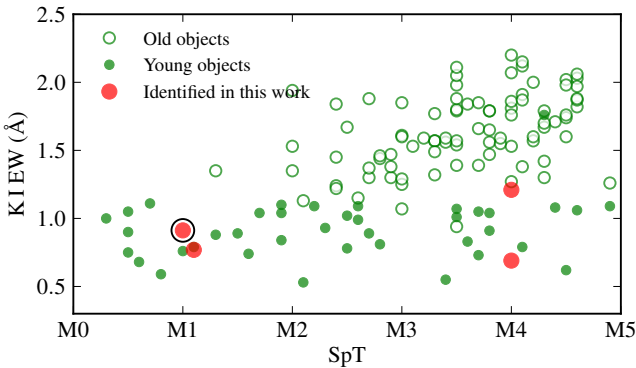


**Fig. 8.** Spectral type versus EW of KI. Green open and filled circles are for old and young objects from Shkolnik et al. (2011), respectively. Red filled circles are objects identified in this work. The black open circle represents the RV-discrepant target 2MASS J02455260+0529240.

Given the S/N and wavelength coverage of the available spectroscopic observations, we could only estimate EWs of Na I (8194.8 Å) for spectral types earlier than  $\approx M2$ . Slesnick et al. (2006) verified that the Na I strength saturates for spectral types earlier than M2. Additionally the work of Schlieder et al. (2012a) verified that this feature is only useful for colours  $V - K \geq 5$ . We therefore have not used this quantity in assessing the membership status of these objects. The values are listed in Table 3 for reference.

The visible spectra of M dwarfs are dominated by molecular bands (titanium oxide: TiO and calcium hydride: CaH). Mould (1976) showed that these bands are gravity-sensitive. Reid et al. (1995) defined a series of band indices, including CaH2 and CaH3, to quantify the strength of these bands. These indices measure the ratio of on-band to off-band flux. We were unable to calculate these spectral indices using our own high-resolution spectra owing to low S/N. However, we have collated values from other works the result of which are shown in Figure 9. The dotted and solid lines represent the lower envelopes of indices for BPC and ABD, respectively. There is a large amount of scatter for both indices ( $\approx 0.1$ ). However, all the objects identified in this work have consistent CaH2 and CaH3 indices by comparison with known members.

Figure 9 shows a comparison of CaH2 and CaH3 indices for the original sample and targets identified in this work. The dotted and solid lines represent the lower envelopes of indices for BPC and ABD, respectively. There is a large amount of scatter for both indices ( $\approx 0.1$ ). All the objects identified in this work have consistent CaH2 and CaH3 indices by a comparison with known members.

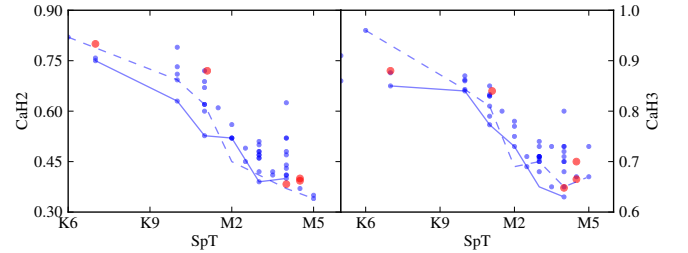


**Fig. 9.** Left panel: spectral type versus CaH2 index for the original sample (blue) and members identified in this work (red). Right panel: same as left, but for CaH3 index. The solid and dotted lines represent the lower envelopes of ABD and BPC, respectively.

#### 6.6. $H_\alpha$ emission

$H_\alpha$  emission can be used as an indication of youth, however, one has to keep in mind this feature can also be observed in older, main-sequence stars. Furthermore, the EW of  $H_\alpha$  is a function of the spectral type of the star at a given age, e.g. Stauffer et al. (1997). In Figure 10 we show the spectral type versus  $H_\alpha$  EW for the original sample and targets identified in this work. Additionally we show the lower envelope of EWs for the original sample of ABD and, similar to Figure 6 of Kraus et al. (2014), show the lower envelope derived in Stauffer et al. (1997) (for the young open clusters IC 2391 and IC 2602, 25-35 Myr). We have grouped the objects by age (ARG, CAR, COL, OCT, THA

all have age estimates  $\approx 30\text{--}40$  Myr and are, hence, plotted together). The envelopes act as an approximate lower boundary, as a function of age, to classify the object as having compatible  $H_\alpha$  properties.

There is one object (2MASS J01354915-0753470) that has a discrepant EW, it is discussed in more detail in Appendix A.

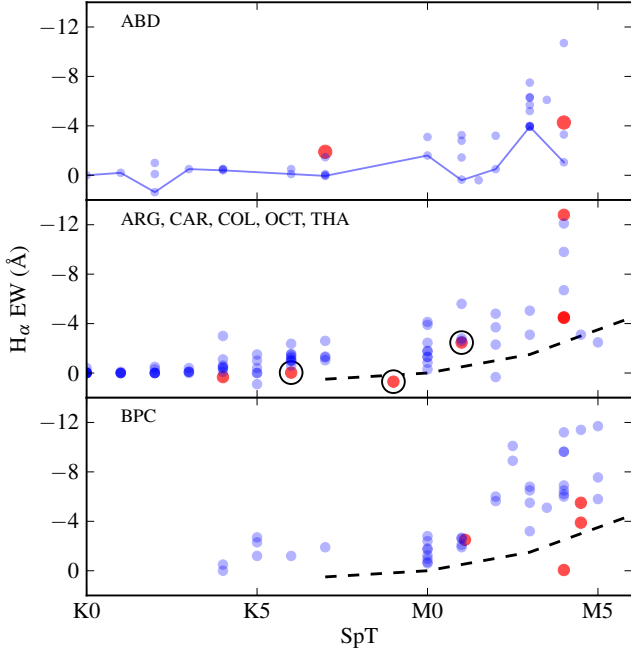


**Fig. 10.** Spectral type versus  $H_\alpha$  EW for the original sample (blue) and objects identified in this work (red). The black rings represent objects with discrepant radial velocities. The blue- and black-dotted lines are the lower envelopes of EWs for the original sample of ABD members and from [Stauffer et al. \(1997\)](#), respectively.

### 6.7. Lithium abundance

If the mass of PMS star is  $\approx 0.06 M_\odot$  or greater its core temperature eventually reaches  $\approx 3$  MK and burns lithium ([Chabrier et al. 1996](#)). The timescale to reach this temperature is mass dependent and once reached, the lithium is depleted rapidly as the mixing timescale is very short in convective stars.

The lithium depletion boundary (LDB) method is based on observing at which luminosity, for a given population, this lithium burning occurs. It is a very powerful technique to calculate the ages of young stars ([Soderblom et al. 2014](#)). One of its main advantages is that it is less model-dependent than other techniques ([Bildsten et al. 1997](#); [Jeffries & Naylor 2001](#)). Lithium EWs can also provide accurate relative ages by comparing the abundance between different groups of stars (see Figure 3 of [da Silva et al. 2009](#)). However, one must be cautious as even for young ages there is a large dispersion in the Li EWs that could be attributed to activity. [Bayo et al. \(2011\)](#) showed that measurements for the same object at different epochs and EWs between objects of the same spectral type can be significantly different.

In Figure 11 we plot the  $V\text{--}K$  colour of the target versus the EW of lithium for 10 detections and non-detections in total. Additionally we show the region of lithium depletion ( $\text{Li}/\text{Li}_0 \leq 0.1$ ) calculated using the evolutionary models of [Baraffe et al. \(2015\)](#).

There are two ways to classify targets as having consistent lithium measurements; one from the empirical abundances from known members, the other from a comparison to the evolutionary models. All of our detections and non-detections are consistent with the models and empirical abundances.

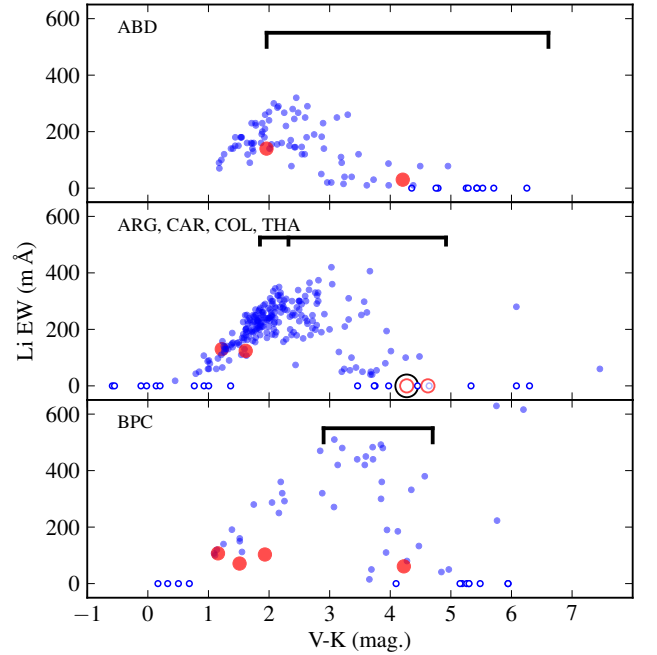


**Fig. 11.**  $V\text{--}K$  magnitude versus Li EW for original sample (blue) and targets identified in this work (red). Filled and open markers represent detections and non-detections, respectively. Black open circles represent sources classified as non-members (“N”) in Table 4. The black lines encompass regions of lithium depletion ( $\text{Li}/\text{Li}_0 \leq 0.1$ ) using the models of [Baraffe et al. \(2015\)](#). In the middle panel there are two minima corresponding to ages of 30 and 40 Myr.

### 6.8. Optical magnitudes

From our compilation of optical photometric values, it is clear that catalogue-catalogue variations in both  $V$  and  $R$  magnitude can be very significant ( $> 2$  mag.). If these magnitudes were used as a further mode of classification for our objects, we could be omitting viable candidates because of an apparent photometric mismatch, which is not necessarily associated with the sources membership status. These apparent variations in magnitudes could be induced by physical phenomena such as flaring ([Montes et al. 2005](#)) at the time of observation from blending of multiple sources or purely poor measurement accuracy. Additionally, optical magnitudes are not available for all of our targets (for example, 18 sources have no  $V$  mag., 35 sources have only one source of  $V$  mag.). Figure 12 demonstrates how the variation in apparent optical magnitudes translates into large un-

**Table 5.** Known members from our original sample that have been identified as wide companions to other known members.

ID	Dist. (pc)	(U, V, W) (kms <sup>-1</sup> )	Comps.
HD 104467	106.5	-11.6, -18.9, -10.2	SB
GSC 09420-00948	110.5	-11.6, -18.7, -10.3	
GSC 09239-01572	114.8	-11.5, -19.9, -8.2	0.3''
GSC 09239-01495	108.8	-10.9, -21, -8.6	
HD 21423	107.5	-13.0, -22.4, -5.2	
CD-36 1289	107.5	-13.7, -21.1, -5.8	
HD 21434	107.8	-12.2, -21.9, -5.7	0.2''
GJ 140	16.9	-24.3, -14, -6.5	3''
GJ 140 C	17.9	-24.1, -13.9, -5.2	
HD 199058	76.0	-6.2, -27.9, -13.3	0.5''
TYC 1090-543-1	76.4	-6.4, -27.2, -13.7	
TYC 112-1486-1	71.0	-13, -15.4, -8.2	0.4''
TYC 112-917-1	67.8	-13.2, -15.5, -8.5	
Eta Tel	47.7	-9.1, -15.5, -8.3	
HD 181327	50.6	-10.1, -16.4, -8.2	
HD 199143	45.7	-7.9, -13.9, -10.9	1.1''
AZ Cap	47.9	-10.1, -15, -9.5	2.2''
HD 217343	32.0	-2.9, -25.3, -14.2	
HD 217379	30.0	-3.8, -27.5, -14.5	1.9''+SB
HD 196982	9.5	-9.8, -15.8, -9.6	
AU Mic	9.8	-10.8, -16.6, -9.9	2.9''
UY Pic	23.9	-7.0, -28.1, -14.6	
CD-48 1893	24.2	-7.0, -28.2, -14.6	
TYC 9300-891-1	147.6	-12.0, -2.8, -9.5	1''
TYC 9300-529-1	147.0	-11.5, -3.7, -9.6	
BD-21 1074A	20.2	-11, -15.6, -9.4	
BD-21 1074B	16.6	-12.2, -15.3, -8.3	0.8''
HD 13246	44.2	-9.2, -20.3, -1.5	SB
CD-60 416	43.2	-9.0, -20.5, -0.8	

certainties in colour and absolute magnitude for existing and new members of the  $\beta$ -Pic moving group. Data points with no uncertainties only have one optical magnitude value. It is interesting to note that many of the identified members lie closer to the zero-age main sequence (ZAMS) than to their respective isochrone. This could be an indication that some of the identified targets in this work are from the older field population. Further spectroscopic observations will allow us to conclude whether these targets are young. Colour-magnitude diagrams of the remaining eight associations are shown in Appendix C.

As mentioned in Section 4.1 we checked all sources with Catalina photometry for any signs of optical flaring that could be associated with variable strong activity (Montes et al. 2005). We found 4 / 36 identified targets in this work, with Catalina photometry, showed significant flaring. We classify significant flaring as two or more observations with values three times the standard deviation of all data. None of these four objects have optical spectra to connect the photometric flare with strong, variable activity. For that reason, this quantity is not used to assess the membership of the target but, it is noted in Table 4.

## 6.9. Revised mass function of the young associations

As mentioned previously, the original works aiming to derive censuses of the young associations suffered from large incompleteness for masses  $<1 M_{\odot}$ . However, recent work has significantly improved members in this mass range.

Figure 13 shows the IMF, when considering all nine young associations as one overall population. This figure includes targets from the original sample, targets identified in this work (a pseudo-random sample of all 84 targets multiplied by the success rate), high-probability targets from Gagné et al. (2015) and consistent targets (based on RV,  $H_{\alpha}$  and/or Li) from Kraus et al. (2014). Although the work of Kraus et al. (2014) was only focussed on the Tucana-Horologium association, this work significantly increased the number of potential members from 62 to 191; therefore even in the context of all nine associations still makes a large difference to the IMF (see the log-scale of Figure 13).

The most considerable improvement from analysis presented here is for stars with masses  $\lesssim 0.5 M_{\odot}$ . We are sensitive to low-mass objects as our initial selection criteria is only based on 2MASS photometry and proper motions. Many other works, such as Rodriguez et al. (2013), use more extensive selection criteria, but at the cost of severely limiting the number of sources with photometry in multiple bands. This is highlighted by Figure 6, which shows only 13 of 84 sources (15%) had photometry in both GALEX and WISE.

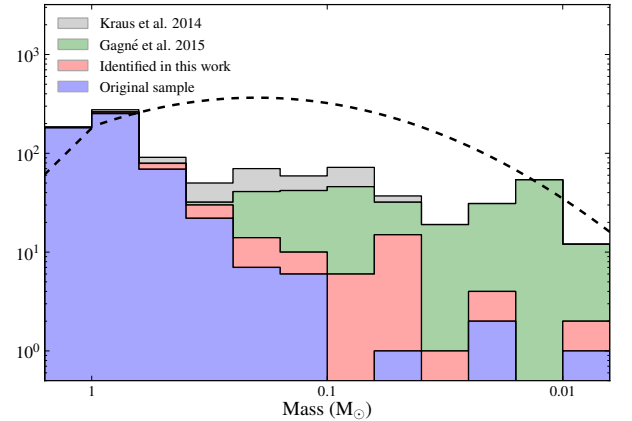


**Fig. 13.** Mass function of the nine young moving groups for objects identified in this analysis (red), Gagné et al. (2015) (green), Kraus et al. (2014) (grey) and the original sample (blue). A power law is fitted for masses  $> 1 M_{\odot}$  ( $\alpha=-2.35$ , Salpeter 1955) and a log-normal ( $\mu=0.2 M_{\odot}$ ,  $\sigma=0.6 \log(M_{\odot})$ ) for masses smaller than  $1 M_{\odot}$  (Chabrier 2003).

## 7. Conclusions

We have identified 84 targets (43:  $0.2-1.3 M_{\odot}$ , 16:  $0.08-0.2 M_{\odot}$ , 25:  $<0.08 M_{\odot}$ ) using our sample of 542 high-probability members. Thirty-three out of 84 sources have spectroscopic parameters either derived here or taken from previous works listed in Table 2. Of these 33 sources, four sources have inconsistent parameters and four have questionable parameters. We can therefore derive a success rate of  $\approx 76-88\%$  using this technique. Additionally only ten out of 33 have been identified in previous works concerned with young associations. Thanks to

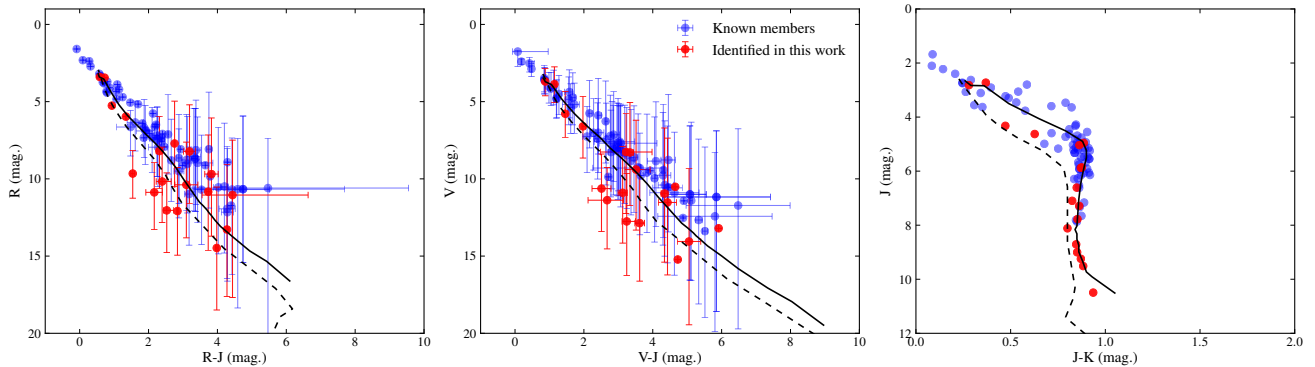


**Fig. 12.** *Left and middle panel:* colour-magnitude diagrams ( $R$ - $J$ ,  $R$ ) and ( $V$ - $J$ ,  $V$ ) for known (blue) and newly proposed (red) members of the  $\beta$ -Pic association. The uncertainties are derived using the upper and lower boundaries of the  $R$  and  $V$  magnitude values, respectively, compiled from our photometric search. In most cases those markers without uncertainties only have one magnitude value. *Right panel:* colour-magnitude diagram ( $J$ - $K$ ,  $J$ ) for known and newly proposed members. The solid and dotted line is the isochrone of Baraffe et al. (2015) using the age of the association and the zero-age main sequence (ZAMS), respectively.

the collation of numerous parameters, we were able to find and use existing additional information from mid- to high-resolution spectra and X-ray observations to successfully complement our photometric–proper motion search for new members. The targets with existing additional information, on which the success rate is derived, are generally brighter in magnitude (average in  $V$ : 12.2 mag. compared to 15.1 mag) and earlier spectral type (average K7 compared to M0) than those currently without further photometric and spectroscopic information. Therefore the derived success rate is only an approximation at this time and should be treated in that way. In the future we aim to take mid- to high-resolution spectra of all the targets identified in this work that currently have no spectroscopic information. With this approach, we can better assess the youth and kinematics of the objects.

As expected by our success rate so far, if many of these new members are confirmed they could have big implications for the formation and dynamical evolution of stars in loose associations. Our initial results are broadly consistent with the mechanism proposed by Reipurth & Mikkola (2012) whereby preferentially lower mass components in three-body systems are ejected from the stellar cores early on their lifetime. These components collectively form *unfolding* triple systems that are potentially in the process of disintegrating into unbound systems. The majority of these wide companions would therefore be associated with tight inner binaries (tightening of the inner binary from angular momentum exchange as the third body is ejected). An evaluation of this mechanism using the young associations will be explored in further work (Elliott et al. in prep.).

Regardless of whether these targets form wide multiple systems or not, if their youth is confirmed, they would make up an ideal sample for the characterisation of low-mass objects and the search for warm planets around nearby stars. New instruments such as SPHERE/VLT (Beuzit et al. 2008) and GPI/GEMINI (Macintosh et al. 2014) have been designed for the purpose of detecting and characterising planets using high-contrast imaging techniques. For a strehl ratio of  $\approx 70\%$  or better in the  $H$  band, the limiting magnitudes for SPHERE and GPI are  $R < 13$  mag and  $I < 10$  mag, respectively. From our sample of identified candidates in this work, 24 have  $R$  magnitudes brighter than the limit of SPHERE. Fifteen of these have been classified as members (denoted by “Y” in Table 4) based on further photometric and

spectroscopic quantities, and nine of these 15 are M-dwarfs. We have therefore, based on this initial work alone, identified crucial new targets to search for warm planets around nearby young stars.

*Acknowledgements.* PE would like to thank A. Tokovinin for a visit in August 2015 that significantly helped to improve the data management of this project, in part making the analysis presented here possible. PE is also grateful to I. Baraffe for a finer grid of models upon request. A. Bayo acknowledges financial support from the Proyecto Fondecyt de Iniciacin 11140572. D. Montes acknowledges financial support from the Spanish Ministerio de Economía y Competitividad under grants AYA2011-30147-C03-03 and AYA2014-54348-C3-3-R. This research has made use of the Washington Double Star catalogue maintained at the U.S. Naval Observatory, the Topcat tool (Taylor 2005), the SIMBAD database, and the VizieR catalogue access tool, CDS, Strasbourg, France (the original description of the VizieR service was published in A&AS143, 23) We have used Catalina (CSS) data in our analysis. The CSS survey is funded by the National Aeronautics and Space Administration under Grant No. NNG05GF22G issued through the Science Mission Directorate Near-Earth Objects Observations Program. The CRTS survey is supported by the U.S. National Science Foundation under grants AST-0909182 and AST-1313422. This publication makes use of VOSA, developed under the Spanish Virtual Observatory project supported from the Spanish MICINN through grant AyA2011-24052.

## References

- Allard, F., Homeier, D., & Freytag, B. 2012, Royal Society of London Philosophical Transactions Series A, 370, 2765
- Alonso-Floriano, F. J., Caballero, J. A., Cortés-Contreras, M., Solano, E., & Montes, D. 2015, A&A, 583, A85
- Andrews, S. M., Rosenfeld, K. A., Kraus, A. L., & Wilner, D. J. 2013, ApJ, 771, 129
- Bailey, III, J. I., White, R. J., Blake, C. H., et al. 2012, ApJ, 749, 16
- Baraffe, I., Homeier, D., Allard, F., & Chabrier, G. 2015, A&A, 577, A42
- Barentsen & et al. 2014, VizieR Online Data Catalog, 2321, 0
- Barrado y Navascués, D., Stauffer, J. R., Song, I., & Caillault, J.-P. 1999, ApJ, 520, L123
- Bayo, A., Barrado, D., Stauffer, J., et al. 2011, A&A, 536, A63
- Bayo, A., Rodrigo, C., Barrado y Navascués, D., et al. 2008, A&A, 492, 277
- Bell, C. P. M., Mamajek, E. E., & Naylor, T. 2015, MNRAS, 454, 593
- Beuzit, J.-L., Feldt, M., Dohlen, K., et al. 2008, in Society of Photo-Optical Instrumentation Engineers (SPIE) Conference Series, Vol. 7014, Ground-based and Airborne Instrumentation for Astronomy II, 701418
- Bianchi, L., Herald, J., Efremova, B., et al. 2011, Ap&SS, 335, 161
- Bildsten, L., Brown, E. F., Matzner, C. D., & Ushomirsky, G. 1997, ApJ, 482, 442
- Binks, A. S. & Jeffries, R. D. 2014, MNRAS, 438, L11
- Binks, A. S. & Jeffries, R. D. 2016, MNRAS, 455, 3345
- Bonnefoy, M., Chauvin, G., Dumas, C., et al. 2009, A&A, 506, 799
- Bowler, B. P., Liu, M. C., Shkolnik, E. L., & Dupuy, T. J. 2013, ApJ, 774, 55

- Caballero, J. A. 2009, *A&A*, 507, 251  
 Caballero, J. A. 2010, *A&A*, 514, A98  
 Chabrier, G. 2003, *PASP*, 115, 763  
 Chabrier, G., Baraffe, I., & Plez, B. 1996, *ApJ*, 459, L91  
 Chauvin, G., Vigan, A., Bonnefoy, M., et al. 2015, *A&A*, 573, A127  
 Cutri, R. M., Skrutskie, M. F., van Dyk, S., et al. 2003, *VizieR Online Data Catalog*, 2246, 0  
 da Silva, L., Torres, C. A. O., de La Reza, R., et al. 2009, *A&A*, 508, 833  
 de Bruijne, J. H. J. & Eilers, A.-C. 2012, *A&A*, 546, A61  
 de la Reza, R., Torres, C. A. O., Quast, G., Castilho, B. V., & Vieira, G. L. 1989, *ApJ*, 343, L61  
 Delorme, P., Lagrange, A. M., Chauvin, G., et al. 2012, *A&A*, 539, A72  
 Desidera, S., Covino, E., Messina, S., et al. 2015, *A&A*, 573, A126  
 Drake, A. J., Djorgovski, S. G., Mahabal, A., et al. 2009, *ApJ*, 696, 870  
 Elliott, P., Bayo, A., Melo, C. H. F., et al. 2014, *A&A*, 568, A26  
 Elliott, P., Huélamo, N., Bouy, H., et al. 2015, *A&A*, 580, A88  
 ESA, ed. 1997, *ESA Special Publication*, Vol. 1200, *The HIPPARCOS and TYCHO catalogues. Astrometric and photometric star catalogues derived from the ESA HIPPARCOS Space Astrometry Mission*  
 Evans, I. N., Primini, F. A., Glotfelty, K. J., et al. 2010, *ApJS*, 189, 37  
 Feigelson, E. D., Lawson, W. A., Stark, M., Townsley, L., & Garmire, G. P. 2006, *ApJ*, 131, 1730  
 Fleming, T. A., Molendi, S., Maccacaro, T., & Wolter, A. 1995, *ApJS*, 99, 701  
 Frith, J., Pinfield, D. J., Jones, H. R. A., et al. 2013, *MNRAS*, 435, 2161  
 Gagné, J., Faherty, J. K., Cruz, K. L., et al. 2015, *ApJS*, 219, 33  
 Girard, T. M., van Altena, W. F., Zacharias, N., et al. 2011, *AJ*, 142, 15  
 Gontcharov, G. A. 2006, *Astronomical and Astrophysical Transactions*, 25, 145  
 Gray, R. O., Corbally, C. J., Garrison, R. F., et al. 2006, *AJ*, 132, 161  
 Hoffleit, D. & Jaschek, C. 1991, *The Bright star catalogue*  
 Høg, E., Fabricius, C., Makarov, V. V., et al. 2000, *A&A*, 355, L27  
 Jeffries, R. D. & Naylor, T. 2001, in *Astronomical Society of the Pacific Conference Series*, Vol. 243, *From Darkness to Light: Origin and Evolution of Young Stellar Clusters*, ed. T. Montmerle & P. André, 633  
 Jordán, A., Brahm, R., Bakos, G. Á., et al. 2014, *AJ*, 148, 29  
 Kastner, J. H., Sacco, G. G., Montez, R., et al. 2011, *ApJ*, 740, L17  
 Kastner, J. H., Thompson, E. A., Montez, R., et al. 2012, *ApJ*, 747, L23  
 Kharchenko, N. V., Piskunov, A. E., Schilbach, E., et al. 2009, *VizieR Online Data Catalog*, 350, 40681  
 Kharchenko, N. V., Scholz, R.-D., Piskunov, A. E., Röser, S., & Schilbach, E. 2007, *Astronomische Nachrichten*, 328, 889  
 Kordopatis, G., Gilmore, G., Steinmetz, M., et al. 2013, *AJ*, 146, 134  
 Kraus, A. L., Shkolnik, E. L., Allers, K. N., & Liu, M. C. 2014, *AJ*, 147, 146  
 Lasker, B. M., Lattanzi, M. G., McLean, B. J., et al. 2008, *AJ*, 136, 735  
 Lawson, W. A., Crause, L. A., Mamajek, E. E., & Feigelson, E. D. 2001, *MNRAS*, 321, 57  
 Lépine, S., Hilton, E. J., Mann, A. W., et al. 2013, *AJ*, 145, 102  
 Looper, D. L., Bochanski, J. J., Burgasser, A. J., et al. 2010, *AJ*, 140, 1486  
 López-Santiago, J., Montes, D., Crespo-Chacón, I., & Fernández-Figueroa, M. J. 2006, *ApJ*, 643, 1160  
 Macintosh, B., Graham, J. R., Ingraham, P., et al. 2014, *Proceedings of the National Academy of Science*, 111, 12661  
 Maldonado, J., Martínez-Arnáiz, R. M., Eiroa, C., Montes, D., & Montesinos, B. 2010, *A&A*, 521, A12  
 Malo, L., Artigau, É., Doyon, R., et al. 2014, *ApJ*, 788, 81  
 Malo, L., Doyon, R., Lafrenière, D., et al. 2013, *ApJ*, 762, 88  
 Mamajek, E. E. 2009, in *American Institute of Physics Conference Series*, Vol. 1158, *American Institute of Physics Conference Series*, ed. T. Usuda, M. Tamura, & M. Ishii, 3–10  
 Martin, E. L. 1997, *A&A*, 321, 492  
 Mason, B. D., Wycoff, G. L., Hartkopf, W. I., Douglass, G. G., & Worley, C. E. 2001, *AJ*, 122, 3466  
 McCarthy, K. & White, R. J. 2012, *AJ*, 143, 134  
 Mermilliod, J. C. 2006, *VizieR Online Data Catalog*, 2168, 0  
 Montes, D., López-Santiago, J., Crespo-Chacón, I., & Fernández-Figueroa, M. J. 2005, in *ESA Special Publication*, Vol. 560, *13th Cambridge Workshop on Cool Stars, Stellar Systems and the Sun*, ed. F. Favata, G. A. J. Hussain, & B. Battrick, 825  
 Montes, D., López-Santiago, J., Gálvez, M. C., et al. 2001, *MNRAS*, 328, 45  
 Montet, B. T., Bowler, B. P., Shkolnik, E. L., et al. 2015, *ApJ*, 813, L11  
 Moor, A., Szabó, G. M., Kiss, L. L., et al. 2013, *MNRAS*, 435, 1376  
 Morin, J., Donati, J.-F., Petit, P., et al. 2008, *MNRAS*, 390, 567  
 Mould, J. R. 1976, *ApJ*, 207, 535  
 Murphy, S. J. & Lawson, W. A. 2015, *MNRAS*, 447, 1267  
 Murphy, S. J., Lawson, W. A., & Bessell, M. S. 2013, *MNRAS*, 435, 1325  
 Nordström, B., Mayor, M., Andersen, J., et al. 2004, *A&A*, 418, 989  
 Pecaui, M. J. & Mamajek, E. E. 2013, *ApJS*, 208, 9  
 Perryman, M. A. C., Lindegren, L., Kovalevsky, J., et al. 1997, *A&A*, 323, L49  
 Pojmanski, G. 2002, *Acta Astron.*, 52, 397  
 Queloz, D. 1995, in *IAU Symposium*, Vol. 167, *New Developments in Array Technology and Applications*, ed. A. G. D. Philip, K. Janes, & A. R. Uppgren, 221  
 Raskin, G., van Winckel, H., Hensberge, H., et al. 2011, *A&A*, 526, A69  
 Reid, I. N., Hawley, S. L., & Gizis, J. E. 1995, *AJ*, 110, 1838  
 Reiners, A. & Basri, G. 2009, *ApJ*, 705, 1416  
 Reipurth, B. & Mikkola, S. 2012, *Nature*, 492, 221  
 Riaz, B., Gizis, J. E., & Harvin, J. 2006, *AJ*, 132, 866  
 Riedel, A. R., Finch, C. T., Henry, T. J., et al. 2014, *AJ*, 147, 85  
 Riviere-Marichalar, P., Elliott, P., Rebollido, I., et al. 2015, *A&A*, 584, A22  
 Rodriguez, D. R., Bessell, M. S., Zuckerman, B., & Kastner, J. H. 2011, *ApJ*, 727, 62  
 Rodriguez, D. R., Zuckerman, B., Kastner, J. H., et al. 2013, *ApJ*, 774, 101  
 Roeser, S., Demleitner, M., & Schilbach, E. 2010, *AJ*, 139, 2440  
 Salpeter, E. E. 1955, *ApJ*, 121, 161  
 Schlieder, J. E., Lépine, S., Rice, E., et al. 2012a, *AJ*, 143, 114  
 Schlieder, J. E., Lépine, S., & Simon, M. 2012b, *ApJ*, 144, 109  
 Schmitt, J. H. M. M., Fleming, T. A., & Giampapa, M. S. 1995, *ApJ*, 450, 392  
 Scholz, R.-D., McCaughrean, M. J., Zinnecker, H., & Lodieu, N. 2005, *A&A*, 430, L49  
 Schütz, O., Meeus, G., & Sterzik, M. F. 2005, *A&A*, 431, 165  
 Shkolnik, E. L., Anglada-Escudé, G., Liu, M. C., et al. 2012, *ApJ*, 758, 56  
 Shkolnik, E. L., Liu, M. C., Reid, I. N., Dupuy, T., & Weinberger, A. J. 2011, *ApJ*, 727, 6  
 Slesnick, C. L., Carpenter, J. M., & Hillenbrand, L. A. 2006, *AJ*, 131, 3016  
 Soderblom, D. R., Hillenbrand, L. A., Jeffries, R. D., Mamajek, E. E., & Naylor, T. 2014, *Protostars and Planets VI*, 219  
 Stauffer, J. R., Hartmann, L. W., Prosser, C. F., et al. 1997, *ApJ*, 479, 776  
 Taylor, M. B. 2005, in *Astronomical Society of the Pacific Conference Series*, Vol. 347, *Astronomical Data Analysis Software and Systems XIV*, ed. P. Shopbell, M. Britton, & R. Ebert, 29  
 Teixeira, R., Ducourant, C., Chauvin, G., et al. 2008, *A&A*, 489, 825  
 Torres, C. A. O., Quast, G. R., da Silva, L., et al. 2006, *A&A*, 460, 695  
 Torres, C. A. O., Quast, G. R., Melo, C. H. F., & Sterzik, M. F. 2008, *Young Nearby Loose Associations*, Vol. 2, 757  
 van Leeuwen, F. 2007, *A&A*, 474, 653  
 Vanderplas, J., Connolly, A., Ivezić, Ž., & Gray, A. 2012, in *Conference on Intelligent Data Understanding (CIDU)*, 47–54  
 Voges, W., Aschenbach, B., Boller, T., et al. 1999, *VizieR Online Data Catalog*, 9010  
 Voges, W., Aschenbach, B., Boller, T., et al. 2000, *VizieR Online Data Catalog*, 9029  
 Vyssotsky, A. N. 1956, *AJ*, 61, 201  
 Watson, M. G., Schröder, A. C., Fyfe, D., et al. 2009, *A&A*, 493, 339  
 Weintraub, D. A. 1990, *ApJS*, 74, 575  
 Wenger, M., Ochsenbein, F., Egret, D., et al. 2000, *A&AS*, 143, 9  
 Wright, E. L., Eisenhardt, P. R. M., Mainzer, A. K., et al. 2010, *AJ*, 140, 1868  
 Xmm-Newton Survey Science Centre, C. 2013, *VizieR Online Data Catalog*, 9044  
 Zacharias, N., Finch, C., Subasavage, J., et al. 2015, *VizieR Online Data Catalog*, 1329, 0  
 Zacharias, N., Finch, C. T., Girard, T. M., et al. 2012, *VizieR Online Data Catalog*, 1322, 0  
 Zacharias, N., Monet, D. G., Levine, S. E., et al. 2005, *VizieR Online Data Catalog*, 1297, 0  
 Zuckerman, B., Rhee, J. H., Song, I., & Bessell, M. S. 2011, *ApJ*, 732, 61  
 Zuckerman, B., Song, I., & Bessell, M. S. 2004, *ApJ*, 613, L65

## Appendix A: Notes on compatibility of individual sources

Identified targets with discrepant or dubious properties (denoted by either "N" or "Y?" in Table 4) are discussed below. We combine all available indicators of youth in the discussion to assess their potential membership. Uncertainties of radial velocity values quoted are  $1.0 \text{ km s}^{-1}$  in the case of measurements performed by the SACY team. This is not a measurement uncertainty but rather it is the average variation seen in single stars from using the CCF technique on optical spectra (see Elliott et al. 2014, for details).

*2MASS J02105345-4603513*: The radial velocity of this target with its associated known member are incompatible  $25.7 \pm 1$

and  $8.5 \pm 1 \text{ km s}^{-1}$ . However, the evidence that these two sources form a young wide binary is strong. It is identified as a multiple system in the WDS catalogue (ID: 02109-4604, observations 1977-2000), McCarthy & White (2012), and Rodriguez et al. (2013). However, because of the angular separation ( $21.5''$ ) there is no observable orbital motion on this timescale. The proper motion values match within 1 sigma (total proper motions:  $54.4 \pm 3.1$  and  $54.2 \pm 2.5 \text{ mas/yr}$ ) and additionally the photometry is compatible in  $V$ ,  $J$ ,  $H$  and  $K$ . 2MASS J02105345-4603513 also shows strong X-ray emission ( $L_x/L_{\text{bol}} = -2.88$ ) and UV excess. It is very likely that 2MASS J02105345-4603513 is a spectroscopic binary and the radial velocity value calculated by Rodriguez et al. (2013) is not the system velocity. For those reasons we conclude 2MASS J02105345-4603513 is a most likely a young source.

2MASS J12573935+3513194: The radial velocities of this target with its associated known member borderline agree ( $2-3\sigma$ ) within measurement uncertainties ( $-9.5 \pm 1.0$  and  $-5.7 \pm 0.5 \text{ km s}^{-1}$ ), however both components have been identified as spectroscopic binaries. The separation between the two components is relatively small ( $16.2''$ ) and the photometry matches well for  $V$ ,  $J$ ,  $H$ , and  $K$ . 2MASS J12573935+3513194 shows strong  $H_\alpha$  emission ( $-4.27$ ), indicating it is young. Additionally the proper motion of the components are both extremely high and agree within uncertainties (total proper motion:  $303.9 \pm 2.8$  and  $317.8 \pm 7.6 \text{ mas/yr}$ ).

2MASS J01334282-0701311: Initially identified as part of a triple system. The components have radial velocities  $-15 \pm 0.1$  (HR 448),  $11.4 \pm 0.2$  (2MASS J01334282-0701311) and  $12.2 \pm 1 \text{ km s}^{-1}$  (G 271-110), respectively. The lowest mass component (G 271-110) in this system is the original known member from Malo et al. (2014). The highest mass component (HR 448) is a well-documented target with extensive radial velocity coverage and therefore this discrepancy is unlikely to arise from variation induced by spectroscopic companion.

2MASS J21212446-6654573: There are two epochs of data for this target, however one radial velocity has huge uncertainties ( $-24.1 \pm 1$  and  $6.4 \pm 14.8 \text{ km s}^{-1}$ ). Torres et al. (2006) also noted this component as a potential spectroscopic binary. The proper motions do not agree within  $3\sigma$  however, the magnitudes of the values are very large,  $142.4 \pm 1.9$  and  $128.3 \pm 1.9 \text{ mas/yr}$ , respectively. The field of view is not crowded and positions of the targets are fully outside the Galactic plane (Galactic longitude and latitude:  $326.596$ ,  $-39.1878$ ) making a chance alignment improbable. The system is also identified as a multiple system (with no additional notes) in the WDS catalogue, with seven observations between 1835-2000. The photometry of both components matches very well in  $V$ ,  $J$ ,  $H$  and  $K$ .

2MASS J04515223-4640497: This target has a hugely discrepant radial velocity with its associated known member ( $51.2 \pm 1.0$  and  $23 \pm 1.0 \text{ km s}^{-1}$ ). It has small emission in  $H_\alpha$  (EW:  $-0.32 \text{ \AA}$ ). As a result of its discrepant radial velocity, this target is not classified as a potential member.

2MASS J08371456-5517343: This target has a hugely discrepant radial velocity with its associated known member ( $81.3 \pm 1.0$  and  $20.8 \pm 1.0 \text{ km s}^{-1}$ ) and low proper motion magnitude ( $12.5 \pm 2.6 \text{ mas/yr}$ ). It has absorption in  $H_\alpha$  therefore there is no evidence it is a young member.

2MASS J01354915-0753470: This target has consistent radial velocity ( $6.3 \pm 0.5$  and  $6.5 \pm 1.0 \text{ km s}^{-1}$ ) and very large and consistent proper motion ( $104.7 \pm 2.8$  and  $98.1 \pm 7.2$ ) with its associated known member, both agree within 1 sigma. The calculated K I EW is consistent with youth, however it does not show  $H_\alpha$  emission. Given its V-K colour this makes the youth of the object questionable.

2MASS J02455260+0529240: The calculated radial velocity is hugely discrepant with its associated known member ( $88.5$  and  $4.3 \text{ km s}^{-1}$ ) and there is no sign of a spectroscopic companion to account for such a discrepancy. The total proper motions are large and agree within 1 sigma ( $83.0 \pm 4.2$  and  $87.6 \pm 0.9 \text{ mas/yr}$ ). However, due to RV value, it is not considered as a potential member.

## Appendix B: Previously identified extremely wide companions

Below we present previous detections of potential wide binary systems in the young associations. We discuss whether these systems were recovered in the analysis presented here and the reasons for why or why not.

*T Cha* – 2MASS J11550485-7919108: This system was first identified in Kastner et al. (2012). In our analysis we did not recover the system as the H-K colour is incompatible ( $<0.03 \text{ mag}$ , beyond criterion, see Figure B.1). As discussed previously at the youngest ages ( $\approx 10 \text{ Myr}$ ) our technique is weaker as infrared excesses are more likely and therefore the companion is less likely to be classified as possibly physical. However, this effect is unlikely to induce any strong bias in our statistics. Kastner et al. (2012) show 2MASS J11550485-7919108 has a modest infrared excess ( $K-W3 \sim 0.8$ ) which is why it was not recovered here. The system is classified as a potential wide binary system because of the detailed analysis performed by Kastner et al. (2012), including  $H_\alpha$ , X-ray and lithium EW analysis, and the recent work of Montet et al. (2015).

*V4046 Sgr* – GSC 07396-00759: First identified in Kastner et al. (2011), this companion does have compatible photometry and kinematics using our method. However, many other sources in the field of view also match the criteria (see Figure B.2) and therefore our upper angular limit is set much smaller ( $10''$ ) than the angular separation of this candidate companion ( $2.82''$ ). It is also noteworthy that the kinematic distances are not compatible between the two sources  $76.9$  and  $95.1 \text{ pc}$ , respectively. Furthermore Kastner et al. (2011) argue that GSC 07396-00759 would itself have to be a spectroscopic multiple system (of approximately equal mass) to account for the discrepancy in magnitudes. However, spectroscopic analysis does not support this. From 3 separate epochs of data there is no evidence for a companion. The radial velocities are  $-5.7$ ,  $-5.0$  and  $-5.7 \text{ km s}^{-1}$  ( $\sigma = 0.3 \text{ km s}^{-1}$ ) from Torres et al. (2006) and this work, which is well below the criterion for multiplicity ( $\sigma > 3 \text{ km s}^{-1}$ ). For these reasons the system is not included in our statistics.

*TWA 1* – 2MASS J11020983-3430355: This system was first identified in Scholz et al. (2005). The system is also recovered here. Figure B.3 shows that 2MASS J11020983-3430355 is the only source with both compatible photometry and kinematics in the field of view. Furthermore the work of Scholz et al. (2005) used spectroscopic analysis to show the source is consistent with being a member of the TW Hydrae moving group. The



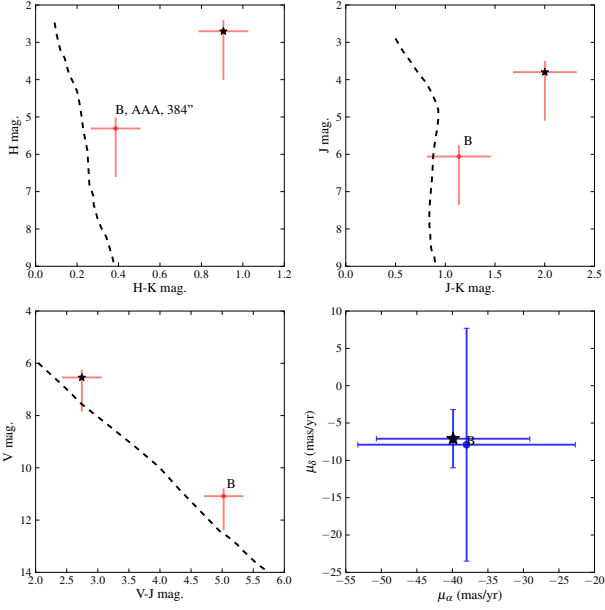


**Fig. B.1.** Photometric and kinematic summary of 2MASS J11550485-7919108.

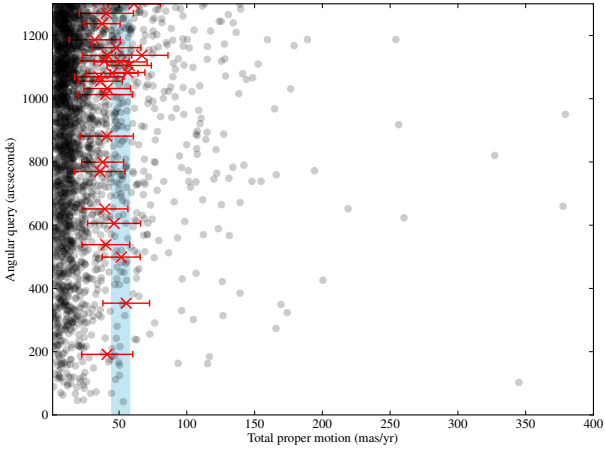


**Fig. B.2.** Considered field of view for V4046 Sgr. The markers are the same as in Figure 1

system is therefore included in our statistics.

*TWA 30 – 2MASS J11321822-3018316:* This system was first identified in [Looper et al. \(2010\)](#). The system was also recovered here, however, initially it was discarded due to the extremely large uncertainties on the proper motion (14.3 mas/yr). The work of [Looper et al. \(2010\)](#) produced much more accurate proper motion values (uncertainties 9 mas/yr) and a radial velocity value ( $12 \pm 3 \text{ km s}^{-1}$ ), showing its Galactic velocity is compatible with that of TWA 30 – (-10.2, -18.3, -4.9) compared with (-11.7, -19.7, -4.1) for TWA 30. Furthermore their spectroscopic analysis showed the source has features consistent with being a young object, member of the TW Hydrae moving group. For these reasons it is included in our statistics.

*51 Eri – 2MASS J04373746-0229282:* This system was first identified in [Feigelson et al. \(2006\)](#) and is also recovered in our analysis. The work of [Feigelson et al. \(2006\)](#) concludes that

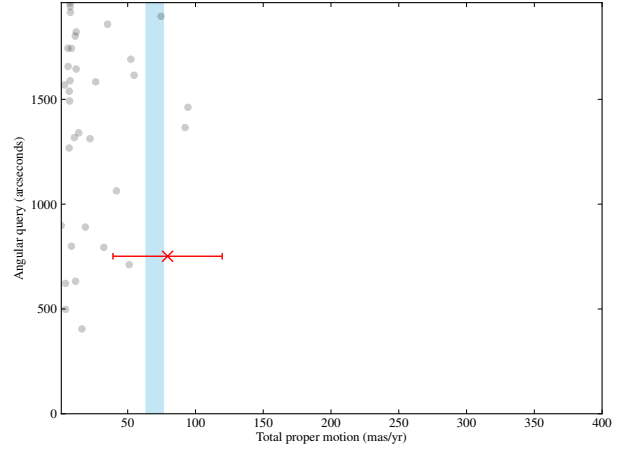


**Fig. B.3.** Considered field of view for TWA 1. The markers are the same as in Figure 1. 2MASS J11020983-3430355 is the only source with compatible proper motion.

these two objects are very likely a physical pair. In recent work [Montet et al. \(2015\)](#) calculated the system velocity of 2MASS J04373746-0229282, itself a close binary, as  $20.8 \pm 0.2 \text{ km s}^{-1}$ . The radial velocity of 51 Eri is  $21.0 \pm 1.2 \text{ km s}^{-1}$ , therefore the two components of the wide binary system are consistent.

### Appendix C: Colour-magnitude diagrams for new candidates

Below are colour-magnitude diagrams (in the same format as Figure 2) for the remaining eight associations.

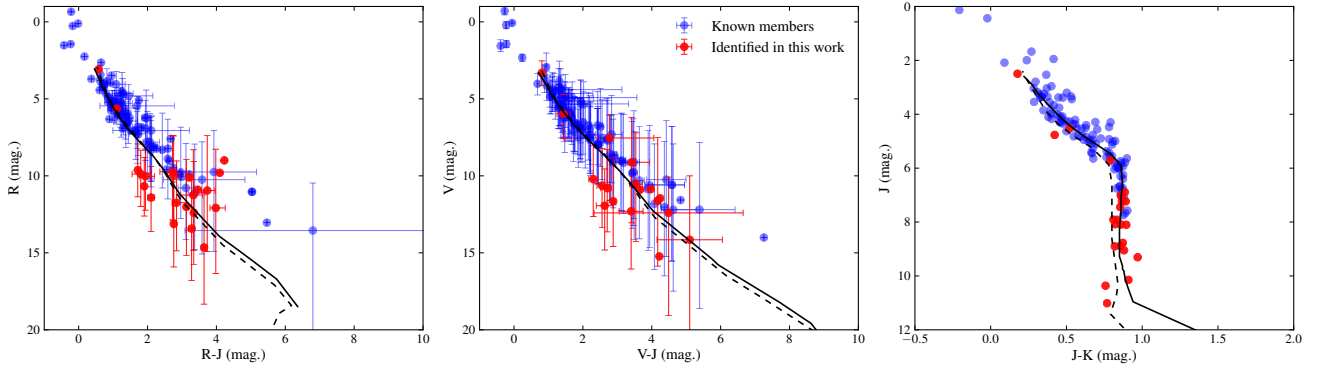


**Fig. C.1.** Colour-magnitude diagrams for the AB Doradus association

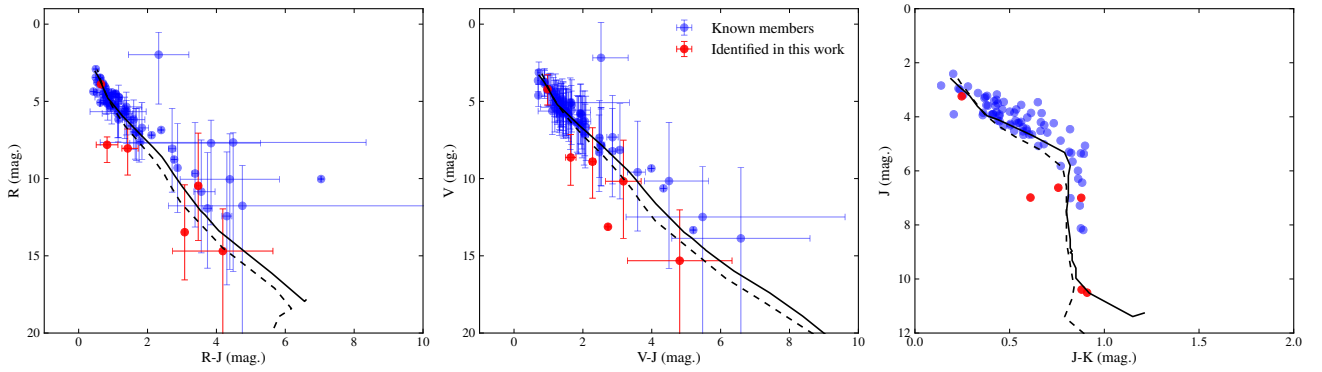


**Fig. C.2.** Colour-magnitude diagrams for the Argus association.

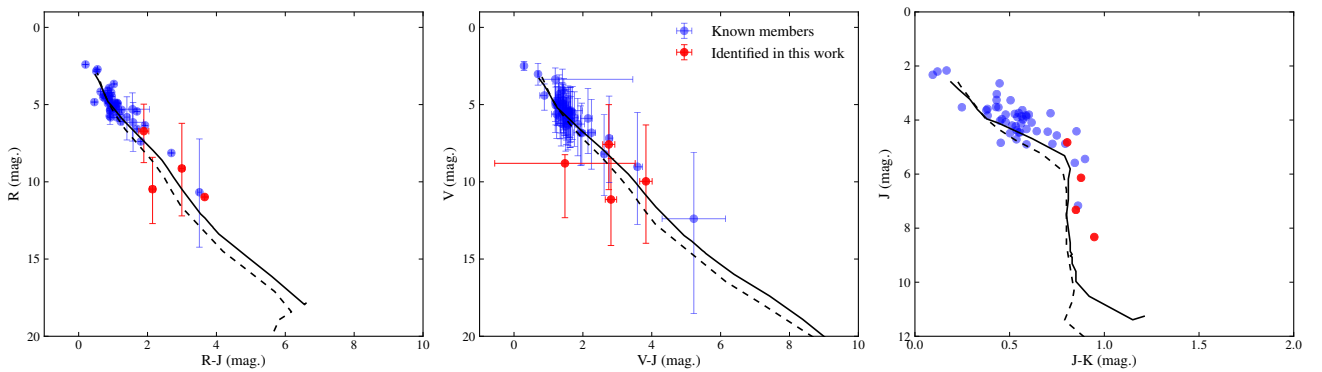


**Fig. C.3.** Colour-magnitude diagrams for the Carina association.

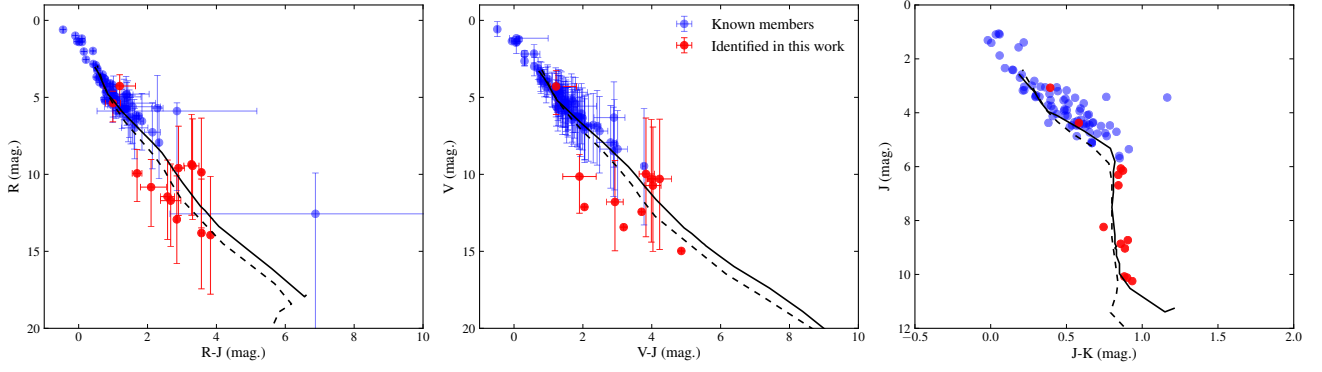


Fig. C.4. Colour-magnitude diagrams for the Columba association.

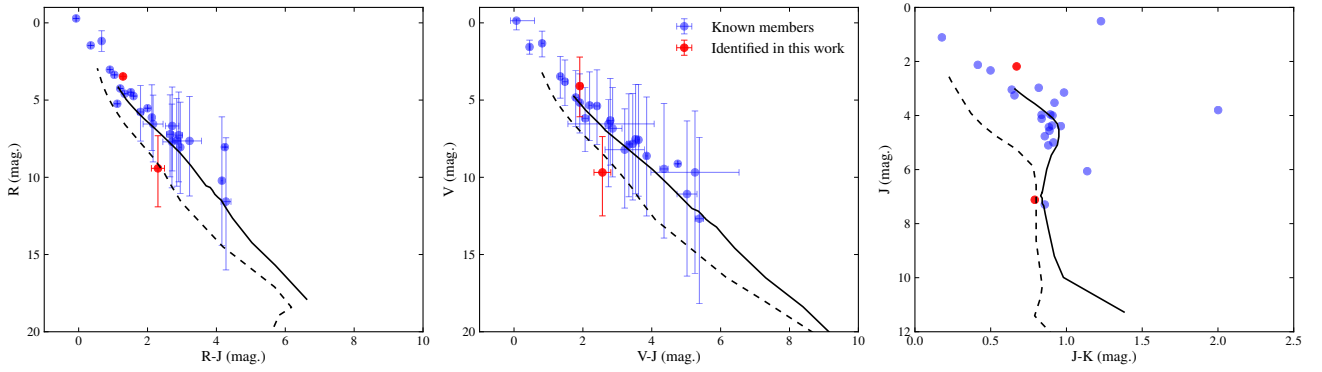


Fig. C.5. Colour-magnitude diagrams for the  $\epsilon$ -Cha association.

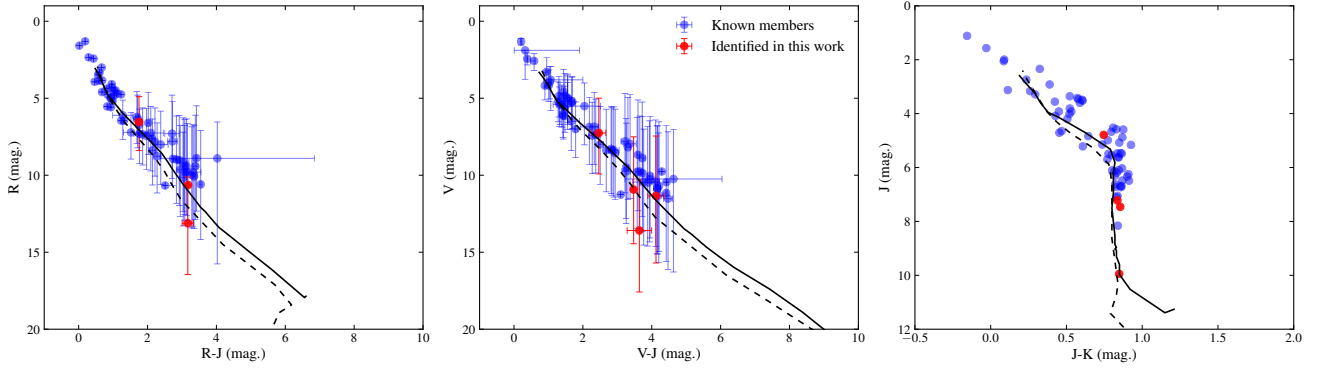
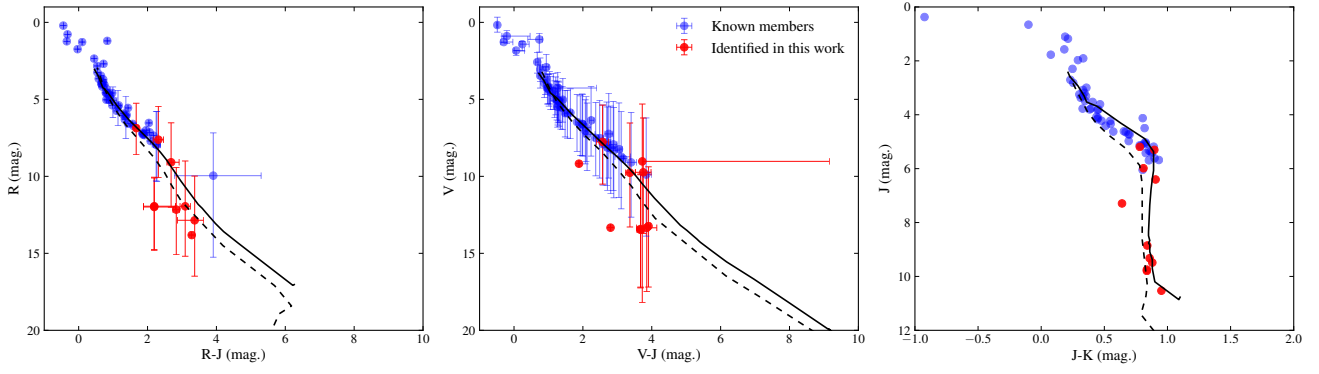
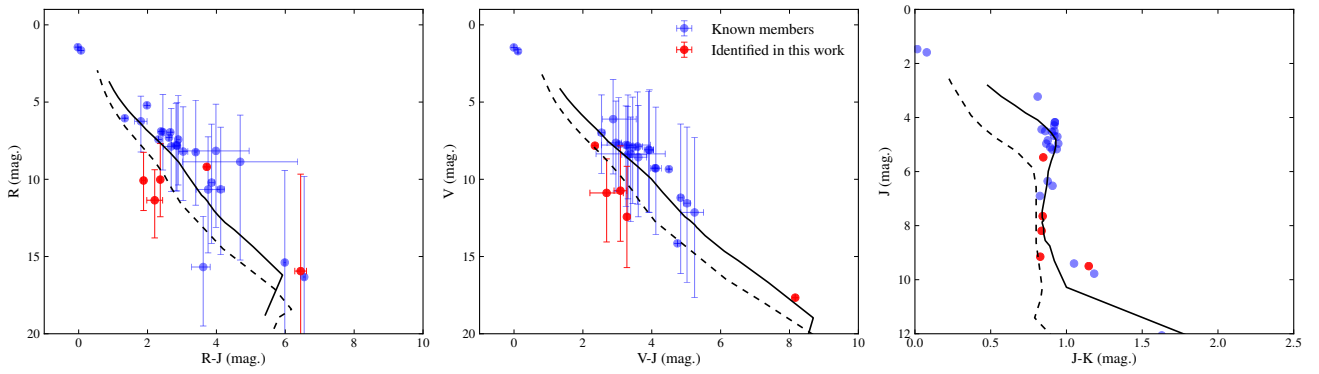


Fig. C.6. Colour-magnitude diagrams for the Octans association.

## Appendix D: Sample used in this work



**Fig. C.7.** Colour-magnitude diagrams for the Tucana-Horologium association.



**Fig. C.8.** Colour-magnitude diagrams for the TW Hydrae association.

**Table D.1.** Basic properties of the original sample used in this work.

ID	RA hh:mm:ss.s	DEC dd:mm:ss.s	Dist. (pc)	<i>J</i> (mag.)	<i>H</i> (mag.)	<i>K</i> (mag.)	$\mu_{\alpha,*}$ (mas/yr)	$\mu_{\delta}$ (mas/yr)	Mem ref.
ABD									
PW And	00:18:20.9	+30:57:22.0	27.3	7.0	6.5	6.4	144.4±1.0	-170.8±0.9	1
V493 And AB	00:34:8.4	+25:23:50.0	49.9	8.5	7.8	7.7	81.5±1.8	-97.6±1.1	3
HD 4277	00:45:50.9	+54:58:40.0	52.7 <sup>(a)</sup>	6.6	6.4	6.4	95.6±1.0	-76.9±1.0	1
HIP 4967	01:03:40.1	+40:51:29.0	29.6 <sup>(a)</sup>	8.1	7.5	7.3	126.7±0.7	-167.2±0.8	1
HD 6569	01:06:26.2	-14:17:47.0	47.4 <sup>(a)</sup>	7.9	7.4	7.3	99.8±1.6	-91.8±2.5	1
BD-12 243	01:20:32.3	-11:28:4.0	34.3 <sup>(a)</sup>	7.0	6.7	6.5	112.0±2.3	-137.7±1.3	1
HS Psc	01:37:23.2	+26:57:12.0	37.4	8.4	7.8	7.6	120.2±0.9	-126.5±1.4	3
CD-46 644	02:10:55.4	-46:03:59.0	73.7	9.3	8.8	8.6	53.3±2.5	-10.8±1.8	1, 5
HD 13482	02:12:15.4	+23:57:29.0	36.6 <sup>(a)</sup>	6.2	5.8	5.7	127.1±1.0	-160.4±1.0	1
HD 16760 b	02:42:21.0	+38:37:21.0	48.4 <sup>(a)</sup>	8.4	7.9	7.8	107.0±8.0	-102.8±8.0	1
HD 16760	02:42:21.3	+38:37:7.0	48.8 <sup>(a)</sup>	7.4	7.1	7.0	76.7±2.2	-108.3±2.3	1
HD 17332 b	02:47:27.2	+19:22:21.0	33.6 <sup>(a)</sup>	6.0	5.7	5.6	117.8±2.5	-160.3±2.5	1
HD 17332 a	02:47:27.4	+19:22:19.0	33.6 <sup>(a)</sup>	5.9	5.6	5.5	117.8±1.0	-160.3±1.0	1
HD 17573	02:49:59.0	+27:15:38.0	50.7 <sup>(a)</sup>	3.7	3.8	3.9	66.8±1.0	-116.5±1.0	1, 2
IS Eri	03:09:42.3	-09:34:47.0	37.4 <sup>(a)</sup>	7.2	6.8	6.7	88.8±1.3	-112.7±1.5	1
HW Cet	03:12:34.3	+09:44:57.0	57.5	8.6	8.1	8.0	60.8±0.8	-88.2±1.1	1
HD 20888	03:17:59.1	-66:55:37.0	54.9 <sup>(a)</sup>	5.8	5.8	5.7	57.3±1.0	13.6±1.0	1, 2
V577 Per	03:33:13.5	+46:15:27.0	34.3 <sup>(a)</sup>	6.8	6.5	6.4	61.8±9.9	-173.8±5.1	1
HIP 17695	03:47:23.3	-01:58:20.0	16.4 <sup>(a)</sup>	7.8	7.2	6.9	178.6±2.2	-278.2±3.1	1
HD 24681	03:55:20.4	-01:43:45.0	53.3	7.7	7.4	7.3	43.4±0.8	-90.7±1.1	1
HD 25457	04:02:36.7	-00:16:8.0	18.8 <sup>(a)</sup>	4.7	4.3	4.2	149.0±1.0	-253.0±1.0	1
HD 25953	04:06:41.5	+01:41:2.0	55.3 <sup>(a)</sup>	6.9	6.7	6.6	37.1±0.6	-94.4±0.8	1
2MASS J04141730-0906544	04:14:17.3	-09:06:54.4	23.8	9.6	9.1	8.8	95.1±5.0	-141.0±5.0	3
TYC 91-82-1	04:37:51.5	+05:03:8.0	87.6	9.2	8.8	8.6	20.8±0.9	-58.9±1.2	1
LP 776-25	04:52:24.4	-16:49:22.0	16.3	7.7	7.1	6.9	118.9±8.0	-211.9±8.0	1, 3
CD-56 1032 N	04:53:30.5	-55:51:32.0	11.1	7.8	7.2	6.9	88.2±42.5	85.8±12.6	1
CD-56 1032 S	04:53:31.2	-55:51:37.0	11.1 <sup>(a)</sup>	7.2	6.6	6.3	133.1±1.4	68.0±1.4	1
2MASS J04571728-0621564	04:57:17.3	-06:21:56.0	45.0	9.5	8.8	8.6	22.9±1.9	-99.1±2.5	3
HD 31652	04:57:22.3	-09:08:0.0	82.4	8.8	8.4	8.4	12.9±1.3	-50.8±1.6	1
CD-40 1701	05:02:30.4	-39:59:13.0	41.3	8.7	8.2	8.1	33.6±0.8	-21.9±0.8	1
HD 32981	05:06:27.7	-15:49:30.0	78.9	8.0	7.8	7.7	16.3±1.3	-44.0±1.6	1
HD 293857	05:11:9.7	-04:10:54.0	76.9	7.8	7.5	7.4	18.1±1.3	-57.6±2.2	1
HD 33999	05:12:35.8	-34:28:48.0	101.4	7.6	7.3	7.2	8.1±0.8	-16.8±1.2	1
HD 35650	05:24:30.2	-38:58:11.0	18.1 <sup>(a)</sup>	6.7	6.1	5.9	42.2±0.9	-57.0±1.1	1
NLTT 15049	05:25:41.7	-09:09:12.0	21.9	8.5	7.9	7.6	39.2±8.0	-188.4±8.0	3
HD 36705 b	05:28:44.4	-65:26:47.0	15.2	8.2	7.7	7.3	0.0±0.0	0.0±0.0	1
AB Dor	05:28:44.8	-65:26:55.0	15.2 <sup>(a)</sup>	5.3	4.8	4.7	33.2±1.0	150.8±1.0	1
UX Col	05:28:56.5	-33:28:16.0	54.1	8.4	7.9	7.8	10.5±0.7	-32.3±0.7	1
CD-30 2476	05:33:18.6	-30:33:27.0	132.9	10.4	10.1	9.9	0.1±1.0	-14.3±0.9	1
CD-34 2331	05:35:4.1	-34:17:52.0	80.5	9.8	9.2	9.1	5.8±0.8	-20.0±0.9	1
UY Pic	05:36:56.9	-47:57:53.0	25.2 <sup>(a)</sup>	6.4	5.9	5.8	25.3±1.0	0.0±1.0	1
WX Col	05:37:12.9	-42:42:56.0	76.4 <sup>(a)</sup>	8.1	7.7	7.7	-12.6±4.7	1.5±2.2	1
2MASS J05385663-0624410	05:38:56.6	-06:24:41.0	114.5	9.6	9.2	9.1	5.6±1.8	-37.3±1.4	1
CP-19 878	05:39:23.2	-19:33:29.0	70.2	8.7	8.2	8.1	4.5±1.6	-44.5±1.5	1
2MASS J05411433-4117585	05:41:14.3	-41:17:59.0	127.3	9.8	9.3	9.1	1.5±1.2	-6.4±1.4	1
CD-26 2425	05:44:13.4	-26:06:15.0	72.3	9.2	8.6	8.5	16.6±1.3	-27.8±1.5	1
HD 38497	05:45:41.3	-14:46:30.0	75.8	7.4	7.1	7.1	-0.1±1.6	-46.8±1.6	1
CD-41 2076	05:48:30.4	-41:27:30.0	65.3	9.2	8.5	8.4	0.6±1.3	-11.7±1.2	1
TZ Col	05:52:16.0	-28:39:25.0	81.3 <sup>(a)</sup>	7.9	7.6	7.5	3.3±0.9	-26.8±0.8	1
TY Col	05:57:50.8	-38:04:3.0	50.1	8.1	7.7	7.6	12.6±1.4	-16.9±1.1	1
BD-13 1328	06:02:21.9	-13:55:33.0	39.7	8.4	7.9	7.8	-8.3±1.0	-91.1±1.0	1
CD-34 2676	06:08:33.9	-34:02:55.0	77.5	8.7	8.3	8.2	3.7±0.8	-19.3±0.9	1
CD-35 2722	06:09:19.2	-35:49:31.0	25.0	7.9	7.3	7.0	-5.0±0.9	-55.1±0.9	1, 3
CD-35 2749	06:11:55.7	-35:29:13.0	59.8	8.8	8.3	8.2	-7.6±2.0	-20.7±1.0	1
HD 45270	06:22:30.9	-60:13:7.0	23.7 <sup>(a)</sup>	5.4	5.2	5.0	-11.3±1.0	64.2±1.0	1
GSC 08894-00426	06:25:56.1	-60:03:27.0	12.2	8.1	7.5	7.2	-23.5±1.5	110.5±1.4	1
AK Pic	06:38:0.4	-61:32:0.0	21.3 <sup>(a)</sup>	5.1	4.7	4.5	-50.1±1.0	72.7±1.0	1
CD-47 2500	06:38:45.5	-47:14:18.0	114.7	9.1	8.7	8.7	-4.4±0.8	0.7±1.4	1
CD-61 1439	06:39:50.0	-61:28:42.0	22.4 <sup>(a)</sup>	7.3	6.6	6.5	-23.8±1.0	77.8±1.8	1
2MASS J06411849-3820360	06:41:18.5	-38:20:36.0	64.7	9.5	8.9	8.8	-9.9±1.2	-16.5±1.0	1
CD-57 1654	07:10:50.6	-57:36:46.0	133.3	9.4	9.0	8.9	-7.7±0.9	7.9±0.8	1
V429 Gem	07:23:43.6	+20:24:59.0	25.7	7.6	7.0	6.9	-67.8±2.9	-231.1±3.5	1
HD 59169	07:26:17.7	-49:40:51.0	111.1 <sup>(a)</sup>	8.4	8.0	7.9	-24.7±6.0	-3.1±1.9	1
V372 Pup	07:28:51.4	-30:14:49.0	15.7 <sup>(a)</sup>	6.6	6.0	5.7	-130.9±8.0	-131.4±8.0	1
CD-84 80	07:30:59.5	-84:19:28.0	67.4	8.4	8.0	7.9	-11.6±1.3	55.1±1.0	1
HD 64982	07:45:35.6	-79:40:8.0	80.6 <sup>(a)</sup>	7.9	7.7	7.6	-11.5±2.0	65.2±7.0	1
HD 82879	09:28:21.1	-78:15:35.0	116.5	8.1	7.9	7.8	-25.8±1.0	18.0±1.4	1
CD-45 5772	10:07:25.2	-46:21:50.0	69.5	8.8	8.2	8.1	-50.1±1.3	-31.3±0.9	1

ID	RA hh:mm:ss.s	DEC dd:mm:ss.s	Dist. (pc)	$J$ (mag.)	$H$ (mag.)	$K$ (mag.)	$\mu_{\alpha,*}$ (mas/yr)	$\mu_{\delta}$ (mas/yr)	Mem ref.
2MASS J10121768-0344441	10:12:17.7	-03:44:44.1	7.9 <sup>(a)</sup>	5.9	5.3	5.0	-150.7±2.6	-241.4±3.3	3
BD+01 2447	10:28:55.5	+00:50:28.0	6.7	6.2	5.6	5.3	-602.3±8.0	-731.9±8.0	1
HD 99827	11:25:17.7	-84:57:16.0	88.5 <sup>(a)</sup>	6.7	6.6	6.5	-48.4±1.0	12.0±1.0	1
2MASS J11254754-4410267	11:25:47.5	-44:10:27.0	51.0	10.3	9.8	9.5	-83.9±2.6	-57.0±7.7	3
2MASS J12194808+5246450	12:19:48.1	+52:46:45.0	28.0 <sup>(a)</sup>	8.3	7.6	7.5	-171.4±1.0	-121.2±1.2	3
2MASS J12574030+3513306	12:57:40.3	+35:13:30.6	19.3 <sup>(a)</sup>	7.4	6.7	6.6	-264.0±1.9	-150.6±2.1	3
PX Vir	13:03:49.7	-05:09:43.0	21.7 <sup>(a)</sup>	6.1	5.7	5.5	-191.1±1.0	-218.7±1.0	1
L 264-18	15:24:48.5	-49:29:47.0	23.5	8.2	7.5	7.3	-120.8±8.0	-241.0±8.0	1
HD 139751	15:40:28.4	-18:41:46.0	36.4 <sup>(a)</sup>	7.7	7.1	6.9	-79.0±4.5	-157.3±1.6	1
HIP 81084	16:33:41.6	-09:33:12.0	30.3 <sup>(a)</sup>	8.4	7.8	7.5	-65.8±1.3	-179.4±1.4	1
HD 152555	16:54:8.1	-04:20:25.0	46.8 <sup>(a)</sup>	6.7	6.5	6.4	-37.2±1.1	-112.9±0.7	1
HD 159911	17:37:46.5	-13:14:47.0	46.3	7.6	7.0	6.8	-16.8±1.4	-124.9±1.6	1
HD 160934	17:38:39.6	+61:14:16.0	33.1 <sup>(a)</sup>	7.6	7.0	6.8	-19.2±0.7	46.7±0.7	1
HD 178085	19:10:57.9	-60:16:20.0	61.4 <sup>(a)</sup>	7.2	7.0	6.9	11.3±1.2	-98.6±1.2	1
HD 181869	19:23:53.2	-40:36:57.0	55.8 <sup>(a)</sup>	4.2	4.2	4.2	31.5±1.0	-120.3±1.0	1, 2
TYC 486-4943-1	19:33:3.8	+03:45:40.0	72.0	9.3	8.8	8.7	16.0±1.6	-66.2±1.5	1
BD-03 4778	20:04:49.4	-02:39:20.0	71.5	8.5	8.0	7.9	27.2±1.1	-72.1±1.9	1
2MASS J20465795-0259320	20:46:58.0	-02:59:32.0	47.5	9.1	8.4	8.3	53.0±2.5	-109.5±1.7	3
HD 199058	20:54:21.1	+09:02:24.0	76.0	7.4	7.0	7.0	35.3±1.0	-58.4±0.6	1
TYC 1090-543-1	20:54:28.0	+09:06:7.0	76.4	9.5	8.9	8.8	36.4±2.7	-57.3±1.8	1
HD 201919	21:13:5.3	-17:29:13.0	39.5	8.3	7.7	7.6	73.9±0.8	-144.4±0.8	1, 3
LO Peg	21:31:1.7	+23:20:7.0	24.8 <sup>(a)</sup>	7.1	6.5	6.4	134.4±0.8	-145.2±0.8	1
GJ 4231	21:52:10.4	+05:37:36.0	30.6 <sup>(a)</sup>	8.2	7.6	7.4	109.8±1.5	-150.0±2.0	1, 3
HD 209952	22:08:14.0	-46:57:40.0	31.0 <sup>(a)</sup>	2.0	2.0	2.0	126.7±1.0	-147.5±1.0	1, 2
HIP 110526a	22:23:29.1	+32:27:34.0	15.1 <sup>(a)</sup>	6.9	6.3	6.1	251.3±8.0	-207.6±8.0	1
HIP 110526b	22:23:29.1	+32:27:32.0	15.1	6.9	6.3	6.1	251.3±8.0	-207.6±8.0	1
HD 217343	23:00:19.3	-26:09:14.0	30.7 <sup>(a)</sup>	6.3	6.0	5.9	110.0±1.0	-160.1±1.0	1
HD 217379A	23:00:28.0	-26:18:43.0	32.7 <sup>(a)</sup>	7.0	6.4	6.3	113.6±8.0	-162.2±8.0	1
HIP 114066	23:06:4.8	+63:55:34.0	24.5 <sup>(a)</sup>	7.8	7.2	7.0	172.7±1.0	-57.8±1.4	1
HD 218860 S	23:11:52.1	-45:08:11.0	49.3 <sup>(a)</sup>	7.5	7.1	7.0	85.3±1.0	-93.3±1.0	1
HIP 115162	23:19:39.6	+42:15:10.0	50.2 <sup>(a)</sup>	7.6	7.3	7.2	78.4±0.5	-65.4±0.6	1
Kap Psc	23:26:56.0	+01:15:20.0	47.2 <sup>(a)</sup>	5.3	5.0	4.9	87.7±1.0	-95.5±1.0	1, 2
LTT 9582	23:32:0.2	-39:17:37.0	23.1	8.9	8.3	8.0	193.4±17.9	-178.4±17.9	3
HD 222575	23:41:54.3	-35:58:40.0	63.6 <sup>(a)</sup>	8.1	7.8	7.6	70.0±0.9	-66.3±1.0	1
HD 223552	23:48:55.5	-28:07:49.0	42.2 <sup>(a)</sup>	4.8	4.6	4.5	100.8±1.0	-105.3±1.0	1, 2
1RXS J235133.3+312720	23:51:33.7	+31:27:23.0	42.8	9.8	9.2	9.0	106.6±1.7	-87.9±3.8	3
HD 224228	23:56:10.7	-39:03:8.0	22.0 <sup>(a)</sup>	6.5	6.0	5.9	205.1±1.9	-186.5±2.1	1
ARG									
FT Psc	00:50:33.2	+24:49:0.0	28.8 <sup>(a)</sup>	8.0	7.3	7.1	198.0±5.1	-14.0±5.4	3
2MASS J03033668-2535329	03:03:36.7	-25:35:32.9	38.6 <sup>(a)</sup>	8.0	7.3	7.1	213.2±8.0	94.5±8.0	3
HIP 15844 a	03:24:6.5	+23:47:6.0	16.9 <sup>(a)</sup>	7.1	6.5	6.3	217.2±8.0	-129.2±8.0	1
HIP 15844 c	03:24:12.9	+23:46:19.0	17.9	8.3	7.7	7.5	199.0±8.0	-112.0±8.0	1
2MASS J04132663-0139211	04:13:26.6	-01:39:21.1	26.2	9.4	8.8	8.5	131.3±7.4	-9.5±3.0	3
CD-29 2360	05:34:59.2	-29:54:4.0	74.9	8.7	8.2	8.0	17.1±0.6	33.1±1.5	1
AP Col	06:04:52.2	-34:33:36.0	8.4	7.7	7.2	6.9	-118.9±5.9	-91.3±5.8	1
CD-56 1438	06:11:53.0	-56:19:5.0	118.6	9.8	9.3	9.2	-2.5±0.9	38.3±1.0	1
TYC 155-2167-1	06:41:9.3	+04:47:19.0	82.3	9.5	8.8	8.7	-7.9±2.2	-9.9±0.8	1
CD-28 3434	06:49:45.4	-28:59:17.0	120.8	9.1	8.7	8.6	-11.3±0.9	20.8±0.8	1
CD-42 2906	07:01:53.4	-42:27:56.0	101.0	9.2	8.7	8.6	-13.8±0.7	35.5±0.7	1
CD-48 2972	07:28:22.0	-49:08:38.0	82.8	8.5	8.1	8.1	-26.7±1.0	44.4±1.0	1
HD 61005	07:35:47.5	-32:12:14.0	35.3 <sup>(a)</sup>	6.9	6.6	6.5	-58.8±0.8	74.0±0.7	1
CD-48 3199	07:47:26.0	-49:02:51.0	103.9	9.3	8.9	8.8	-22.4±2.1	36.1±0.9	1
CD-43 3604	07:48:49.8	-43:27:6.0	86.5	8.9	8.3	8.2	-26.8±1.3	39.6±1.0	1
2MASS J07535548-5710073	07:53:55.5	-57:10:7.0	145.7	10.3	9.8	9.7	-18.3±1.2	26.9±1.0	1
HD 67945	08:09:38.6	-20:13:50.0	77.0	7.4	7.2	7.2	-37.8±1.3	20.4±1.5	1
PMM 5314	08:28:34.6	-52:37:4.0	142.7	9.7	9.6	9.5	-24.1±1.0	22.7±1.5	1
PMM 7422	08:28:45.6	-52:05:27.0	141.4	9.3	9.1	8.9	-22.6±1.0	24.6±0.9	1
PMM 7956	08:29:51.9	-51:40:40.0	157.7	9.8	9.4	9.2	-23.0±1.1	18.8±0.9	1
PMM 6974	08:34:18.1	-52:15:58.0	147.4	10.5	10.0	9.9	-22.6±2.0	23.0±0.9	1
PMM 4280	08:34:20.5	-52:50:5.0	154.8	9.2	8.9	8.8	-21.0±0.9	22.5±0.9	1
PMM 6978	08:35:1.2	-52:14:1.0	147.3	10.4	9.9	9.8	-23.3±0.9	22.3±0.9	1
PMM 2456	08:35:43.7	-53:21:20.0	141.1	10.3	9.7	9.6	-23.6±1.8	24.3±1.3	1
PMM 351	08:36:24.2	-54:01:6.0	149.2	9.2	8.9	8.8	-24.4±2.0	20.7±1.3	1
PMM 3359	08:36:55.0	-53:08:34.0	144.8	10.1	9.7	9.6	-23.1±0.9	23.6±1.0	1
PMM 5376	08:37:2.3	-52:46:59.0	161.9	11.4	10.7	10.5	-20.8±1.4	20.9±1.4	1
PMM 4324	08:37:47.0	-52:52:12.0	152.3	8.8	8.6	8.5	-22.4±1.0	22.0±1.0	1
PMM 665	08:37:51.6	-53:45:46.0	154.8	10.1	9.7	9.6	-21.1±1.2	22.7±1.7	1
PMM 4336	08:37:55.6	-52:57:11.0	141.0	9.9	9.4	9.3	-21.2±0.9	17.9±1.0	1
PMM 4362	08:38:22.9	-52:56:48.0	147.3	9.8	9.4	9.4	-23.5±0.9	22.4±0.8	1
PMM 4413	08:38:55.7	-52:57:52.0	154.2	9.1	8.8	8.7	-22.3±0.9	21.6±0.9	1

ID	RA hh:mm:ss.s	DEC dd:mm:ss.s	Dist. (pc)	<i>J</i> (mag.)	<i>H</i> (mag.)	<i>K</i> (mag.)	$\mu_{\alpha,*}$ (mas/yr)	$\mu_{\delta}$ (mas/yr)	Mem ref.
CD-58 2194	08:39:11.6	-58:34:28.0	102.2	8.9	8.5	8.4	-32.7±1.0	35.4±1.0	1
PMM 686	08:39:22.6	-53:55:6.0	158.1	10.6	10.0	9.9	-21.3±1.6	21.7±1.6	1
V364 Vel	08:39:53.0	-52:57:57.0	167.4	10.3	9.9	9.8	-21.1±1.0	19.3±1.0	1
V365 Vel	08:40:6.2	-53:38:7.0	155.5	9.3	9.0	8.9	-20.0±1.4	23.4±1.3	1
PMM 8415	08:40:16.3	-52:56:29.0	133.8	10.2	9.7	9.6	-25.7±1.2	24.9±1.1	1
PMM 1759	08:40:18.3	-53:30:29.0	141.8	11.1	10.4	10.2	-26.2±1.7	21.2±1.7	1
PMM 1142	08:40:49.1	-53:37:45.0	159.2	9.7	9.4	9.3	-18.4±1.2	23.6±1.2	1
PMM 1174	08:41:22.7	-53:38:9.0	146.8	8.7	8.5	8.5	-23.6±1.9	22.7±1.2	1
V368 Vel	08:41:57.8	-52:52:14.0	141.5	11.1	10.4	10.3	-24.0±1.2	23.9±1.3	1
PMM 756	08:43:0.4	-53:54:8.0	154.6	9.8	9.4	9.3	-23.5±1.1	20.4±1.1	1
PMM 5811	08:43:17.9	-52:36:11.0	157.9	8.4	8.3	8.2	-21.3±1.1	21.6±1.1	1
PMM 2888	08:43:52.3	-53:14:0.0	147.3	8.8	8.7	8.6	-25.5±1.1	20.2±1.3	1
PMM 2012	08:43:59.0	-53:33:44.0	136.8	10.2	9.8	9.7	-20.9±1.4	12.7±1.4	1
V376 Vel	08:44:5.2	-52:53:17.0	165.5	9.6	9.3	9.2	-21.3±1.4	19.7±1.0	1
PMM 1373	08:44:10.2	-53:43:34.0	142.8	10.4	10.0	9.8	-24.8±1.5	10.6±1.5	1
V377 Vel	08:44:26.2	-52:42:32.0	173.3	10.0	9.6	9.6	-21.4±1.3	17.5±1.0	1
V379 Vel	08:45:26.9	-52:52:2.0	139.9	10.7	10.2	10.1	-25.2±1.1	23.4±1.1	1
V380 Vel	08:45:39.1	-52:26:0.0	137.8	8.9	8.7	8.6	-52.0±0.9	22.0±1.0	1
PMM 2182	08:45:48.0	-53:25:51.0	152.8	9.1	8.9	8.8	-26.3±1.0	18.5±2.1	1
CD-57 2315	08:50:8.1	-57:45:59.0	107.2	8.6	8.1	8.0	-34.1±2.0	31.0±1.0	1
2MASS J09020394-5808497	09:02:3.9	-58:08:50.0	138.1	9.9	9.5	9.4	-24.2±1.3	26.2±1.3	1
CD-62 1197	09:13:30.3	-62:59:9.0	116.1	8.9	8.4	8.3	-34.1±1.1	27.4±1.0	1
TYC 7695-335-1	09:28:54.1	-41:01:19.0	153.0	9.8	9.3	9.1	-28.7±1.1	13.6±1.1	1
BD-20 2977	09:39:51.4	-21:34:17.0	93.3	8.8	8.5	8.4	-50.0±0.9	7.8±0.9	1
TYC 9217-641-1	09:42:47.4	-72:39:50.0	143.8	10.4	10.0	9.8	-30.1±1.3	18.9±1.3	1
CD-39 5833	09:47:19.9	-40:03:10.0	113.4	9.4	9.0	8.9	-40.6±1.2	16.3±1.6	1
HD 85151a	09:48:43.2	-44:54:8.0	65.9	8.0	7.7	7.6	-68.4±8.0	33.5±3.0	1
HD 85151b	09:48:43.4	-44:54:9.0	65.9	8.0	7.7	7.6	3.9±7.6	1.6±3.7	1
CD-65 817	09:49:9.0	-65:40:21.0	134.9	9.1	8.8	8.7	-31.4±7.6	16.1±6.9	1
HD 309851	09:55:58.3	-67:21:22.0	105.1	8.7	8.4	8.3	-42.4±0.9	25.7±1.2	1
2MASS J10142048-8138423	10:14:20.5	-81:38:42.0	125.7	10.0	9.3	9.1	-37.0±1.3	18.5±2.3	1
HD 310316	10:49:56.1	-69:51:22.0	115.0	8.8	8.4	8.3	-43.5±1.2	13.5±0.9	1
CP-69 1432	10:53:51.5	-70:02:16.0	147.1	9.4	9.2	9.0	-32.6±1.3	12.1±1.0	1
HD 103742	11:56:42.3	-32:16:5.0	33.7 <sup>(a)</sup>	6.5	6.2	6.1	-166.1±1.0	-7.7±1.0	1
CD-42 7422	12:06:32.9	-42:47:51.0	106.9	9.2	8.7	8.6	-50.3±1.3	-2.5±1.0	1
CD-74 673	12:20:34.4	-75:39:29.0	50.1	8.6	8.1	7.9	-109.4±2.0	4.2±1.1	1
CD-75 652	13:49:12.9	-75:49:48.0	77.1	8.4	8.0	8.0	-62.2±1.0	-31.5±1.9	1
2MASS J13591045-1950034	13:59:10.4	-19:50:3.4	10.7	8.3	7.8	7.4	-552.7±8.0	-183.1±8.0	3
HD 129496	14:46:21.4	-67:46:16.0	84.8	7.8	7.5	7.4	-47.6±1.4	-39.7±1.0	1
NY Aps	15:12:23.4	-75:15:16.0	50.3 <sup>(a)</sup>	7.8	7.5	7.4	-75.6±1.4	-73.5±1.2	1
2MASS J18083702-0426259	18:08:37.0	-04:26:25.9	167.5 <sup>(a)</sup>	5.8	5.2	4.9	-8.6±1.3	-15.7±1.2	3
CD-52 9381	20:07:23.8	-51:47:27.0	29.4	8.2	7.6	7.4	85.9±0.7	-143.9±0.7	1, 3
2MASS J20531465-0221218	20:53:14.7	-02:21:21.8	37.9	9.3	8.7	8.4	186.8±8.0	15.7±8.0	3
2MASS J23205766-0147373	23:20:57.7	-01:47:37.3	41.0	9.4	8.8	8.5	168.6±8.0	26.2±8.0	3
2MASS J23581366-1724338	23:58:13.7	-17:24:33.8	39.1	8.3	7.7	7.4	222.6±4.1	12.8±1.5	3

## BPC

2MASS J00172353-6645124	00:17:23.5	-66:45:12.0	36.3	8.6	7.9	7.7	102.9±1.0	-15.0±1.0	3
GJ 3076	01:11:25.4	+15:26:21.0	19.3	9.1	8.5	8.2	192.0±8.0	-130.0±8.0	3
Barta 161 12	01:35:13.9	-07:12:52.0	37.9	9.0	8.4	8.1	93.0±1.7	-48.0±2.2	3, 5
G 271-110	01:36:55.1	-06:47:38.0	24.0	9.7	9.1	8.9	172.6±8.0	-84.2±8.0	3
HIP 10679	02:17:24.7	+28:44:30.0	40.0 <sup>(a)</sup>	6.6	6.4	6.3	98.2±1.0	-67.4±1.0	1
HD 14082	02:17:25.3	+28:44:42.0	39.5 <sup>(a)</sup>	6.0	5.8	5.8	94.3±1.0	-72.2±1.0	1
BD+30 397 b	02:27:28.1	+30:58:41.0	42.4	8.8	8.1	7.9	81.5±4.6	-69.1±3.2	1
AG Tri	02:27:29.3	+30:58:25.0	42.4 <sup>(a)</sup>	7.9	7.2	7.1	80.4±0.9	-70.1±1.3	1
EXO 0235.2-5216	02:36:51.7	-52:03:4.0	28.6	8.4	7.8	7.5	102.2±0.8	1.2±0.8	1, 3
HD 29391	04:37:36.1	-02:28:25.0	29.4 <sup>(a)</sup>	4.7	4.8	4.5	44.2±1.0	-64.4±1.0	1
V1005 Ori	04:59:34.8	+01:47:1.0	24.2 <sup>(a)</sup>	7.1	6.5	6.3	37.5±0.8	-93.5±0.9	1
CD-57 1054	05:00:47.1	-57:15:25.0	26.9 <sup>(a)</sup>	7.1	6.4	6.2	35.5±0.9	74.4±0.9	1
HIP 23418aa	05:01:58.8	+09:58:59.0	37.8 <sup>(a)</sup>	7.2	6.7	6.4	17.2±8.0	-82.0±8.0	1, 3
BD-21 1074b	05:06:49.5	-21:35:4.0	20.2	7.0	6.4	6.1	33.1±2.7	-33.2±2.0	1, 3
2MASS J05200029+0613036	05:20:0.3	+06:13:4.0	67.8	9.3	8.7	8.6	9.4±1.9	-34.7±2.1	1
RX J0520.5+0616	05:20:31.8	+06:16:11.0	71.0	9.2	8.7	8.6	9.5±1.8	-32.8±2.1	1
2MASS J05241914-1601153	05:24:19.1	-16:01:15.0	26.8	8.7	8.1	7.8	16.0±2.5	-34.8±3.5	3
AF Lep	05:27:4.8	-11:54:3.0	27.0 <sup>(a)</sup>	5.3	5.1	4.9	17.7±1.0	-49.5±1.0	1
Beta Pic	05:47:17.1	-51:03:59.0	19.5 <sup>(a)</sup>	3.7	3.5	3.5	4.7±1.0	83.1±1.0	1
2MASS J06131330-2742054	06:13:13.3	-27:42:5.4	29.2	8.0	7.4	7.1	-13.1±1.6	-0.3±1.3	3
AO Men	06:18:28.2	-72:02:41.0	38.6 <sup>(a)</sup>	7.5	7.0	6.8	-6.4±0.9	76.4±0.8	1
2MASS J09133435-7550099	09:13:34.4	-75:50:10.0	62.7	11.9	11.3	11.0	0.0±0.0	0.0±0.0	1
TWA22	10:17:26.9	-53:54:27.0	17.6	8.6	8.1	7.7	-177.0±3.3	-10.3±3.3	1
2MASS J14142141-1521215	14:14:21.4	-15:21:21.5	30.2 <sup>(a)</sup>	7.4	6.8	6.6	-141.1±2.3	-187.9±4.6	3
V343 Nor	15:38:57.5	-57:42:27.0	38.4 <sup>(a)</sup>	6.4	6.0	5.9	-43.6±2.0	-95.6±1.5	1

ID	RA hh:mm:ss.s	DEC dd:mm:ss.s	Dist. (pc)	<i>J</i> (mag.)	<i>H</i> (mag.)	<i>K</i> (mag.)	$\mu_{\alpha,*}$ (mas/yr)	$\mu_{\delta}$ (mas/yr)	Mem ref.
CD-27 11535	17:15:3.6	-27:49:40.0	87.3	8.2	7.5	7.4	-5.2±0.8	-43.6±0.8	1
V824 Ara	17:17:25.5	-66:57:4.0	31.5 <sup>(a)</sup>	5.3	4.9	4.7	-21.8±1.0	-136.9±1.0	1
HD 155555 c	17:17:31.3	-66:57:6.0	31.5	8.5	7.9	7.6	-11.0±2.0	-143.0±2.0	1
GSC 08350-01924	17:29:20.7	-50:14:53.0	66.3	8.9	8.2	8.0	-5.8±1.5	-62.7±5.1	1, 3
CD-54 7336	17:29:55.1	-54:15:49.0	68.4	7.9	7.5	7.4	-9.8±3.2	-60.0±1.7	1
HD 161460	17:48:33.7	-53:06:43.0	71.0	7.3	6.9	6.8	-3.6±1.0	-58.4±1.3	1
HD 164249	18:03:3.4	-51:38:56.0	48.1 <sup>(a)</sup>	6.2	6.0	5.9	4.0±1.0	-86.5±1.0	1
V4046 Sgr	18:14:10.5	-32:47:33.0	76.9	8.1	7.4	7.2	5.5±1.2	-50.9±1.9	1, 3
GSC 07396-00759	18:14:22.1	-32:46:10.0	95.2	9.4	8.8	8.5	1.9±5.7	-41.2±2.6	1, 3
HD 168210	18:19:52.2	-29:16:33.0	72.4 <sup>(a)</sup>	7.5	7.2	7.1	3.5±1.4	-46.4±1.5	1
2MASS J18420694-5554254	18:42:6.9	-55:54:25.0	51.9	9.5	8.8	8.6	9.7±12.1	-81.2±2.8	3
HD 172555	18:45:26.9	-64:52:17.0	28.6 <sup>(a)</sup>	4.4	4.3	4.3	32.5±1.0	-148.8±1.0	1
CD-64 1208	18:45:37.0	-64:51:46.0	28.6	6.9	6.3	6.1	25.9±8.0	-184.2±8.0	1
Smethells 20	18:46:52.6	-62:10:36.0	52.4	8.7	8.0	7.9	13.6±1.4	-79.4±1.4	1, 3
CD-31 16041	18:50:44.5	-31:47:47.0	53.2	8.3	7.7	7.5	16.4±1.6	-72.8±1.1	1, 3
PZ Tel	18:53:5.9	-50:10:50.0	51.5 <sup>(a)</sup>	6.9	6.5	6.4	19.1±1.1	-81.8±1.1	1
TYC 6872-1011-1	18:58:4.2	-29:53:5.0	82.6	8.9	8.2	8.0	12.2±1.3	-45.7±2.5	1, 3
CD-26 13904	19:11:44.7	-26:04:9.0	78.9	8.1	7.6	7.4	17.9±1.4	-45.0±1.9	1
Eta Tel	19:22:51.2	-54:25:26.0	48.3 <sup>(a)</sup>	5.1	5.1	5.0	25.6±1.0	-82.7±1.0	1
HD 181327	19:22:58.9	-54:32:17.0	51.8 <sup>(a)</sup>	6.2	6.0	5.9	24.0±1.0	-81.8±1.0	1
2MASS J19233820-4606316	19:23:38.2	-46:06:32.0	72.2	9.1	8.4	8.3	17.2±1.0	-55.0±1.1	3
2MASS J19312434-2134226	19:31:24.3	-21:34:22.6	26.0	8.7	8.1	7.8	58.7±6.2	-109.5±2.3	3
UCAC3 116-474938	19:56:2.9	-32:07:19.0	58.4	9.0	8.3	8.1	35.2±1.8	-59.9±1.5	1, 3
TYC 7443-1102-1	19:56:4.4	-32:07:38.0	56.3	8.7	8.0	7.8	31.9±1.4	-65.1±1.2	1, 3
2MASS J20013718-3313139	20:01:37.2	-33:13:14.0	63.4	9.2	8.5	8.2	27.0±3.2	-58.6±2.0	1, 3
HD 190102	20:04:18.1	-26:19:46.0	46.8 <sup>(a)</sup>	7.0	6.7	6.6	32.3±1.0	-75.1±1.0	1
HD 191089	20:09:5.2	-26:13:26.0	52.3 <sup>(a)</sup>	6.3	6.1	6.1	39.2±1.0	-68.3±1.0	1
2MASS J20100002-2801410	20:10:0.0	-28:01:41.0	48.0	8.7	8.0	7.7	40.7±3.0	-62.0±1.7	3
2MASS J20333759-2556521	20:33:37.6	-25:56:52.1	48.3	9.7	9.1	8.9	52.8±1.7	-75.9±1.3	3
AT Mic S	20:41:51.1	-32:26:10.0	9.5	5.8	5.2	4.9	286.2±8.0	-377.2±8.0	1
AT Mic N	20:41:51.2	-32:26:7.0	9.5 <sup>(a)</sup>	5.8	5.2	4.9	269.3±8.0	-365.7±8.0	1
2MASS J20434114-2433534 A	20:43:41.1	-24:33:53.0	45.1	8.6	8.0	7.8	57.2±1.2	-70.2±1.8	3
2MASS J20434114-2433534 B	20:43:41.1	-24:33:53.0	45.1	8.6	8.0	7.8	57.2±1.2	-70.2±1.8	1
AU Mic	20:45:9.5	-31:20:27.0	9.8	5.4	4.8	4.5	287.8±3.7	-359.0±3.7	1
HD 199143	20:55:47.7	-17:06:51.0	45.7 <sup>(a)</sup>	6.2	5.9	5.8	58.8±1.0	-62.8±1.0	1
AZ Cap	20:56:2.7	-17:10:54.0	47.9	7.8	7.2	7.0	57.6±1.1	-59.9±1.2	1, 3
GSC 06354-00357	21:10:5.3	-19:19:57.0	32.6	8.1	7.4	7.2	0.0±0.0	0.0±0.0	1
2MASS J21100535-1919573	21:10:5.3	-19:19:57.0	32.6	8.1	7.4	7.2	89.0±0.9	-89.9±1.8	3
TYC 2211-1309-1	22:00:41.6	+27:15:14.0	46.6	8.6	7.9	7.7	74.9±1.2	-16.8±0.5	1, 3
CP-72 2713	22:42:48.9	-71:42:21.0	37.3	7.8	7.1	6.9	92.7±0.8	-51.1±0.8	1, 3
WW PsA	22:44:58.0	-33:15:2.0	20.1 <sup>(a)</sup>	7.8	7.2	6.9	178.7±1.0	-123.0±2.0	1
TX PsA	22:45:0.0	-33:15:26.0	20.1	8.7	8.1	7.8	171.1±1.3	-125.2±4.3	1
2MASS J23301341-2023271	23:30:13.4	-20:23:27.1	16.2 <sup>(a)</sup>	7.2	6.6	6.3	314.5±8.0	-208.1±8.0	3
BD-13 6424	23:32:30.9	-12:15:52.0	27.9	7.5	6.8	6.6	137.4±1.0	-81.0±1.0	1, 3
CAR									
HD 8813	01:23:25.9	-76:36:42.0	46.5 <sup>(a)</sup>	7.2	6.9	6.8	99.0±0.8	-18.7±0.9	1
WISE J025901.49-423220.4	02:59:1.5	-42:32:20.0	103.3	12.2	11.7	11.4	39.9±4.1	-6.9±4.4	1
CD-65 149	03:06:14.5	-65:21:32.0	90.0	8.6	8.2	8.0	42.6±1.3	7.1±0.8	1
HD 19545	03:07:50.8	-27:49:52.0	54.6 <sup>(a)</sup>	5.9	5.9	5.8	66.3±1.0	-19.1±1.0	1, 2
HD 22213	03:34:16.4	-12:04:7.0	52.4	7.3	7.0	6.8	75.6±2.3	-34.3±1.5	1
CD-45 1384	04:03:53.4	-44:39:32.0	109.1	9.0	8.6	8.5	32.0±1.1	1.2±1.1	1
CD-44 1533	04:22:45.7	-44:32:52.0	103.7	9.0	8.7	8.6	31.2±0.9	4.0±0.9	1
BD-20 951	04:52:49.5	-19:55:2.0	72.4	8.0	7.5	7.3	38.7±0.9	-15.6±0.9	1
HD 269620	05:29:27.1	-68:52:5.0	91.2	8.4	8.2	8.1	21.1±1.4	28.3±1.2	1
AT Col	05:37:5.3	-39:32:26.0	66.2	7.9	7.5	7.3	31.1±1.3	8.0±1.3	1
HD 269921	05:38:34.5	-68:53:7.0	90.8	8.9	8.4	8.4	18.8±1.1	29.5±1.3	1
HD 42270	05:53:29.3	-81:56:53.0	54.0	7.5	7.0	6.9	28.6±1.2	64.2±1.2	1
CD-48 2324	06:28:6.1	-48:26:53.0	141.8	9.5	9.1	9.0	7.3±1.2	11.6±1.2	1
CD-37 2984	06:39:46.7	-37:50:10.0	75.3	9.3	8.8	8.7	11.3±0.7	9.6±0.8	1
CD-52 1641	06:41:12.5	-52:07:39.0	99.2	9.1	8.5	8.5	7.5±0.8	18.9±0.8	1
CD-41 2572	06:45:37.9	-41:12:41.0	80.7	9.2	8.8	8.7	11.4±1.8	10.1±1.7	1
HD 51062	06:53:47.4	-43:06:51.0	94.4 <sup>(a)</sup>	7.5	7.2	7.1	5.5±3.6	11.0±0.9	1
CD-57 1709	07:21:23.7	-57:20:37.0	100.5	9.2	8.8	8.7	0.8±1.0	22.1±0.8	1
CD-42 3328	07:33:21.2	-42:55:42.0	125.1	9.9	9.6	9.4	-2.9±1.0	9.1±0.9	1
CD-60 1850	07:43:42.9	-61:07:17.0	91.0	9.2	8.7	8.5	2.2±1.3	26.4±1.3	1
HIP 38712	07:55:31.4	+08:51:47.0	39.0 <sup>(a)</sup>	5.1	5.0	5.0	-7.4±1.0	-89.9±1.0	1
TYC 8557-1251-1	07:55:31.6	-54:36:51.0	123.0	9.8	9.3	9.2	-1.7±1.2	16.5±2.5	1
2MASS J08110934-5555563	08:11:9.3	-55:55:56.0	129.0	9.9	9.5	9.4	-5.9±1.0	15.7±1.2	1
BD-07 2388	08:13:51.0	-07:38:25.0	42.6	7.6	7.1	6.9	-23.7±1.5	-46.0±1.1	1
CD-38 4458	08:26:10.0	-39:02:5.0	142.8	9.0	8.7	8.6	-6.4±1.1	7.2±1.1	1



ID	RA hh:mm:ss.s	DEC dd:mm:ss.s	Dist. (pc)	<i>J</i> (mag.)	<i>H</i> (mag.)	<i>K</i> (mag.)	$\mu_{\alpha,*}$ (mas/yr)	$\mu_{\delta}$ (mas/yr)	Mem ref.
CP-54 1712	08:37:10.9	-55:18:10.0	180.8	9.8	9.4	9.4	-5.9±1.0	10.6±1.8	1
CD-61 2010	08:42:0.5	-62:18:26.0	121.4	9.4	9.0	8.8	-10.2±0.8	18.6±0.8	1
CD-75 392	08:50:5.4	-75:54:38.0	91.4	9.3	8.8	8.7	-15.1±1.5	33.1±0.9	1
CD-53 2515	08:51:56.4	-53:55:57.0	137.1	9.3	8.9	8.7	-11.7±1.0	11.3±1.0	1
2MASS J08521921-6004443	08:52:19.2	-60:04:44.0	163.9	9.9	9.5	9.4	-6.5±1.6	13.2±1.3	1
2MASS J08563149-5700406	08:56:31.5	-57:00:41.0	191.6	10.3	9.9	9.8	-8.2±1.4	8.9±2.7	1
TYC 8582-3040-1	08:57:45.6	-54:08:37.0	143.2	9.9	9.5	9.3	-11.9±1.8	10.4±2.3	1
CD-49 4008	08:57:52.2	-49:41:51.0	102.9	9.1	8.8	8.6	-17.3±0.9	10.9±0.8	1
CD-54 2499	08:59:28.7	-54:46:49.0	109.5	8.8	8.5	8.4	-15.9±1.3	14.0±1.2	1
CD-55 2543	09:09:29.4	-55:38:27.0	115.2	8.8	8.5	8.4	-14.8±1.4	14.8±1.8	1
TYC 8174-1586-1	09:11:15.8	-50:14:15.0	117.2	10.2	9.6	9.5	-15.9±8.3	10.7±2.3	1
CD-54 2644	09:13:16.9	-55:29:3.0	131.7	8.9	8.5	8.4	-15.0±1.9	10.3±1.9	1
HD 309751	09:31:44.7	-65:14:53.0	141.6	8.8	8.5	8.4	-13.1±1.8	14.6±1.2	1
CD-48 4797	09:33:14.3	-48:48:33.0	47.0	8.9	8.3	8.1	-46.6±1.4	23.0±1.6	1, 3
CP-62 1293	09:43:8.8	-63:13:4.0	69.4	9.0	8.7	8.6	-33.1±1.1	26.9±1.0	1
TYC 9217-417-1	09:59:57.7	-72:21:47.0	83.6	9.5	8.9	8.7	-28.3±1.1	27.8±1.0	1
BD-19 3018	10:27:37.3	-20:27:11.0	60.2	8.4	8.0	7.9	-51.5±1.2	-24.5±3.0	1
CD-69 783	10:41:23.0	-69:40:43.0	86.5	8.9	8.5	8.4	-33.5±1.6	19.5±1.6	1
TYC 8962-1747-1	11:08:7.9	-63:41:47.0	88.2	9.1	8.5	8.3	-37.1±1.9	8.3±1.9	1
HD 107722	12:23:29.0	-77:40:51.0	59.0	7.4	7.2	7.1	-65.7±0.9	11.8±0.9	1
HD 152598	16:52:58.1	+31:42:6.0	29.2 <sup>(a)</sup>	4.7	4.5	4.6	-90.8±1.0	-17.3±1.0	1
TYC 9486-927-1	21:25:27.5	-81:38:28.0	36.3	8.2	7.6	7.3	58.9±1.5	-109.4±1.0	1
BD-03 5579	23:09:37.1	-02:25:55.0	63.0	8.6	8.0	7.8	55.7±1.8	-45.1±1.6	1

## COL

HD 984	00:14:10.2	-07:11:57.0	47.2 <sup>(a)</sup>	6.4	6.2	6.1	102.8±1.0	-66.4±1.0	1, 2
BD+17 232	01:37:39.4	+18:35:33.0	65.1	7.5	6.9	6.7	68.6±0.8	-47.3±0.6	1
CD-52 381	01:52:14.6	-52:19:33.0	83.4	9.1	8.5	8.4	51.3±1.2	-6.7±1.1	1
BD-16 351	02:01:35.6	-16:10:1.0	80.9	8.6	8.1	8.0	53.5±1.5	-30.3±1.9	1
CD-53 386	02:01:53.7	-52:34:53.0	106.9	9.2	8.7	8.6	38.5±2.0	-10.0±1.4	1
CD-44 753	02:30:32.4	-43:42:23.0	51.3	8.0	7.4	7.2	80.3±0.9	-13.3±0.9	1, 3, 5
HD 16754	02:39:48.0	-42:53:30.0	45.5 <sup>(a)</sup>	4.7	4.6	4.5	88.2±1.0	-17.8±1.0	1, 2
TYC 8862-19-1	02:58:4.0	-62:41:14.0	92.6	9.6	9.0	8.9	40.5±1.5	5.5±1.0	1
BD-11 648	03:21:49.7	-10:52:18.0	128.1	9.8	9.4	9.3	31.0±1.2	-14.5±1.6	1
GSC 08499-00304	03:24:15.0	-59:01:13.0	92.9	9.5	8.9	8.7	37.5±1.1	9.6±1.1	1, 3
CD-36 1289	03:25:51.9	-35:56:26.0	107.5	8.6	8.2	8.1	34.6±1.0	-1.8±1.0	1
HD 21423	03:25:55.8	-35:55:15.0	107.5 <sup>(a)</sup>	6.2	6.2	6.2	36.3±1.0	-4.4±1.0	1
HD 21434	03:25:59.0	-35:57:30.0	107.8	6.7	6.6	6.6	34.2±2.0	-5.1±2.0	1
V1221 Tau	03:28:15.0	+04:09:48.0	81.5	8.0	7.6	7.4	46.9±0.9	-33.8±0.7	1
HD 21997	03:31:53.6	-25:36:51.0	71.9 <sup>(a)</sup>	6.2	6.1	6.1	53.9±1.0	-14.9±1.0	1
HIP 17248	03:41:37.3	+55:13:7.0	35.4 <sup>(a)</sup>	8.3	7.6	7.5	95.7±0.8	-119.2±1.0	1, 2
HD 23384	03:47:10.6	+51:42:23.0	57.5 <sup>(a)</sup>	6.2	6.1	6.1	60.2±1.0	-74.6±1.0	1
TYC 65-1471-1	03:48:58.8	+01:10:54.0	111.1	8.9	8.4	8.3	33.6±1.0	-20.9±0.8	1
BD-04 700	03:57:37.2	-04:16:16.0	106.5	9.2	8.8	8.8	33.7±1.3	-18.0±1.4	1
HD 26980	04:14:22.6	-38:19:2.0	80.7 <sup>(a)</sup>	7.9	7.7	7.6	38.6±0.9	3.0±0.8	1
HD 27679	04:21:10.3	-24:32:21.0	78.0	8.2	7.9	7.8	38.3±0.9	-6.9±1.1	1
CD-43 1395	04:21:48.7	-43:17:33.0	141.0	8.9	8.5	8.4	20.5±0.9	4.9±1.0	1
2MASS J04240094-5512223	04:24:0.9	-55:12:22.0	66.4	9.8	9.2	8.9	42.4±2.1	17.2±2.1	1, 3, 5
CD-44 1568	04:27:20.5	-44:20:39.0	86.2	9.2	8.7	8.6	32.5±1.1	4.6±1.1	1
CD-36 1785	04:34:50.8	-35:47:21.0	80.1	9.3	8.8	8.6	33.4±0.9	0.4±0.9	1
BD+08 742	04:42:32.1	+09:06:1.0	105.6	9.6	9.2	9.1	26.7±0.8	-27.8±1.1	1
HD 30447	04:46:49.5	-26:18:9.0	80.1 <sup>(a)</sup>	7.1	7.0	6.9	30.5±1.1	-2.4±1.8	1
2MASS J04515303-4647309	04:51:53.0	-46:47:31.0	77.5	9.8	9.1	8.9	30.5±1.5	12.2±1.5	1, 3, 5
HD 31242 N	04:51:53.5	-46:47:13.0	68.1	8.5	8.2	8.2	33.5±1.1	16.1±1.3	1
HD 272836	04:53:5.2	-48:44:39.0	78.6	8.9	8.4	8.2	29.3±0.9	14.9±0.9	1
BD-08 995	04:58:48.6	-08:43:40.0	86.8	8.8	8.5	8.3	25.2±1.3	-22.4±1.2	1
HD 31647 b	04:59:15.4	+37:53:30.0	52.4	7.0	5.9	5.9	46.3±2.5	-97.8±2.5	1
HD 31647 a	04:59:15.4	+37:53:25.0	52.4 <sup>(a)</sup>	4.9	5.0	4.9	46.3±1.0	-97.8±1.0	1, 2
HD 32372	05:00:51.9	-41:01:7.0	76.3 <sup>(a)</sup>	8.1	7.9	7.8	33.4±0.8	10.7±0.9	1
HD 32309	05:01:25.6	-20:03:7.0	60.6 <sup>(a)</sup>	5.0	5.0	5.0	36.4±1.0	-16.5±1.0	1, 2
AS Col	05:20:38.0	-39:45:18.0	48.3 <sup>(a)</sup>	6.4	6.2	6.1	38.4±1.0	13.1±1.0	1
CD-43 1846	05:26:23.0	-43:22:36.0	84.7 <sup>(a)</sup>	8.1	7.9	7.8	21.2±1.3	10.3±2.9	1
HD 35996	05:26:24.0	-43:22:33.0	71.4 <sup>(a)</sup>	7.4	7.3	7.2	23.8±1.2	12.9±1.0	1
HD 35841	05:26:36.6	-22:29:24.0	94.0	8.0	7.8	7.8	18.0±0.8	-7.9±1.0	1
HD 274561	05:28:55.1	-45:34:58.0	86.8	9.6	9.1	9.0	19.2±1.0	13.8±1.0	1
HD 36329	05:29:24.1	-34:30:56.0	70.9 <sup>(a)</sup>	7.3	7.1	6.9	25.8±0.8	5.9±0.8	1
AG Lep	05:30:19.1	-19:16:32.0	115.1	8.4	8.0	7.9	14.1±1.5	-7.3±1.2	1
AH Lep	05:34:9.2	-15:17:3.0	61.3	7.2	7.0	6.9	26.4±1.3	-24.1±1.2	1, 2
HD 37286	05:36:10.3	-28:42:29.0	52.9 <sup>(a)</sup>	6.0	5.9	5.9	25.8±1.0	-3.0±1.0	1, 2
HD 37484	05:37:39.6	-28:37:35.0	56.8 <sup>(a)</sup>	6.5	6.3	6.3	24.3±1.0	-4.1±1.0	1, 2
TYC 119-1242-1	05:37:45.3	+02:30:57.0	70.8	9.0	8.4	8.3	18.6±3.7	-39.8±2.0	1

ID	RA hh:mm:ss.s	DEC dd:mm:ss.s	Dist. (pc)	<i>J</i> (mag.)	<i>H</i> (mag.)	<i>K</i> (mag.)	$\mu_{\alpha,*}$ (mas/yr)	$\mu_{\delta}$ (mas/yr)	Mem ref.
TYC 119-497-1	05:37:46.5	+02:31:26.0	67.0	9.0	8.4	8.2	21.8±2.4	-41.4±1.3	1
BD-08 1195	05:38:35.0	-08:56:40.0	82.0	8.5	8.1	8.0	16.7±0.9	-22.3±1.6	1
CD-34 2406	05:42:34.3	-34:15:42.0	89.8	9.2	9.0	8.7	14.6±1.5	7.0±0.9	1
HD 38207	05:43:21.0	-20:11:21.0	86.3	7.7	7.5	7.5	17.4±1.4	-6.2±1.5	1
HD 38206	05:43:21.7	-18:33:27.0	75.2 <sup>(a)</sup>	5.8	5.8	5.8	18.9±1.0	-14.0±1.0	1
HD 38397	05:43:35.8	-39:55:25.0	55.3 <sup>(a)</sup>	7.1	6.8	6.8	25.8±1.1	13.1±1.2	1, 2
CD-38 2198	05:45:16.3	-38:36:49.0	134.1	9.6	9.2	9.1	10.7±1.1	5.7±1.7	1
CD-29 2531	05:50:21.4	-29:15:21.0	107.8	9.6	9.2	9.1	11.6±1.0	2.1±0.8	1
CD-52 1363	05:51:1.2	-52:38:13.0	110.5	9.1	8.7	8.6	10.1±1.5	17.2±0.9	1
HD 40216	05:55:43.2	-38:06:16.0	54.4 <sup>(a)</sup>	6.5	6.3	6.2	20.5±1.0	9.3±1.0	1
RT Pic	06:00:41.3	-44:53:50.0	52.6 <sup>(a)</sup>	7.7	7.4	7.3	17.4±0.9	21.3±0.9	1, 2
V1358 Ori	06:19:8.1	-03:26:20.0	49.2 <sup>(a)</sup>	6.8	6.6	6.6	10.4±0.4	-43.3±0.4	1
AB Pic	06:19:12.9	-58:03:16.0	46.1 <sup>(a)</sup>	7.6	7.1	7.0	16.2±0.8	45.7±0.8	1
CD-40 2458	06:26:6.9	-41:02:54.0	94.5	8.5	8.2	8.0	5.0±1.2	11.3±1.3	1
TYC 4810-181-1	06:31:55.2	-07:04:59.0	87.5	9.8	9.2	9.1	7.0±2.0	-19.2±1.6	1
HD 295290	06:40:22.3	-03:31:59.0	60.2	7.4	7.0	7.0	3.4±1.0	-37.9±0.7	1
HD 48370	06:43:1.0	-02:53:19.0	34.1	6.7	6.4	6.3	14.5±0.6	-71.0±1.1	1
HD 49855	06:43:46.2	-71:58:35.0	58.1 <sup>(a)</sup>	7.7	7.4	7.3	4.6±0.9	60.9±0.8	1
CD-36 3202	06:52:46.7	-36:36:17.0	101.5	9.4	8.9	8.7	-1.6±0.9	6.2±0.8	1
TYC 9178-284-1	06:55:25.2	-68:06:21.0	108.3	9.7	9.1	8.9	1.2±1.0	26.4±1.4	1
HD 51797	06:56:23.5	-46:46:55.0	77.7	8.4	7.9	7.8	-1.6±1.0	18.5±0.9	1
HD 55279	07:00:30.5	-79:41:46.0	58.8 <sup>(a)</sup>	8.3	7.8	7.7	1.9±0.9	59.8±0.9	1
CD-39 3026	07:01:51.8	-39:22:4.0	119.9	9.9	9.4	9.3	-0.1±0.8	7.9±0.8	1
CD-63 408	08:24:6.0	-63:34:3.0	118.6	8.6	8.2	8.1	-13.7±1.1	18.2±1.6	1
V479 Car	09:23:35.0	-61:11:36.0	87.7 <sup>(a)</sup>	8.6	8.1	8.0	-24.5±2.5	12.7±1.3	1
CP-52 2481	09:32:26.1	-52:37:40.0	101.9	9.4	9.0	8.8	-26.8±1.5	6.9±2.0	1
HD 298936	10:13:14.8	-52:30:54.0	50.5	7.9	7.4	7.2	-60.9±1.5	13.9±0.8	1
BD+44 3670	21:00:47.0	+45:30:10.0	57.8	7.3	7.0	6.9	39.2±1.1	8.6±0.5	1, 2
TYC 1158-1185-1 S	22:42:48.8	+13:30:54.0	50.2	8.6	8.0	8.0	72.8±1.3	-41.0±1.5	1
TYC 1158-1185-1 N	22:42:48.9	+13:30:53.0	50.2	8.6	8.0	8.0	72.8±1.3	-41.0±1.5	1, 3
V342 Peg	23:07:28.7	+21:08:3.0	39.4 <sup>(a)</sup>	5.4	5.3	5.2	107.9±1.0	-49.6±1.0	1, 2
HD 222439	23:40:24.5	+44:20:2.0	51.6 <sup>(a)</sup>	4.6	4.6	4.6	80.7±1.0	-18.7±1.0	1, 2

ECH

EG Cha	08:36:56.2	-78:56:46.0	108.7	8.2	7.5	7.3	-26.8±1.0	25.2±1.1	1
RX J0902.9-7759	09:02:51.3	-77:59:35.0	100.0	10.1	9.5	9.2	-33.9±1.7	22.0±1.7	1
2MASS J09053087-8134572	09:05:30.9	-81:34:57.0	93.9	12.2	11.6	11.3	-35.2±9.6	27.2±9.6	1
2MASS J09152912-7608471	09:15:29.1	-76:08:47.0	117.5	9.3	8.7	8.5	-28.2±1.3	18.7±1.4	1
2MASS J09345604-7804193	09:34:56.1	-78:04:19.0	121.6	9.8	9.1	8.9	-27.5±1.4	18.3±1.3	1
RX J1005.3-7749	10:05:20.0	-77:48:42.0	91.6	9.8	9.1	8.9	-44.4±1.9	10.1±1.9	1
DZ Cha	11:49:31.9	-78:51:1.0	102.7	9.4	8.7	8.5	-41.1±4.3	-9.4±1.7	1, 3
T Cha	11:57:13.5	-79:21:32.0	107.5	9.0	7.9	7.0	-39.9±3.6	-7.1±1.3	1
EE Cha	11:58:35.2	-77:49:31.0	108.7 <sup>(a)</sup>	6.3	6.2	6.1	-42.0±1.0	-9.1±1.0	1
Eps Cha	11:59:37.6	-78:13:19.0	111.1 <sup>(a)</sup>	5.0	5.0	5.0	-41.2±1.0	-8.5±1.0	1
HIP 58490	11:59:42.3	-76:01:26.0	101.0 <sup>(a)</sup>	9.1	8.5	8.3	-39.5±1.5	-6.1±1.8	1
2MASS J12000511-7811346	12:00:5.0	-78:11:34.0	111.1	5.8	5.2	4.6	-39.0±1.0	-5.7±1.0	1
DX Cha	12:00:5.1	-78:11:35.0	115.0 <sup>(a)</sup>	5.8	5.2	4.6	-39.0±1.0	-5.7±1.0	1
HD 104467	12:01:39.1	-78:59:17.0	106.5	7.3	7.0	6.8	-40.7±1.1	-5.5±1.0	1
2MASS J12020369-7853012	12:02:3.8	-78:53:1.0	110.5	9.2	8.5	8.3	-39.0±5.3	-5.8±1.7	1
2MASS J12043615-7731345	12:04:36.2	-77:31:35.0	116.9	9.8	9.1	8.9	-36.8±1.6	-1.7±1.6	1
HD 105923	12:11:38.1	-71:10:36.0	117.1	7.7	7.3	7.2	-36.9±1.7	-8.1±1.1	1
2MASS J12164593-7753333	12:16:46.0	-77:53:33.0	116.3	10.1	9.5	9.2	-36.1±1.6	-9.9±1.6	1
2MASS J12194369-7403572	12:19:43.8	-74:03:57.0	108.9	9.7	9.0	8.9	-40.1±1.9	-6.6±1.9	1
RX J1220.4-7407	12:20:21.9	-74:07:39.0	114.8	9.3	8.6	8.4	-37.8±1.8	-6.1±1.8	1
CD-74 712	12:39:21.3	-75:02:39.0	108.6	8.4	8.0	7.8	-38.9±1.5	-13.7±1.6	1
TYC 9245-535-1	12:56:8.4	-69:26:54.0	119.3	8.9	8.2	8.0	-34.9±2.6	-15.3±3.3	1
CD-69 1055	12:58:25.6	-70:28:49.0	106.7	8.2	7.7	7.5	-39.4±1.6	-17.4±1.1	1
MP Mus	13:22:7.5	-69:38:12.0	106.1	8.3	7.6	7.3	-39.1±1.2	-19.9±1.6	1

OCT

2MASS J00530603-8250259	00:53:6.0	-82:50:25.9	129.0	10.1	9.5	9.3	22.2±1.2	22.1±1.2	4
CD-50 245	00:55:25.3	-49:56:57.0	65.6	8.7	8.4	8.3	38.2±1.3	27.8±1.1	1
CD-46 287	01:01:16.7	-45:56:37.0	78.0	9.4	8.9	8.7	32.0±0.8	21.9±1.7	1
HIP 10670	02:17:18.9	+33:50:50.0	34.5 <sup>(a)</sup>	3.8	3.9	4.0	45.7±1.0	-52.2±1.0	1
CD-41 702	02:29:0.3	-41:07:33.0	59.9	9.0	8.5	8.3	23.1±1.0	34.8±0.9	1
HIP 16095	03:27:18.7	+12:44:7.0	87.7 <sup>(a)</sup>	6.3	6.3	6.3	10.4±1.0	-7.6±1.0	1
2MASS J03302115-6412207	03:30:21.1	-64:12:20.7	121.0	12.1	11.5	11.3	8.7±6.2	26.0±6.1	4
HD 23208	03:42:39.8	-20:32:44.0	50.3 <sup>(a)</sup>	7.7	7.3	7.2	3.2±1.6	26.4±1.6	1
2MASS J04085395-7203535	04:08:54.0	-72:03:53.5	89.0	10.8	10.2	9.9	-4.6±2.2	38.6±2.0	4
HIP 19496	04:10:35.8	+25:21:45.0	98.0 <sup>(a)</sup>	8.2	8.0	7.9	2.8±0.7	-19.5±0.5	1

ID	RA hh:mm:ss.s	DEC dd:mm:ss.s	Dist. (pc)	<i>J</i> (mag.)	<i>H</i> (mag.)	<i>K</i> (mag.)	$\mu_{\alpha,*}$ (mas/yr)	$\mu_{\delta}$ (mas/yr)	Mem ref.
2MASS J04105436-6924209	04:10:54.4	-69:24:20.9	89.0	11.4	10.8	10.5	-4.8±3.2	36.0±3.3	4
CD-58 860	04:11:55.7	-58:01:47.0	87.1	8.8	8.5	8.4	-4.0±1.4	32.8±2.4	1
2MASS J04224274-6137581	04:22:42.7	-61:37:58.1	98.0	11.7	11.1	10.9	-4.3±2.5	31.1±2.4	4
CD-43 1451	04:30:27.3	-42:48:47.0	122.8	9.3	8.9	8.7	0.3±0.8	19.2±0.8	1
EX Eri	04:46:25.7	-28:05:15.0	56.2 <sup>(a)</sup>	5.8	5.7	5.7	-4.5±1.0	17.5±1.0	1
2MASS J04593927-3426546	04:59:39.3	-34:26:54.6	86.0	11.2	10.5	10.2	-14.7±1.8	21.8±1.8	4
2MASS J05015289-6101308	05:01:52.9	-61:01:30.8	120.0	11.5	10.9	10.6	-7.2±2.3	24.4±2.2	4
2MASS J05060048-4545196	05:06:0.5	-45:45:19.6	116.0	12.0	11.4	11.2	-9.5±3.0	20.1±3.9	4
CD-72 248	05:06:50.6	-72:21:12.0	145.8	9.2	8.8	8.7	-6.1±1.1	21.3±1.2	1
2MASS J05181994+0829132	05:18:20.0	+08:29:13.0	88.3	9.6	9.0	8.9	-6.3±2.1	-9.9±1.2	1
2MASS J05184173-4907129	05:18:41.7	-49:07:12.9	136.0	11.2	10.5	10.4	-12.1±1.6	13.6±1.6	4
HD 274576	05:28:51.4	-46:28:19.0	117.1	9.3	8.9	8.8	-11.3±1.0	19.5±1.1	1
2MASS J05321635-4132446	05:32:16.4	-41:32:44.6	141.0	11.4	10.7	10.5	-5.4±5.1	17.6±16.9	4
BD-20 1111	05:32:29.3	-20:43:33.0	129.7	9.1	8.7	8.7	-9.8±1.3	8.3±1.5	1
2MASS J05410719-2409179	05:41:7.2	-24:09:17.9	111.0	10.9	10.3	10.2	-8.1±1.6	11.0±1.6	4
CD-47 1999	05:43:32.1	-47:41:11.0	166.7	9.0	8.8	8.6	-8.2±0.9	14.5±0.8	1
2MASS J05541279-4044059	05:54:12.8	-40:44:5.9	143.0	12.5	11.8	11.6	-11.3±5.6	11.1±5.3	4
2MASS J05581182-3500496	05:58:11.8	-35:00:49.0	105.8	9.8	9.5	9.4	-14.6±1.0	17.2±1.2	1
2MASS J05584222-5639409	05:58:42.2	-56:39:40.9	138.0	11.8	11.2	11.0	-11.1±2.7	18.7±2.6	4
2MASS J06002910-5531015	06:00:29.1	-55:31:1.5	126.0	11.8	11.2	10.9	-12.6±2.8	15.4±2.7	4
CD-49 2037	06:03:35.4	-49:11:26.0	173.8	9.7	9.2	9.1	-10.1±3.7	13.2±2.4	1
2MASS J06055373-2541242	06:05:53.7	-25:41:24.2	110.0	11.7	11.1	10.8	-13.4±2.5	14.9±2.8	4
2MASS J06124600-3836083	06:12:46.0	-38:36:8.3	85.0	11.7	11.1	10.9	-23.5±3.2	18.3±3.1	4
2MASS J06204718-3619482	06:20:47.2	-36:19:48.2	116.0	10.0	9.4	9.2	-15.5±1.5	12.6±1.5	4
2MASS J06205027-7905195	06:20:50.3	-79:05:19.5	130.0	10.7	10.1	9.8	-16.6±1.9	22.1±1.8	4
CD-66 395	06:25:12.4	-66:29:10.0	126.1	9.5	9.1	9.0	-12.8±1.4	22.1±1.3	1
CD-30 3394N	06:40:4.9	-30:33:3.0	137.1	8.8	8.6	8.6	-16.1±1.6	10.3±1.2	1
CD-30 3394S	06:40:5.7	-30:33:9.0	137.1	8.8	9.2	8.7	-13.4±1.4	9.3±1.2	1
2MASS J06434892-5130461	06:43:48.9	-51:30:46.1	140.0	12.0	11.3	11.1	-15.6±2.2	18.2±2.4	4
2MASS J06555474-4046498	06:55:54.7	-40:46:49.8	132.0	11.7	11.1	10.9	-17.5±3.1	9.9±2.9	4
2MASS J07402971-7148232	07:40:29.7	-71:48:23.0	168.9	9.7	9.2	9.1	-15.2±1.8	12.4±2.2	1
2MASS J08145586-7613014	08:14:55.9	-76:13:1.4	139.0	11.2	10.5	10.4	-22.9±1.9	10.1±1.9	4
2MASS J16405331-7234127	16:40:53.3	-72:34:12.7	134.0	12.7	12.1	11.9	-17.4±5.7	8.7±8.7	4
BD-18 4452N	17:13:11.6	-18:34:25.0	16.7	7.3	6.7	6.5	44.0±3.5	-67.1±4.4	1
2MASS J17214553-8026396	17:21:45.5	-80:26:39.6	162.0	12.3	11.7	11.5	8.2±4.2	-20.9±4.5	4
2MASS J17325153-7336111	17:32:51.5	-73:36:11.1	167.0	10.6	10.0	9.8	9.1±1.9	-20.4±1.8	4
HD 155177	17:42:9.0	-86:08:5.0	132.0	7.9	7.7	7.6	11.5±1.1	-22.5±0.9	1
BD+01 3657	18:22:17.2	+01:42:25.0	26.8 <sup>(a)</sup>	7.6	7.0	6.9	83.2±0.9	-19.8±0.5	1
2MASS J18494869-7157100	18:49:48.7	-71:57:10.0	147.1	9.3	8.9	8.7	7.9±3.6	-16.5±5.4	1
CP-79 1037	19:47:3.9	-78:57:43.0	150.8	9.8	9.4	9.3	16.1±3.4	-14.3±1.7	1
CP-82 784	19:53:56.8	-82:40:42.0	132.7	9.2	8.8	8.6	21.3±0.9	-13.2±0.9	1
2MASS J19545336-6450090	19:54:53.4	-64:50:9.0	166.0	10.7	10.0	9.8	15.8±2.1	-13.8±2.2	4
2MASS J19545407-6450343	19:54:54.1	-64:50:34.3	181.0	11.2	10.5	10.3	16.9±2.3	-9.1±2.3	4
2MASS J20293579-6317079	20:29:35.8	-63:17:7.9	140.0	10.8	10.2	10.0	23.4±1.7	-12.3±1.6	4
2MASS J20410187-7813502	20:41:1.9	-78:13:50.2	157.0	11.4	10.8	10.6	23.0±6.2	-5.1±5.4	4
HIP 102218	20:42:40.6	-10:58:11.0	67.6 <sup>(a)</sup>	6.9	6.7	6.7	37.0±1.1	-6.2±1.3	1
HD 197157	20:44:2.3	-51:55:15.0	24.2 <sup>(a)</sup>	3.9	3.7	3.8	155.9±1.0	-53.6±1.0	1
CD-33 15436	21:11:55.2	-32:58:37.0	54.8	8.9	8.4	8.3	61.3±0.8	-11.5±1.2	1
2MASS J22540018-7807039	22:54:0.2	-78:07:3.9	99.0	10.6	9.9	9.8	37.0±2.0	11.0±2.0	4
HK Aqr	23:08:19.6	-15:24:36.0	31.6 <sup>(a)</sup>	8.0	7.3	7.1	107.7±1.7	-19.3±1.0	1
EQ Peg B	23:31:52.6	+19:56:14.0	6.1	7.1	6.6	6.3	-78.1±6.3	108.4±6.3	1
CD-87 121	23:58:17.7	-86:26:24.0	109.3	8.5	8.1	8.0	26.4±1.0	16.0±0.8	1

## THA

HD 105	00:05:52.5	-41:45:11.0	39.4 <sup>(a)</sup>	6.5	6.2	6.1	97.5±1.0	-76.3±1.0	1
HD 987	00:13:53.0	-74:41:18.0	44.5 <sup>(a)</sup>	7.4	7.1	7.0	78.1±1.3	-51.3±1.3	1
HD 1466	00:18:26.1	-63:28:39.0	41.5 <sup>(a)</sup>	6.5	6.2	6.1	89.4±1.0	-59.5±1.0	1
HIP 1910	00:24:9.0	-62:11:4.0	43.7 <sup>(a)</sup>	8.4	7.7	7.5	82.6±2.7	-51.1±0.8	1, 5
CT Tuc	00:25:14.7	-61:30:48.0	44.6 <sup>(a)</sup>	8.6	7.9	7.7	84.7±1.9	-54.8±1.2	1, 5
HD 2884	00:31:32.7	-62:57:30.0	41.5 <sup>(a)</sup>	4.7	4.7	4.5	83.6±1.0	-54.8±1.0	1
HD 2885	00:31:33.5	-62:57:56.0	42.5 <sup>(a)</sup>	4.3	4.2	4.1	94.0±1.0	-46.3±1.0	1
HD 3003	00:32:43.9	-63:01:53.0	45.5 <sup>(a)</sup>	5.1	5.2	5.0	86.7±1.0	-50.3±1.0	1
HD 3221	00:34:51.2	-61:54:58.0	43.9 <sup>(a)</sup>	7.3	6.7	6.5	83.7±1.3	-50.2±0.8	1, 5
CD-78 24	00:42:20.3	-77:47:40.0	50.1	8.2	7.7	7.5	77.6±0.9	-30.4±1.2	1, 5
HD 8558	01:23:21.3	-57:28:51.0	49.5 <sup>(a)</sup>	7.2	6.9	6.8	89.1±0.8	-38.9±0.7	1
CC Phe	01:28:8.7	-52:38:19.0	36.0 <sup>(a)</sup>	7.4	6.9	6.8	103.7±0.7	-44.1±0.7	1
2MASS J01521830-5950168	01:52:18.3	-59:50:17.0	37.9	8.9	8.3	8.1	109.2±1.8	-25.7±1.8	1, 3, 5
DK Cet	01:57:49.0	-21:54:5.0	40.8 <sup>(a)</sup>	6.9	6.6	6.5	103.9±0.9	-47.8±0.9	1
HD 12894	02:04:35.1	-54:52:54.0	47.8 <sup>(a)</sup>	5.7	5.5	5.4	75.7±1.0	-25.1±1.0	1
HD 13183	02:07:18.1	-53:11:56.0	51.1 <sup>(a)</sup>	7.3	7.0	6.9	88.2±1.4	-23.5±1.1	1
HD 13246	02:07:26.1	-59:40:46.0	44.2	6.5	6.3	6.2	91.1±1.0	-18.3±1.0	1

ID	RA hh:mm:ss.s	DEC dd:mm:ss.s	Dist. (pc)	<i>J</i> (mag.)	<i>H</i> (mag.)	<i>K</i> (mag.)	$\mu_{\alpha,*}$ (mas/yr)	$\mu_{\delta}$ (mas/yr)	Mem ref.
CD-60 416	02:07:32.2	-59:40:21.0	43.2	8.3	7.7	7.5	94.4±1.9	-21.8±1.8	1, 5
HD 14228	02:16:30.6	-51:30:43.0	47.2 <sup>(a)</sup>	4.0	4.0	4.1	90.7±1.0	-22.0±1.0	1
HD 16978	02:39:35.4	-68:16:1.0	46.6 <sup>(a)</sup>	4.4	4.4	4.3	86.8±1.0	-0.2±1.0	1
CD-53 544	02:41:46.8	-52:59:52.0	41.4	7.6	6.9	6.8	97.4±1.3	-13.1±1.1	1, 3, 5
CD-58 553	02:42:33.0	-57:39:37.0	48.5	8.6	8.0	7.8	82.7±0.9	-8.3±1.7	1, 3, 5
HD 17250	02:46:14.6	+05:35:33.0	54.3 <sup>(a)</sup>	6.9	6.6	6.5	75.4±0.8	-44.6±0.5	1, 2
HD 20121 a	03:12:25.8	-44:25:11.0	42.6 <sup>(a)</sup>	5.1	4.9	4.8	82.7±1.0	-2.6±1.0	1, 2
HD 20385	03:16:40.7	-03:31:49.0	49.2 <sup>(a)</sup>	6.5	6.2	6.1	78.6±1.0	-43.8±1.0	1
CD-35 1167	03:19:8.7	-35:07:0.0	44.6	8.6	7.9	7.7	86.4±1.3	-21.0±1.0	1, 3, 5
CD-46 1064	03:30:49.1	-45:55:57.0	42.2	7.8	7.3	7.1	88.8±1.2	-5.0±1.1	1
CD-44 1173	03:31:55.7	-43:59:14.0	44.0	8.3	7.7	7.5	85.0±1.4	-8.2±1.9	1, 3, 5
HD 22705	03:36:53.4	-49:57:29.0	43.3 <sup>(a)</sup>	6.5	6.3	6.1	89.7±1.0	0.3±1.0	1
HD 24636	03:48:11.5	-74:41:39.0	54.0 <sup>(a)</sup>	6.4	6.2	6.1	63.5±1.0	24.9±1.0	1, 2
HD 24701	03:48:35.9	-37:37:13.0	50.7 <sup>(a)</sup>	3.9	4.6	4.8	75.8±1.0	-10.7±1.0	1, 2
HD 25042	04:00:32.0	-41:44:54.0	48.5 <sup>(a)</sup>	7.2	6.9	6.9	69.1±0.9	1.2±1.8	1
BD-15 705	04:02:16.5	-15:21:30.0	52.9	8.2	7.7	7.6	66.7±1.5	-28.2±1.3	5
BD-12 943	04:36:47.1	-12:09:21.0	62.3	8.3	7.9	7.8	50.4±2.7	-22.7±1.5	1
HD 29615	04:38:43.9	-27:02:2.0	56.2 <sup>(a)</sup>	7.3	7.0	6.9	49.7±1.7	-9.7±1.3	1
TYC 8083-455-1	04:48:0.7	-50:41:26.0	54.8	8.7	8.1	7.9	53.1±2.1	15.7±2.3	1, 3, 5
HD 32195	04:48:5.2	-80:46:45.0	61.0 <sup>(a)</sup>	7.2	7.0	6.9	46.2±0.8	41.6±0.9	1
BD-19 1062	04:59:32.0	-19:17:42.0	64.1	8.8	8.2	8.1	43.7±0.9	-13.4±1.0	1
BD-09 1108	05:15:36.5	-09:30:51.0	77.5	8.5	8.2	8.1	31.7±1.2	-20.0±1.3	1
CD-30 2310	05:18:29.0	-30:01:32.0	66.2	9.1	8.4	8.3	37.4±0.9	1.6±1.0	1
TYC 8098-414-1	05:33:25.6	-51:17:13.0	51.6	9.0	8.4	8.2	43.8±2.1	25.1±2.1	1, 3, 5
CD-27 2520	05:49:6.6	-27:33:56.0	74.3	8.8	8.4	8.3	26.0±1.2	3.2±1.1	1
HD 47875	06:34:41.0	-69:53:6.0	68.4	7.8	7.4	7.3	18.7±1.1	40.9±1.3	1
HD 53842	06:46:13.5	-83:59:30.0	55.8 <sup>(a)</sup>	6.6	6.4	6.3	19.7±1.0	61.6±1.0	1
HD 86356	09:51:50.7	-79:01:38.0	74.5	8.6	8.1	8.0	-26.7±0.8	38.1±0.8	1
2MASS J10010873-7913074	10:01:8.8	-79:13:8.0	75.1	10.1	9.4	9.2	-25.7±1.5	38.5±1.6	1
2MASS J11401658-8321003	11:40:16.6	-83:21:0.0	74.2	9.3	8.7	8.6	-41.6±1.1	27.5±1.1	1
HD 193924	20:25:38.9	-56:44:6.0	54.9 <sup>(a)</sup>	2.3	2.5	2.5	6.9±1.0	-86.0±1.0	1
HD 202917	21:20:50.0	-53:02:3.0	42.9 <sup>(a)</sup>	7.4	7.0	6.9	30.1±1.0	-94.5±1.0	1
HIP 107345	21:44:30.1	-60:58:39.0	46.5 <sup>(a)</sup>	8.8	8.1	7.9	39.6±2.4	-91.9±1.8	1, 5
HD 207575	21:52:9.7	-62:03:9.0	45.3 <sup>(a)</sup>	6.4	6.1	6.0	44.0±1.0	-92.0±1.0	1
HD 207964	21:55:11.4	-61:53:12.0	46.5 <sup>(a)</sup>	5.2	5.2	4.9	44.5±1.0	-91.1±1.0	1
2MASS J22021626-4210329	22:02:16.3	-42:10:33.0	44.6	8.9	8.2	8.0	50.4±1.0	-90.9±1.5	3, 5
TYC 9344-293-1	23:26:10.7	-73:23:50.0	44.2	8.8	8.2	7.9	72.9±1.0	-67.4±1.0	1, 3, 5
CD-86 147	23:27:49.4	-86:13:19.0	58.4	8.0	7.6	7.5	54.7±0.9	-42.2±0.9	1
DS Tuc	23:39:39.5	-69:11:45.0	45.7 <sup>(a)</sup>	7.1	6.8	6.7	82.9±1.8	-78.8±4.0	1
TWA									
CE Ant	10:42:30.1	-33:40:17.0	34.5	7.8	7.1	6.9	-114.9±8.7	-18.7±4.7	1
TW Hya	11:01:51.9	-34:42:17.0	51.0 <sup>(a)</sup>	8.2	7.6	7.3	-68.7±1.8	-13.1±1.2	1
HD 96819	11:08:44.0	-28:04:50.0	55.6 <sup>(a)</sup>	5.3	5.4	5.2	-72.8±1.0	-22.2±1.0	1
CD-29 8887	11:09:13.8	-30:01:40.0	46.5	7.6	6.9	6.7	-88.4±1.0	-21.2±0.8	1
TWA 3A	11:10:27.9	-37:31:52.0	36.4	7.7	7.0	6.8	-105.9±0.9	-17.3±1.0	1
V1215 Cen	11:13:26.5	-45:23:43.0	96.2	9.4	8.7	8.5	-43.9±1.4	-7.4±1.4	1, 3
V1217 Cen	11:21:5.5	-38:45:16.0	64.1	9.0	8.3	8.1	-66.6±1.5	-11.7±1.5	1, 3
V547 Hya	11:21:17.2	-34:46:46.0	55.6	8.4	7.7	7.5	-85.4±0.9	39.9±1.0	1
TV Cr1	11:22:5.3	-24:46:40.0	43.1 <sup>(a)</sup>	6.4	5.8	5.6	-88.8±1.6	-32.6±5.0	1
CD-33 7795	11:31:55.3	-34:36:27.0	50.0	7.7	7.0	6.7	-79.6±0.8	-22.6±0.9	1, 3
TWA5 b	11:31:55.4	-34:36:29.0	50.0	7.7	7.0	6.7	-79.6±0.8	-22.6±0.9	1
TWA30 a	11:32:18.3	-30:19:52.0	45.5	9.6	9.0	8.8	-87.8±1.3	-25.2±1.3	3
V549 Hya	11:32:41.2	-26:52:9.0	38.6	9.8	9.3	9.0	-95.3±2.2	-28.6±4.7	1
V550 Hya	11:32:41.2	-26:51:56.0	42.7	8.3	7.7	7.4	-99.2±6.2	-32.2±6.2	1
TWA26	11:39:51.1	-31:59:21.0	38.2	12.7	12.0	11.5	-96.0±11.6	-40.3±11.6	1
V1239 Cen	11:48:24.2	-37:28:49.0	70.6 <sup>(a)</sup>	8.7	8.0	7.8	-44.2±1.8	-18.0±0.9	1
TWA23	12:07:27.4	-32:47:0.0	53.8	8.6	8.0	7.8	-70.4±1.4	-29.7±1.1	1, 3
TWA27	12:07:33.4	-39:32:54.0	52.3	13.0	12.4	11.9	-80.1±17.9	-15.1±17.9	1
V1249 Cen	12:15:30.7	-39:48:43.0	54.1	8.2	7.5	7.3	-73.2±0.8	-27.7±0.8	1, 3
TWA32	12:26:51.4	-33:16:13.0	68.1	10.7	10.1	9.8	-61.6±2.0	-23.0±4.9	1
TWA16	12:34:56.4	-45:38:7.0	78.1	9.0	8.3	8.1	-47.5±1.3	-20.2±0.8	1
V1252 Cen	12:35:4.2	-41:36:39.0	61.7	9.1	8.5	8.2	-70.1±1.1	-28.9±1.1	1, 3
TWA11a	12:36:1.0	-39:52:10.0	73.0 <sup>(a)</sup>	5.8	5.8	5.8	-56.7±1.0	-25.0±1.0	1

Notes. <sup>(a)</sup> Distances from parallax measurements

References. 1: SACY works (Torres et al. 2008; Elliott et al. 2014), 2: Zuckerman et al. (2011), 3: Malo et al. (2014), 4: Murphy & Lawson (2015), 5: Kraus et al. (2014).

**Appendix E: All properties and references of targets identified in this work**